The Complete Research Report

Project Name…

Thermal and Hydraulic Performance of the Combined Enhanced Tube, Freely Rotating Swirl Generator and Nanofluids

Investigator…

Asst. Prof. Dr. Weerapun Duangthongsuk

February 2018

Project code: TRG 5880269

The Complete Research Report

Project Name…

Thermal and Hydraulic Performance of the Combined Enhanced Tube, Freely Rotating Swirl Generator and Nanofluids

Researcher…

Asst. Prof. Dr. Weerapun Duangthongsuk
Mechanical Engineering Department
Faculty of Engineering
Southeast Asia University

Supported by the Thailand Research Fund (TRF)

บทคัดย่อ

รหัสโครงการ: TRG 5880269

ชื่อโครงการ: สมรรถนะทางความร้อนและการไหลของท่อแลกเปลี่ยนความร้อนสมรรถนะสูงที่ทำงานร่วมกับอุปกรณ์สร้างการไหลวนที่หมุนได้อย่างอิสระและของไหลนาโน

ชื่อนักวิจัย:
ผศ. ดร. วีระพันธ์ ด้วงทองสุข
สาขาวิชาวิศวกรรมเครื่องกล คณะวิศวกรรมศาสตร์ มหาวิทยาลัยเอเชียอาคเนย์

E-mail Address: wdaungthongsuk@yahoo.com, weerapund@sau.ac.th

ระยะเวลาโครงการ : 2 ปี นับตั้งแต่ 2 กรกฎาคม 2558 – 30 มิถุนายน 2560

งานวิจัยนี้เป็นการศึกษาเชิงทดลองในการหาลักษณะเฉพาะการถ่ายเทความร้อนและความดันลดของของไหลนาโนที่ไหลผ่านท่อแลกเปลี่ยนความร้อนสมรรถนะสูงชนิด Internally grooved tube (IGT) และท่อแลกเปลี่ยนความร้อนสมรรถนะสูงที่ติดตั้งอุปกรณ์สร้างการไหลวนชนิดหมุนได้อย่างอิสระภายใน (IGT+SG) โดยศึกษาภายใต้สภาวะการไหลแบบปั่นป่วน จากนั้นนำข้อมูลการทดลองไปเปรียบเทียบกับท่อเรียบปกติ (CST) ของไหลนาโนที่ใช้ในการทดลอง คือ ชนิดที่ใส่อนุภาคของ SiO_2 ลงในน้ำ โดยมีความเข้มข้นโดยปริมาตรเท่ากับ 0.2, 0.4 และ 0.6 vol.% ท่อทดสอบที่ใช้เป็นแบบท่อสองชั้นไหลสวนทางกัน มีความยาว 1.3 เมตร โดยที่ของไหลนาโนไหลอยู่ภายในและแลกเปลี่ยนความร้อนกับน้ำร้อนที่ไหลอยู่ในท่อวงแหวน ท่อในทั้งแบบ CST, IGT และ IGT+SG ทำมาจากสแตนเลส ที่มีขนาดเส้นผ่านศูนย์กลางภายนอก 9.53 มิลลิเมตร เส้นผ่านศูนย์กลางภายใน 7.53 มิลลิเมตร ส่วนท่อนอกทำมาจากอะครีลิกใสที่มีขนาดเส้นผ่านศูนย์กลางภายนอก 33.9 มิลลิเมตร และมีเส้นผ่านศูนย์กลางภายใน 27.8 มิลลิเมตร อุปกรณ์ไหลวนที่ติดตั้งภายในท่อมีจำนวน 6 ตัว แต่ละตัวยาว 42 มิลลิเมตร มีมุมบิด 60 องศา ทำมาจากพลาสติคเพื่อลดน้ำหนัก และทุกตัวสามารถหมุนได้อย่างอิสระเมื่อมีของไหลไหลผ่าน ที่ทางเข้าของท่อทดสอบทำการติดตั้งท่อพลาสติคใสเพื่อลดการสูญเสียความร้อนตามความยาวท่อ งานวิจัยนี้ทำการศึกษาผลของเลขเรย์โนลด์ ความเข้มข้นของของไหลนาโน ท่อแลกเปลี่ยนความร้อนสมรรถนะสูง และการติดตั้งอุปกรณ์สร้างการไหลวนในท่อแลกเปลี่ยนความร้อนสมรรถนะสูง ที่มีต่อค่าสมรรถนะทางความร้อนและความดันลดที่เกิดขึ้น จากการทดลอง สำหรับกรณีที่ใช้น้ำเป็นของไหลทำงาน พบว่า ท่อ IGT+SG ให้ค่าสัมประสิทธิ์การถ่ายเทความร้อนที่สูงที่สุด โดยสูงกว่าท่อ IGT ประมาณ 12 เปอร์เซ็นต์ และสุงกว่าท่อ CST ประมาณ 24 เปอร์เซ็นต์ ขณะเดียวกันความดันลดก็สูงที่สุดด้วยเช่นกัน โดยสูงกว่าท่อ IGT และ

CST ประมาณ 2.9 และ 3.1 เท่า ตามลำดับ สำหรับกรณีการใช้ของไหลนาโนเป็นของไหลทำงานที่ความเข้มข้นระหว่าง 0.2 ถึง 0.6 เปอร์เซ็นต์โดยปริมาตรนั้น พบว่าสามารถเพิ่มสมรรถนะการถ่ายเทความร้อนได้ 6 ถึง 22 เปอร์เซ็นต์ สุดท้ายงานวิจัยนี้ได้นำข้อมูลจากการทดลองทั้งหมด มาสร้างสหสัมพันธ์สำหรับทำนายค่าเลขนัสเซลและความดันลด จากการไหลของของไหลนาโนที่ไหลผ่านท่อ IGT และ IGT+SG ในรูปแบบที่ง่ายต่อการใช้งาน และให้ผลสอดคล้องกับการทดลอง

คำหลัก : ของไหลนาโน, ท่อแลกเปลี่ยนความร้อนสมรรถนะสูง, เลขนัสเซล, ความดันลด, อุปกรณ์สร้างการไหลวน

Abstract

Project Code: TRG 5880269

Project Title: Thermal and Hydraulic Performance of the Combined Enhanced Tube, Freely Rotating Swirl Generator and Nanofluids

Investigator:

Asst. Prof. Dr. Weerapun Duangthongsuk

Mechanical Engineering Department, Faculty of Engineering,

Southeast Asia University

E-mail Address: wdaungthongsuk@yahoo.com, weerapund@sau.ac.th

Project Period: 2 July 2015 – 30 June 2017

This study reports the heat transfer and pressure drop characteristics of nanofluids flow in the internally grooved tube (IGT) and the internally grooved tube fitted with freely rotating swirl generator (IGT+SG) under turbulent flow regime, experimentally. The data are compared with the common smooth tube (CST). SiO_2 nanoparticles dispersed in water with particle concentrations of 0.2, 0.4 and 0.6 vol.% are used as working fluid. Double tube counter flow heat exchanger is used as the test section. The test section is a 1.3 m length with nanofluids flows inside the tube while hot water flows in the annular. The inner tube is CST, IGT and IGT+SG which made from stainless steel with a 9.53 mm outer diameter and a 7.53 mm inner diameter. Similarly, the outer tube is made from acrylic tubing and has a 33.9 mm outer diameter and 27.8 mm inner diameter. Six freely rotating swirl generators with length of 42 mm and twisted angle of 60^o are equipped along the test section. They are made from plastic. The test section is thermally isolated from its upstream and downstream section by plastic tubes in order to reduce the heat loss along the axial direction. The effects of Reynolds number, particle concentrations, enhanced tube and swirl flow devices fitted in the enhanced tube on the thermal performance and pressure drop are presented. For water, the results indicated that IGT+SG gave highest heat transfer coefficient compared with the IGT and CST around 12% and 24%, respectively. At the same time, highest pressure drops are obtained and greater than those of the IGT and CST average 2.9 and 3.1 times,

respectively. The heat transfer coefficients of nanofluid are higher than the common water approximately 6.0 to 22% at particle fraction ranged between 0.2 and 0.6 vol.% for case of IGT. As a result, IGT gave larger thermal performance factor than that of the IGT+SG for all of the test conditions. Finally, new heat transfer and pressure drop correlations for predicting the Nusselt number and pressure drop of nanofluid flowing through IGT and IGT+SG are proposed in the simple forms.

Keywords: nanofluid, enhanced tube, Nusselt number, pressure drop, swirl generator

Output จากโครงการวิจัยที่ได้รับทุนจาก สกว.

1. ผลงานตีพิมพ์ในวารสารวิชาการนานาชาติ

- Duangthongsuk, W. and Wongwises, S., 2017, “An experimental investigation on the heat transfer and pressure drop characteristics of nanofluid flowing in microchannel heat sink with multiple zigzag flow channel structures”, *Experimental Thermal and Fluid Science*, Vol. 87, pp. 30-39. ISI Scimago Q1
- Duangthongsuk, W. and Wongwises, S., “A comparison of the thermal and hydraulic performances between miniature pin fin and microchannel heat sinks with nanofluids cooled”, *Heat and Mass Transfer*, **In revision**
- Duangthongsuk, W. and Wongwises, S., “Turbulent forced convective heat transfer and flow feature of nanofluids flow in an enhanced tube fitted with swirl generator”, *Experimental Thermal and Fluid Science*, **In preparation**

ผลงานตีพิมพ์ในที่ประชุมวิชาการระดับนานาชาติ

- Duangthongsuk, W., 2017, “Thermal and Hydraulic Performances of Nanofluids Flow in Microchannel Heat Sink with Multiple Zigzag Flow Channels”, MATEC Web of Conferences **95**, 03011

2. การนำผลงานวิจัยไปใช้ประโยชน์
   - เชิงสาธารณะ (มีเครือข่ายความร่วมมือ/สร้างกระแสความสนใจในวงกว้าง)
   - เชิงวิชาการ (มีการพัฒนาการเรียนการสอน/สร้างนักวิจัยใหม่)

3. อื่นๆ
   - Heat Transfer and Pressure Drop Investigations of Nanofluids Flow in a Enhanced Tube Fitted with Swirl Flow Device**,** การประชุมวิชาการประจำปี “**นักวิจัยรุ่นใหม่..พบ..เมธีวิจัยอาวุโส สกว.**” ครั้งที่ 16, 11 – 13 มกราคม 2560, โรงแรม เดอะรีเจ้นท์ บีชชะอำ, เพชรบุรี

ACKNOWLEDGEMENT

This research work would not have been possible without the help and active collaboration of many people to whom I acknowledge my indebtedness and sincere gratitude and appreciation.

Firstly, I would like to express sincere thanks to the Thailand Research Fund (TRF), and the Southeast Asia University to provide financial support (Grant No. TRG 5880269) for this study. I am very grateful to thanks my mentor, Prof. Dr. Somchai Wongwises, for his valuable suggestion, attentive interest, guidance and kind recommendations in the present research. Thank you the students in the Mechanical Engineering Department, Southeast Asia University for their help.

CONTENTS

LIST OF TABLES

LIST OF FIGURES

LIST OF SYMBOLS

A	=	area, m^2
B	=	base thickness, mm
C_p	=	specific heat, J/kgK
d	=	nanoparticle diameter, m
D_H	=	hydraulic diameter, m
h	=	heat transfer coefficient, W/m^2K
k	=	thermal conductivity, W/mK
$\dot{m}$	=	mass flow rate, kg/s
Nu	=	Nusselt number
Pow	=	pumping power, W
ΔP	=	Pressure drop, Pa
Pr	=	Prandtl number
q	=	heat flux, W/m^2
Q	=	heat transfer rate, W
Re	=	Reynolds number
T	=	temperature, ^oC
u	=	mean velocity, m/s
$\dot{V}$	=	volume flow rate, m^3/s

Greek symbols

ϕ	=	volume fraction
ρ	=	density, kg/m^3

μ	=	viscosity, kg/ms

Subscript

h	=	heating fluid
in	=	inlet
m	=	mean
out	=	outlet
p	=	particles
nf	=	nanofluid
s	=	surface
TS	=	test section

CHAPTER 1 INTRODUCITON

1.1 Rationale

Heat transfer enhancement techniques are means to augment thermal performance, a drastic reduction in size and cost of heat exchangers. In general, two heat transfer enhancement techniques are applied include passive technique and active technique, respectively. For passive technique, special surface geometries, such as a rough surface, an extended surface, enhanced tube, fluid additives, displaced insert devices, or swirl flow devices are used to increase the heat transfer performance. Similarly, the active technique requires external forces, such as an electrical field, stirring of the fluid, fluid and surface vibration, or jet impingement. Focusing on passive techniques, the use of an enhanced tube such as internally grooved tube, micro fin tube, corrugated tube and spiral flute tube to replace the common plain tube is an interest technique for considering. Many investigators have been reported that various types of enhanced tube can increase the thermal performance by increasing fluid mixing, unsteadiness, turbulence flow, or limiting the growth of the fluid boundary layers close to the heat transfer surfaces and no additional pressure drop are observed. Furthermore, displaced insert devices or swirl generator devices can be fitted inside and outside of the tubes to create swirl flow, thereby reducing the thermal boundary layer thickness. Thus, an increase in heat transfer performance is obtained. However, the addition of some devices into the main flow can caused an increase in the drop of pressure. The last interest passive technique for increasing the heat transfer performance is fluid additives named “Nanofluid”. Normally, common heat transfer fluids such as oil, water and ethylene glycol are widely used in many industries, including power generation, chemical processes, heating and cooling processes. Their heat transfer performances are rather limited by poor thermal properties when compared with most solids. This is the

important reason why the development of heat transfer devices is retarded. Many researchers have tried to develop special heat transfer fluids for increasing of their thermal properties. A novel way is to suspend small solid particles in the common fluid to form colloidal. Different types of solid particles, such as polymeric, metallic and non-metallic can be added into the common heat transfer fluids. In the early studies, however, use of suspended particles of millimeter or even micrometer-size demonstrated unusually high thermal enhancement, but some extreme problems are also experienced, such as poor stability of the suspension, clogging of flow channels, eroding of pipelines and increase in pressure drop in practical applications. Although the solutions show better thermal performance compared to common heat transfer fluids, they are still not suitable for use as heat transfer fluids in practical applications, especially for the mini and/or micro-channel or even electronic cooling equipment. So far, the concept of nanofluid can be solve the above-mentioned problem. This term refer to the use of nanoparticle (normally less than 100 nm) to disperse in common heat transfer fluids. This concept was first introduced by Masuda et al. [1] in 1993. However, 2 years later, the name of nanofluid was first called by S.U.S Choi [2] and successively gained popularity. Many investigator have reported that nanofluids have shown a number of potential advantages, such as better long-term stability, little or no penalty in pressure drop, significantly greater thermal conductivity and can have drastically heat transfer performance [3, 4, 5, 6]. Nanofluids are expected to be ideally used for practical applications.

From the above three types of passive technique, a significant increase in heat transfer performance and minimizing of the pressure drop value are the most proper methods for enhancing the thermal performance of heat exchangers. Up to now, the combination of these three techniques for increasing the heat transfer performance and minimizing the

pressure drop across the equipment are still lacked. In my opinion, this is a good chance to discover the thermal and hydraulic performance of the three combined techniques. Examples of the enhanced tube, swirl generator device and nanofluid are expressed in Figs. 1, 2 and 3, respectively as follows:

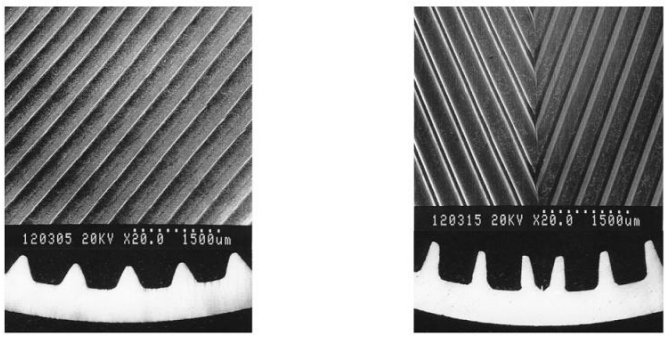

a) Internally grooved tube (Goto et al. [7])

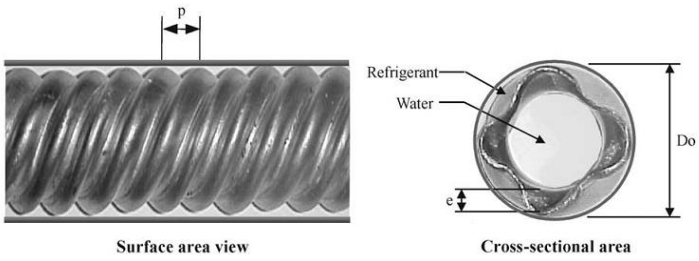

b) Spiral fluted tube (Rousseau et al. [8])

c) Corrugated tube [9]

Fig. 1.1 Examples of enhanced tube.

a) Turbine type swirl generator inserts (Duangthongsuk & Wongwises [10, 11])

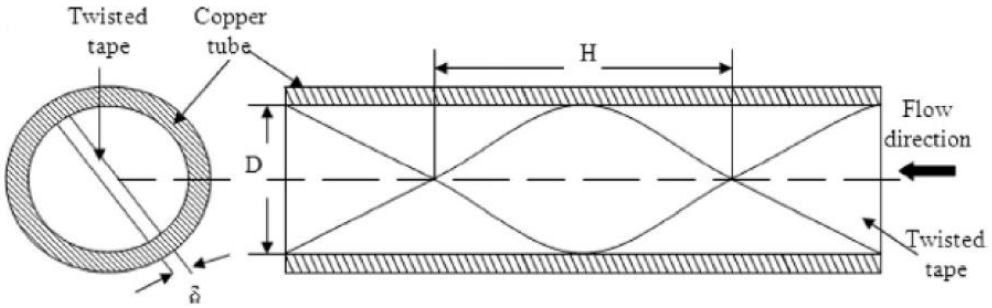

b) Twisted tape insert (Azmi et al. [12])

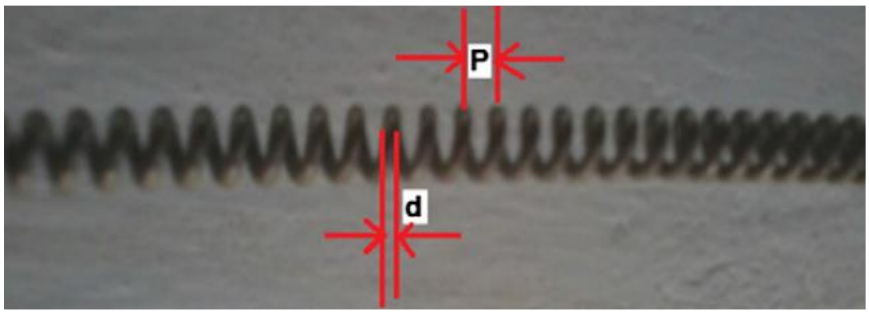

c) Wire coil insert (Reddy & Rao [13])

Fig. 1.2 Examples of swirl generator inserts.

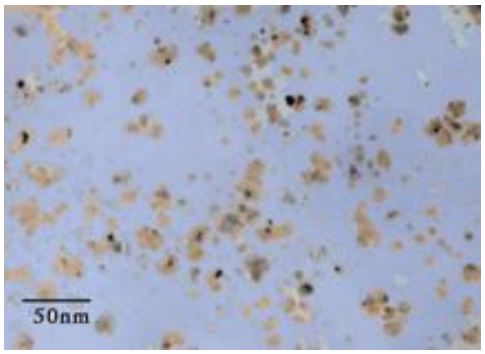

a) Cu-water nanofluid [14]

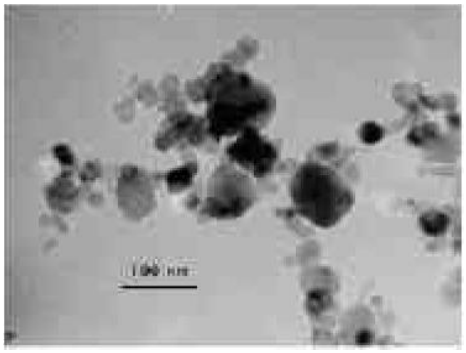

b) CuO-ethylene glycol nanofluid [14]

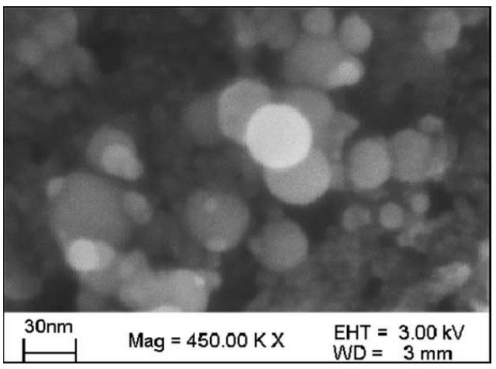

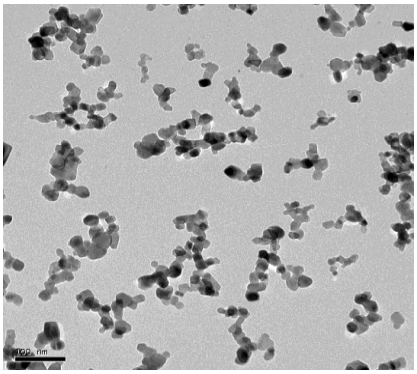

c) Al_2O_3-H_2O (Wen & Ding [15]) d) TiO_2 –H_2O (Duangthongsuk & Wongwises [16])

Fig. 1.3 TEM images of various type of nanofluids**.**

1.2 Objectives

1. To investigate the heat transfer and friction factor of nanofluids flowing through an internally grooved tube fitted with freely rotating swirl generators (IGT+SG).

2. To study the effects of the parameters such as Reynolds number, particle concentration and freely rotating swirl flow device on the heat transfer performance and friction characteristics of internally grooved tube fitted with freely rotating swirl generators (IGT+SG) compared with common smooth tube (CST) and internally grooved tube (IGT).

3. To propose the new correlations to predict the Nusselt number and pressure drop of nanofluids flowing through IGT and IGT+SG using nanofluids as coolant.

1.3 Scope

1. Enhanced tube used in the present study is an internally grooved tube with nominal diameter of 9.53 mm.

2. The SiO_2 nanoparticles suspended in water with particle concentrations less than 0.6 vol.% are used as working fluid and flow under turbulent flow regime.

3. Length of the test section is about 1,300 mm.
4. Double tube counter flow heat exchanger is used as the test section.
5. Nanofluids temperature is about 25 ^{o}C.

1.4 Significance and Usefulness

1. The results obtained from this study are expected to be suitable for applying the combined enhanced tube and swirl flow device using nanofluids to practical use.
2. The experimental system can be used to study the other types of the enhanced tube and swirl flow device including outer swirl generator.
3. The new heat transfer and pressure drop correlations can be used to predict the thermal and flow behaviors of nanofluid flowing through the enhanced tube fitted with swirl flow device.

CHAPTER 2 FUNDAMENTAL AND LITERATURE REVIEW

The purpose of this chapter is to describe the fundamental and basic theory of nanofluids and heat transfer enhancement techniques, respectively. Moreover, review the literature mentioning the heat transfer performance and flow characteristics of nanofluids flowing through enhanced tube equipped with various types of swirl generator including the experimental and numerical investigations. The detail of above mentioned is expressed in the following subsection.

2.1 Fundamental of Nanofluids

2.1.1 Making of Nanofluids

Materials for base fluids and nanoparticles are diverse. Stable and highly conductive nanofluids are produced by one- and two-step production methods. Both approaches to creating nanoparticle suspensions suffer from agglomeration of nanoparticles, which is a key issue in all technology involving nanopowders. Thus, synthesis and suspension of nearly nonagglomerated or monodispersed nanoparticles in liquids is the key to significant enhancement in the thermal properties of nanofluids (Das et al. [17]).

2.1.2 Nanoparticles Materials and Conventional Base Fluids

Modern fabrication technology provides great opportunities to process materials actively at nanometer scales. Nanostructured or nanophase materials are made of nanometer-sized substances engineered on the atomic or molecular scale to produce either new or enhanced physical properties not exhibited by conventional bulk solids. All physical mechanisms have a critical length scale below which the physical properties of materials are changed. Therefore, particles smaller than 100 nm exhibit

properties different from those of conventional solids. The noble properties of nanophase materials come from the relatively high surface area/volume ratio, which is due to the high proportion of constituent atoms residing at the grain boundaries. The thermal, mechanical, optical, magnetic, and electrical properties of nanophase materials are superior to those of conventional materials with coarse grain structures. Consequently, research and development investigation of nanophase materials has drawn considerable attention from both material scientists and engineers (Duncan and Rouvray, [18]).

1. Nanoparticle material types. Nanoparticles used in nanofluids have been made of various materials, such as oxide ceramics (Al_2O_3, CuO), nitride ceramics (AlN, SiN), carbide ceramics (SiC, TiC), metals (Cu, Ag, Au), semiconductors (TiO_2, SiC), carbon nanotubes, and composite materials such as alloyed nanoparticles Al70Cu30 or nanoparticle core–polymer shell composites. In addition to nonmetallic, metallic, and other materials for nanoparticles, completely new materials and structures, such as materials “doped” with molecules in their solid–liquid interface structure, may also have desirable characteristics (Das et al. [17]).

2. Host liquid types. Many types of liquids, such as water, ethylene glycol, and oil, have been used as host liquids in nanofluids (Das et al. [17]).

2.1.3 Methods of Nanoparticle Manufacture

Fabrication of nanoparticles can be classified into two broad categories: physical processes and chemical processes (Kimoto et al. [19], Granqvist and Buhrman [20]). Currently, a number of methods exist for the manufacture of nanoparticles. Typical physical methods include inert-gas condensation (IGC), developed by Granqvist and Buhrman [20], and mechanical grinding. Chemical methods include chemical vapor

deposition (CVD), chemical precipitation, microemulsions, thermal spray, and spray pyrolysis. A sonochemical method has been developed to make suspensions of iron nanoparticles stabilized by oleic acid (Suslick et al., [21]). The current processes for making metal nanoparticles include IGC, mechanical milling, chemical precipitation, thermal spray, and spray pyrolysis. Most recently, Chopkar et al. [22] produced alloyed nanoparticles Al70Cu30 using ball milling. In ball milling, balls impart a lot of energy to slurry of powder, and in most cases some chemicals are used to cause physical and chemical changes. These nanosized materials are most commonly produced in the form of powders. In powder form, nanoparticles are dispersed in aqueous or organic host liquids for specific applications (Das et al. [17]).

2.1.4 Dispersion of Nanoparticles in Liquids

Stable suspensions of nanoparticles in conventional heat transfer fluids are produced by two methods: the two-step technique and the single-step technique. The two-step method first makes nanoparticles using one of the above-described nanoparticle processing techniques and then disperses them into base fluids. The single-step method simultaneously makes and disperses nanoparticles directly into base fluids. In either case, a well-mixed and uniformly dispersed nanofluid is needed for successful production or reproduction of enhanced properties and interpretation of experimental data. For nanofluids prepared by the two-step method, dispersion techniques such as high shear and ultrasound can be used to create various particle–fluid combinations. Most nanofluids containing oxide nanoparticles and carbon nanotubes reported in the open literature are produced by the two-step process. If nanoparticles are produced in dry powder form, some agglomeration of individual nanoparticles may occur due to strong attractive van der Waals forces between nanoparticles. This undesirable

agglomeration is a key issue in all technology involving nanopowders. Making nanofluids using the two-step processes has remained a challenge because individual particles quickly agglomerate before dispersion, and nanoparticle agglomerates settle out in the liquids. Well-dispersed stable nanoparticle suspensions are produced by fully separating nanoparticle agglomerates into individual nanoparticles in a host liquid. In most nanofluids prepared by the two-step process, the agglomerates are not fully separated, so nanoparticles are dispersed only partially. Although nanoparticles are dispersed ultrasonically in liquid using a bath or tip sonicator with intermittent sonication time to control overheating of nanofluids, this two-step preparation process produces significantly poor dispersion quality. Because the dispersion quality is poor, the conductivity of the nanofluids is low. Therefore, the key to success in achieving significant enhancement in the thermal properties of nanofluids is to produce and suspend nearly monodispersed or nonagglomerated nanoparticles in liquids.

A promising technique for producing nonagglomerating nanoparticles involves condensing nanophase powders from the vapor phase directly into a flowing low-vapor pressure fluid. This approach, developed in Japan 20 years ago by Akoh et al. [23] which is called the VEROS (vacuum evaporation onto a running oil substrate) technique. VEROS has been essentially ignored by the nanocrystalline-materials community because of subsequent difficulties in separating the particles from the fluids to make dry powders or bulk materials. Based on a modification of the VEROS process developed in Germany (Wagener et al. [24) Moreover, Eastman et al. [25] developed a direct evaporation system that overcomes the difficulties of making stable and well-dispersed nanofluids. The direct evaporation–condensation process yielded a uniform distribution of nanoparticles in a host liquid. In this much-longed-for way to making

nonagglomerating nanoparticles, they obtained copper nanofluids with excellent dispersion characteristics and intriguing properties. The thermal conductivity of ethylene glycol, the base liquid, increases by 40% at a Cu nanoparticle concentration of only 0.3 vol%. This is the highest enhancement observed for nanofluids except for those containing carbon nanotubes. However, the technology used by Eastman et al. has two main disadvantages. First, it has not been scaled up for large-scale industrial applications. Second, it is applicable only to low-vapor-pressure base liquids. Clearly, the next step is to see whether they can compete with the chemical one-step method described below. Zhu et al. [26] developed a one-step chemical method for producing stable Cu-in-ethylene glycol nanofluids by reducing copper sulfate pentahydrate ($CuSO_4 \cdot 5H_2O$) with sodium hypophosphite ($NaH_2PO_2 \cdot H_2O$) in ethylene glycol under microwave irradiation. They claim that this one-step chemical method is faster and cheaper than the one-step physical method. The thermal conductivity enhancement approaches that of Cu nanofluids prepared by a one-step physical method developed by Eastman et al. [27]. Although the two-step method works well for oxide nanoparticles, it is not as effective for metal nanoparticles such as copper. For nanofluids containing high-conductivity metals, it is clear that the single-step technique is preferable to the two-step method (Das et al. [17]).

The first-ever nanofluids with carbon nanotubes, nanotubes-in-synthetic oil (PAOs), were produced by a two-step method (Choi et al. [28]). Multiwalled carbon nanotubes (MWNTs) were produced in a CVD reactor, with xylene as the primary carbon source and ferrocene to provide the iron catalyst. MWNTs having a mean diameter of~25 nm and a length of~50μm contained an average of 30 annular layers. Chopkar et al. [22] used ball milling to produce $Al_{70}Cu_{30}$ nanoparticles and dispersed

their alloyed nanoparticles in ethylene glycol (Das et al. [17]).

2.2 Heat Transfer Enhancement Classification

In general, heat transfer enhancement techniques are classified in three categories such as passive method, active method, and compound method which are described as follows:

2.2.1 Passive method

These methods need no external power and usually utilize geometrical or surface modifications to the flow tube by additional devices or joining inserts. These methods increase the rate of heat transfer by changing the flow treatment which also causes the pressure drop to increase. Various passive techniques are described as follows:

- Coiled tubes: Coiled tubes are appropriate for more compact heat exchangers. These methods produce secondary flows which support higher heat transfer coefficient.
- Extended surfaces: They are used to create swirl turbulence and secondary flow.
- Rough surfaces (Corrugated tube, Rib):
- Swirl flow devices: These devices produce secondary recirculation on the axial flow for single phase or two-phase flows heat exchanger. In this part we investigate the previous work in which authors used twisted tape, conical ring, snail entry tabulators, vortex rings, coiled wire and other kinds of tabulators.

Passive thermal management refers to technologies that rely solely on the thermo-dynamics of conduction, convection and radiation to complete the heat transfer process. These technologies are the most commonly used, the least expensive and the easiest to implement. Passive techniques generally use surface or geometrical modifications to the flow by incorporating inserts or additional devices. They promote higher heat transfer

coefficients by disturbing or altering the existing flow behavior (except for extended surfaces) which also leads to increase in the pressure drop. In case of extended surfaces, effective heat transfer area on the side of the extended surface is increased. Passive techniques hold the advantage over the active techniques as they do not require any direct input of external power. These techniques do not require any direct input of external power; rather they use it from the system itself which ultimately leads to an increase in fluid pressure drop

2.2.2 Active method

For this method, some external power input needs in order to reach augment in the rate of heat transfer. Because of the need of equipment, this method has limit application in many practical applications. In comparison to the passive techniques, these techniques have not shown much potential as it is difficult to provide external power input in many cases. Various active techniques are as follows:

- Mechanical Aids: These devices stir the fluid by mechanical means or by rotating the surface. Examples of the mechanical aids include rotating tube exchangers and scrapped surface heat and mass exchangers.
- Surface vibration: They have been used primarily in single phase flows. A low or high frequency is applied to facilitate the surface vibrations which results in higher convective heat transfer coefficients.
- Fluid vibration: Instead of applying vibrations to the surface, pulsations are created in the fluid itself. This kind of vibration enhancement technique is employed for single phase flows.
- Electrostatic fields: Electrostatic field like electric or magnetic fields or a combination of the two from DC or AC sources is applied in heat exchanger systems which induces greater bulk mixing, force convection or electromagnetic

pumping to enhance heat transfer. This technique is applicable in heat transfer process involving dielectric fluids.

- Injection: In this technique, same or other fluid is injected into the main bulk fluid through a porous heat transfer interface or upstream of the heat transfer section. This technique is used for single phase heat transfer process.
- Suction: This method is used for both two phase heat transfer and single phase heat transfer process. Two phase nucleate boiling involves the vapor removal through a porous heated surface whereas in single phase flows fluid is withdrawn through the porous heated surface

Active thermal management refers to technologies that must introduce energy – typically from an external device – to augment the heat transfer process. A key benefit is that they increase the rate of fluid flow during convection which dramatically increases the rate of heat removal. These techniques are more complex from the use and design point of view as the method requires some external power input to cause the desired flow modification and improvement in the rate of heat transfer. It finds limited application because of the need of external power in many practical applications. In comparison to the passive techniques, these techniques have not shown much potential as it is difficult to provide external power input in many cases. In these cases, external power is used to facilitate the desired flow modification and the concomitant improvement in the rate of heat transfer.

Finally, the compound method uses for complex design, so it has limited applications.

2.3 Literature Review

Usually, heat transfer enhancement techniques are widely used to increase the thermal performance the heat transfer equipment. Minimizing in the pressure drop value should be considered at the same time. Combination of various enhancement techniques for improving the heat transfer performance are explored by a number of researchers in the past decade ago. The recent published articles respect to this aspect are summarized as follows:

For experimental approach, Sharma et al. [29] examined the heat transfer and friction characteristics of a common tube fitted with twisted tape using Al_2O_3-water nanofluids as coolant and flow in transition regime. Sundar and Sharma [30, 31] reported the turbulent heat transfer performance of Al_2O_3-water nanofluids flow in a common tube with twisted tape inserts and with longitudinal strip inserts. Similarly, Heat transfer and flow characteristics of Al_2O_3-water nanofluids flowing through a common plain tube with wire coil inserts under laminar flow case were reported by Chandrasekar and colleges [32] in 2010. Darzi et al. [33] presented the thermal and hydraulic performance of helically corrugated tubes using SiO_2-water nanofluids as working fluid. Wongcharee and Eiamsa-ard [34, 35] examined the heat transfer and friction factor of CuO-water nanofluids flow in a corrugated tube equipped with twisted tapes. Raja Sekhar and co-workers [36] reported the local heat transfer coefficient and friction characteristics of Al_2O_3-water nanofluids flowing through a common smooth tube with twisted tape inserts in laminar flow regime. Naik et al. [37] reported the heat transfer and friction factor of CuO-water nanofluids flow in a common plain tube fitted with twisted tape and wire coil under turbulent flow regime. Azmi and co-workers [38] studied the convective heat transfer coefficient and friction factor of TiO_2-water nanofluids flowing through a common tube with twisted tape inserts under turbulent flow condition. Darzi

and Sedighi [39] studied the heat transfer performance and friction factor of Al_2O_3-water nanofluids flowing through various helically corrugated tubes under turbulent flow condition. Reddy and Rao [13] investigated the turbulent heat transfer performance and friction factor of TiO_2-ethylene glycol and water based nanofluids flow in double tube counter flow heat exchanger with helical coil inserts. Maddah et al. [40] studied the turbulent heat transfer performance of Al_2O_3-water nanofluids flow in horizontal double tube pipes with twisted tapes inserts in turbulent flow case. Eiamsa-ard and Kiatkittipong [41] presented the thermal and hydraulic performance of a common tube fitted with multiple twisted tape using TiO_2-water nanofluids as working fluid medium both experimental and numerical approach. Esmaeilzadeh and colleges [42] presented the laminar heat transfer and friction factor of a circular tube with twisted tape inserts using Al_2O_3-water nanofluids as working fluid.

For numerical approach, Azmi et al. [43] presented a numerical model to predict the heat transfer performance of SiO_2- water nanofluids flow in a common tube equipped with twisted tape and then compared with the measured data.

As mentioned above, a number of researchers reported that the nanofluids show dramatically higher heat transfer performance compared to common base fluids. Little or no penalty drop in pressure were obtained. Similarly, many investigators have been indicated that the common tube equipped with the swirl flow devices gave drastically greater heat transfer performance than those of the conventional tubes. Moreover, it clearly seen that combination at least two enhancement techniques are used to increase the thermal performance, especially nanofluids combined with twisted tape inserts and nanofluids flow in the enhanced tubes. Other swirl flow device such as wire coil and helical are a few reported. There is the only work of Wongcharee and Eiamsa-ard [35] that studied the heat transfer and friction characteristics of three combined techniques

including nanofluid, enhanced tube and swirl flow device. However, twisted tape inserts used in their study was fixed and not freely rotating and equipped with full length of the test tube which caused in high pressure drop.

Thus, this study is aimed to determine the heat transfer and pressure drop of nanofluids flowing in internally grooved equipped with freely rotating swirl generators (IGT+SG) which is expected to increase the thermal performance and minimize the pressure drop. Then, the measured data for IGT+SG are compared with the common internally grooved tube (IGT) and the common smooth tube (CST). For swirl flow device, turbine type swirl generator with short length tabulators are used and freely rotating when fluid is forced through these device. Under this conduct, improving in the heat transfer performance and minimizing in the pressure drop may obtained. SiO_2 nanoparticles dispersed in water are used as working fluid with particle concentrations of 0.2, 0.4 and 0.6 vol.%. The effects of Reynolds number, particle concentrations, and freely swirl flow inserts on the heat transfer performance and pressure drop characteristics are presented and compared. Finally, new heat transfer and pressure drop correlations are proposed to predict the Nusselt number and pressure drop of nanofluids flowing through IGT and IGT+SG working with nanofluids.

CHAPTER 3 SAMPLE PREPARATION, EXPERIMENTAL APPARATUS AND PROCEDURE

This chapter presents the method to prepare the nanofluid solution, experimental system and experimental procedure, respectively. For the experimental system, the apparatus are conducted for measuring the convective heat transfer and pressure drop of nanofluids flow through IGT+SG and IGT. Then, the measured are compared with the CST. The details are described in the following sections.

3.1 Sample Preparation

Nanofluid preparation is of crucial importance when using the nanofluid as a working fluid. The term "nanofluid" does not mean a simple mixture between solid particles and base fluid. In order to prepare nanofluids by dispersing the nanoparticles in a base fluid, proper mixing, and stabilization of the particles is required. Normally, there are three effective methods used to attain stability of suspension against sedimentation of the nanoparticles which are outlined as follows: 1) control the ph value of the suspensions, 2) add surface activators or surfactants, 3) use ultrasonic vibration. All of these techniques aim to change the surface properties of suspended nanoparticles and suppress the formation of clustering particles in order to obtain stable suspensions. In this study, SiO_2 nanoparticles with mean diameters of 15 nm and particle volume fractions of 0.2, 0.4 and 0.6 vol.% are used in this study. Nanofluid with various concentrations were prepared by dispersing a specific amount of the nanoparticles in the deionized water (DI water) base fluid. Moreover, an ultrasonic vibrator was used to sonicate the solution continuously for about two hours in order to break down

agglomeration of the nanoparticles. The thermophysical properties of nanoparticle were expressed in the following table.

Table 3.1 Thermophysical properties of SiO_2 nanoparticle used in the present study

Properties	SiO_2 nanoparticle
Density (kg/m^3)	2,648
Specific heat (kJ/kg ^oC)	0.742
Thermal conductivity (W/m^{2o}C)	1.37
Mean diameter, d (nm)	15

3.2 Convective Heat Transfer and Pressure Drop Measurement

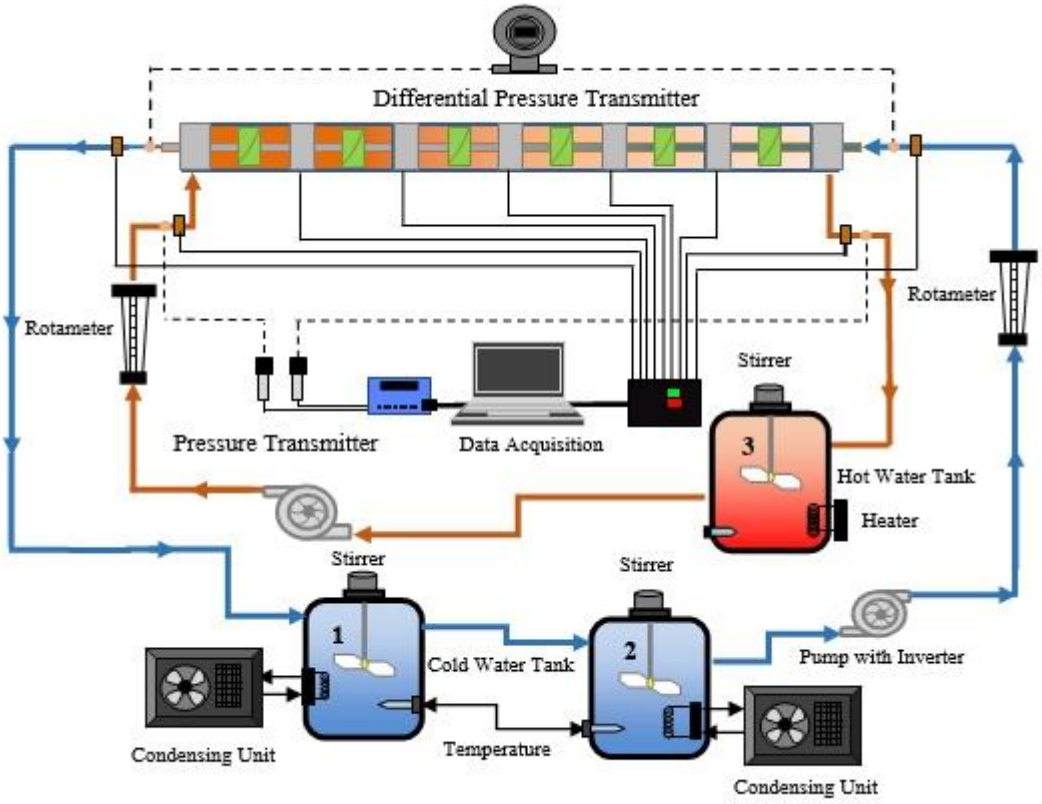

Fig. 3.1 Schematic diagram of the experimental apparatus

In the present study, experimental approach is used to investigate the heat transfer performance and flow characteristics of nanofluids flowing through IGT and IGT+SG. The experimental system is shown schematically in Fig. 3.1. It mainly consists of a test

section, two cold water tanks, a magnetic gear pump, a hot water pump, a hot water tank and a receiver tank. The test section is a 1.3 m long counter flow horizontal double tube heat exchanger with nanofluid flowing inside the tube while hot water flows in the annular. The inner tube is CST, IGT and IGT+SG which made from stainless steel with a 9.53 mm outer diameter and a 7.53 mm inner diameter. Similarly, the outer tube is made from acrylic tubing and has a 33.9 mm outer diameter and 27.8 mm inner diameter. The test section is thermally isolated from its upstream and downstream section by plastic tubes in order to reduce the heat loss along the axial direction. The differential pressure transmitter and T-type thermocouple are mounted at both ends of the test section to measure pressure drop and the bulk temperature of the nanofluid, respectively. Thermocouples are mounted at different longitudinal positions on the inner tube surface of the wall. The inlet and exit temperatures of hot water are measured using T-type thermocouples which are inserted into the flow directly. The cooler tank No. 1 with a 3.5 kW cooling capacity and a thermostat is used to keep the nanofluid temperature constant at desired value. Similarly, the cold water tank No.2 of 30 L with 3.5 kW cooling capacity is used to reduce the nanofluid temperature leaving from the test section to the temperature of tank No.1. Both tank are made from stainless steel with 30 L capacity. For hot water tank, a 3 kW electric heater with a thermostat is installed to keep the temperature of the hot water constant. The nanofluid flow rate is controlled by adjusting the rotation speed of the magnetic pump. The hot water flow rate is measured by a rotameter whereas the nanofluids flow rate is evaluated by the time taken for a given volume of nanofluid to be discharged. Calibrations of all instruments used in this study are performed for estimating the accuracy of the measured data.

After steady state reached, wall temperatures, inlet and exit temperatures of the nanofluids, mass flow rates of the nanofluids, and pressure drop across the test section are recorded.

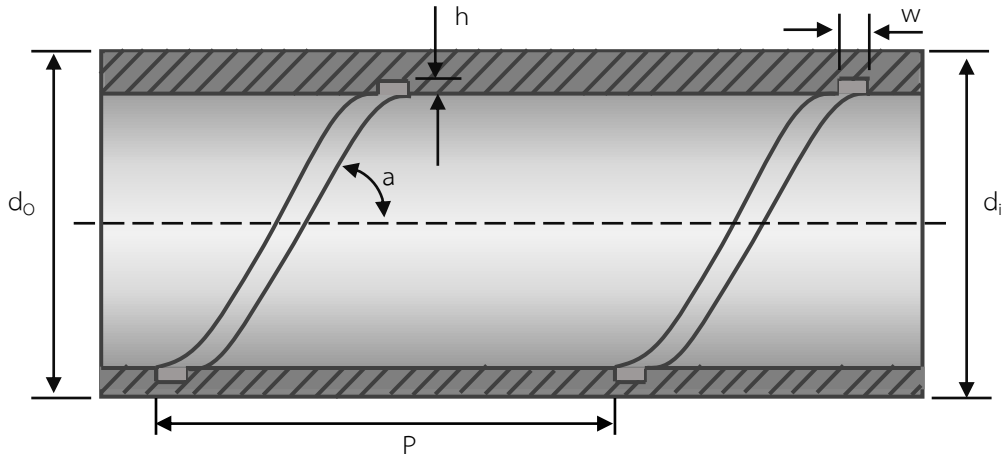

a) Internally grooved tube (IGT)

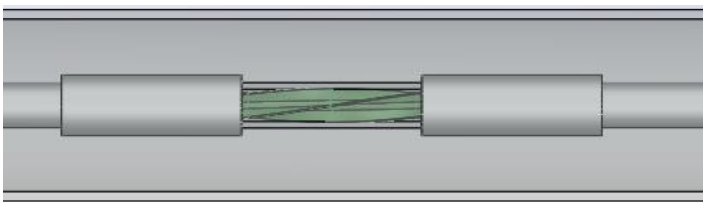

b) Swirl generator fitted in the outer and inner of the IGT (IGT+SG)

Fig. 3.2 Configuration of the enhanced tube and swirl generator used in the present study

Table 3.2 Important dimensions of IGT used in the present work

Dimension	**IGT**
d_o (mm)	9.53
d_i (mm)	7.1
h (mm)	0.2
N_S (Number of start)	10
P (mm)	305
w (mm)	0.2
α	5^o

3.3 Experimental Procedure

Experiments were conducted with various mass flow rates of working fluids and particle concentration whereas the temperature of nanofluid was kept constant at desired values. The working fluid flow rate (water, nanofluids and hot water) was adjusted using an inverter for controlling the speed of pump. The nanofluid temperature at the inlet of the test section was kept constant at a required value using the cooling coil controlled via temperature controller. Similarly, the heat load supplied to the test sections can be varied by adjusting the hot water temperature and hot water flow rate. During the test run, the system was allowed to approach the steady state before any data was recorded. After stabilization, inlet and exit temperatures of the nanofluids and hot water, wall temperatures, flow rates of nanofluid and hot water and pressure drop across the test section were recorded. The test runs were done at inlet temperatures of nanofluid at 25^{o}C and hot water temperature of 36 ^{o}C. The Reynolds number of nanofluids ranged between 6,000 and 18,000.

CHAPTER 4 DATA REDUCTION

The objective of this chapter is to explore the data reduction of the measured data. The data reduction to provide the heat transfer coefficient, Nusselt number, Reynolds number and pumping power of nanofluids flowing through enhanced tube equipped with swirl generator which is summarized as follows:

4.1 Calculation Methodology

In the present study, the heat transfer performance and flow characteristics of nanofluid flowing in enhanced tube fitted with freely rotating swirl generator are evaluated. Thus, the heat transfer rate, heat transfer coefficient and Nusselt number of nanofluids can be computed from the following equation.

The heat transfer rate into the nanofluid is expressed as:

$$Q_{nf} = \dot{m}_{nf} Cp_{nf} (T_{out} - T_{in})_{nf} \tag{4.1}$$

where Q_{nf} is the heat transfer rate of the nanofluid, $\dot{m}_{nf}$ is the mass flow rate of the nanofluid T_{in} and T_{out} are the temperature of the nanofluid at inlet and exit of the test section.

The heat transfer coefficient and the Nusselt numbers of the nanofluid can be calculated from the following equations.

$$h_{nf} = \frac{Q_{nf}}{A_S (T_S - T_{nf})} \tag{4.2}$$

$$Nu_{nf} = \frac{h_{nf} D}{k_{nf}} \tag{4.3}$$

where h_{nf} is the heat transfer coefficient of the nanofluid, T_S is the average wall temperature of the test section, T_{nf} is the bulk temperature of the nanofluid, Nu_{nf} is the Nusselt number of the nanofluid, D is the diameter of the test section and k_{nf} is the thermal conductivity of the nanofluid.

The Reynolds number is defined as:

$$\mathrm{Re} = \frac{\rho_{nf} u_m D}{\mu_{nf}} \tag{4.4}$$

where ρ_{nf} is the density of the nanofluid, u_m is the mean velocity of the nanofluid and μ_{nf} is the viscosity of the nanofluid.

Similarly to the heat transfer performance, the pumping power across the test sections is calculated from:

$$Pow = \dot{V}\Delta P \tag{4.5}$$

where Pow is the pumping power across the test sections block, ΔP is the measured pressure drop across the test section block, and $\dot{V}$ is the volume flow rate of the working fluid.

4.2 Thermophysical Properties of Nanofluid

The physical and thermal properties of nanofluid such as density, viscosity, specific heat and thermal conductivity presented in the above equations are calculated using the following equations:

The density and specific heat of the nanofluid are calculated according to Pak and Cho equation [44], which are expressed as follows:

$$\rho_{nf} = \phi\rho_p + (1-\phi)\rho_w \tag{4.6}$$

and

$$Cp_{nf} = \phi Cp_p + (1-\phi)Cp_w \tag{4.7}$$

where ϕ is the volume fraction of the nanoparticles, ρ_p is the density of the nanoparticles and ρ_w is the density of the base fluid, Cp_{nf} is the specific heat of the nanofluid, Cp_p is the specific heat of the nanoparticles and Cp_w is the specific heat of the base fluid.

For viscosity of the nanofluid, Drew and Passman [45] suggested the well-known Einstein's equation for calculating viscosity, which applicable to spherical particle in volume fractions less than 5.0 vol.% and is defined as follows:

$$\mu_{nf} = (1+2.5\phi)\mu_w \tag{4.8}$$

where μ_{nf} is the viscosity of the nanofluid and μ_w is the viscosity of the base fluid.

For thermal conductivity of the nanofluid, one well-known formula for calculating the thermal conductivity of nanofluid is the Hamilton and Crosser [46] model, which is expressed in the following form:

$$k_{nf} = \left[\frac{k_p + (n-1)k_w - (n-1)\phi(k_w - k_p)}{k_p + (n-1)k_w + \phi(k_w - k_p)}\right]k_w \tag{4.9}$$

$$n = 3/\psi \tag{4.10}$$

In which, n is the empirical shape factor and ψ is the sphericity, defined as the ratio of the surface area of a sphere (with the same volume as the given particle) to the surface area of the particle. The sphericity is 1 and 0.5 for the spherical and cylindrical shapes, respectively. Moreover, k_{nf} is the thermal conductivity of the nanofluid, k_p is the thermal conductivity of the nanoparticles and k_w is the thermal conductivity of the base fluid. For the case of pressure drop, the measured pressure drop of enhanced tube equipped with freely rotating swirl generator are compared with the common plain tube. Finally, the thermophysical properties of the nanofluid shown in the above equations are calculated from water and nanoparticles at average bulk temperature.

CHAPTER 5 RESULTS AND DISCUSSION

The objective of this chapter is to present the results and discussion of the heat transfer performance and friction characteristics of the SiO_2-water nanofluids flowing through common smooth tube (CST), internally grooved tube (IGT) and internally grooved tube fitted with five short-length swirl generators (IGT+SG). The results of the present study were expressed as follows:

5.1 Experimental system validation

Before starting to determine the convective heat transfer coefficient and friction factor of the nanofluid, the reliability and accuracy of the experimental system are estimated by using water as the working fluid and flows in common smooth tube (CST). The results of the experimental heat transfer coefficient and friction factors are compared with those obtained from the Dittus-Boelter equation [47] and Colebrook equation [48] which are defined as follows:

The Dittus-Boelter equation is defined as:

$$Nu = 0.023\mathrm{Re}^{0.8}\,\mathrm{Pr}^{0.4} \tag{5.1}$$

where Nu is the Nusselt number, Re is the Reynolds number, and Pr is the Prandtl number.

The Colebrook equation is defined as:

$$\frac{1}{\sqrt{f}} = -2.0\ell og\left(\frac{\varepsilon/d_i}{3.7} + \frac{2.51}{\mathrm{Re}\sqrt{f}}\right) \tag{5.2}$$

where ε is the roughness of the test tube.

As shown in Figures 5.1 and 5.2, an agreement between the experimental results and the calculated values for pure water can be seen.

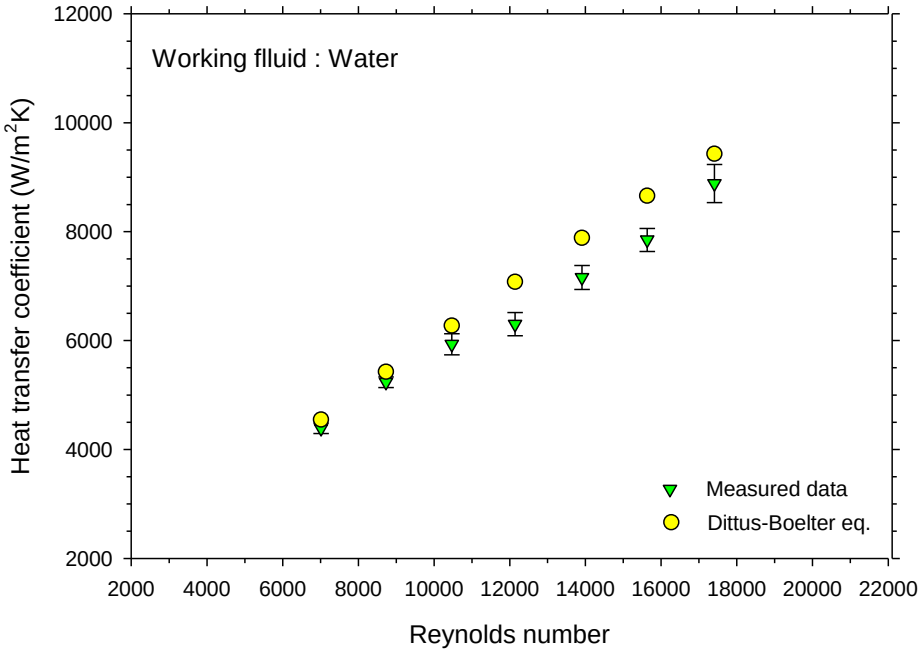

Fig. 5.1 Comparison between measured heat transfer coefficient and that calculated from Dittus-Boelter equation [47]

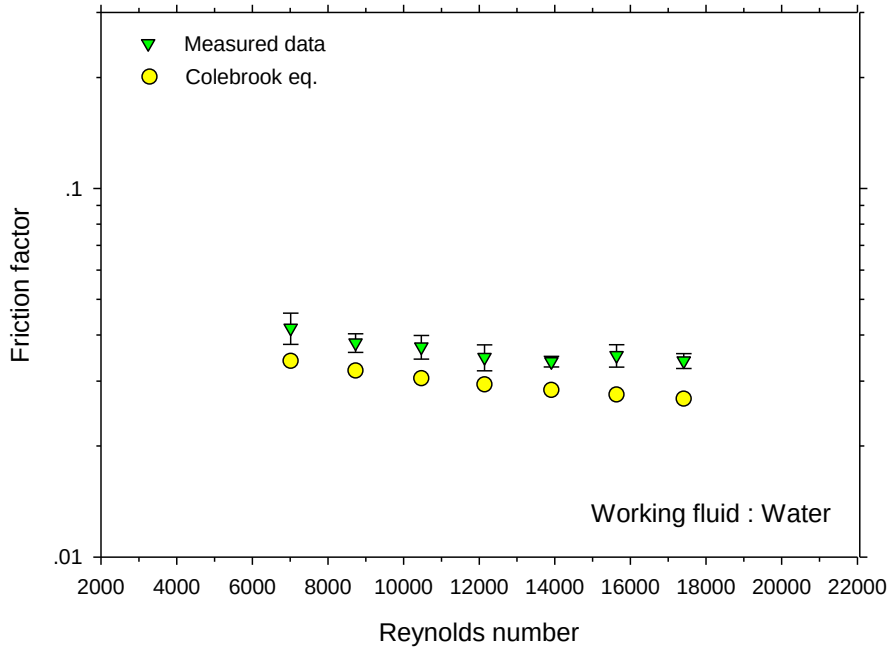

Fig. 5.2 Comparison between measured friction factor and that calculated from Colebrook equation [48]

5.2 Effect of the test section types on the heat transfer and pressure drop (data for water)

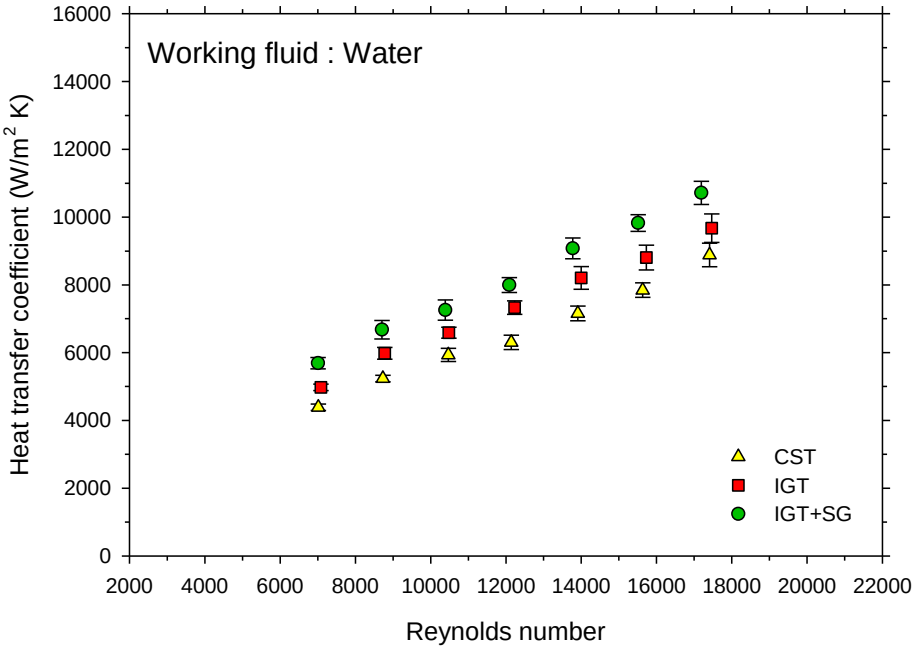

Fig. 5.3 Nusslet number as a function of the test section type as well as Reynolds number

Relationship between the heat transfer coefficient and Reynolds number in the common smooth tube (CST), enhanced tube (IGT) and the enhanced tube fitted with swirl generator (IGT+SG) was illustrated as shown in Fig. 5.3. For all case, it clearly seen that the heat transfer coefficient increased with increasing Reynolds number. Furthermore, it was also evidently seen that the heat transfer coefficient of the IGT+SG was significantly larger than that of the IGT and CST by about 11% and 23%, respectively. In general, for ICT, the internally grooved surface created the mixing of fluid and tend to decrease the thermal boundary layer thickness near the groove surface which lead to increase the heat transfer performance compared to the CST. In addition, in the present work, six short-length tabulator swirl generators with freely rotating were located inside the IGT called “IGT+SG” was also conducted. When the fluid flows past

the SG_S, the swirling flow after the SG_S were created which lead to increase the mixing of the fluid near the tube wall. As a results, superior heat transfer performance was obtained compared to the common IGT and CST. The heat transfer enhancement ratio between IGT and IGT+SG compare with the CST was plotted as shown in Fig. 5.4. For the case of IGT, the heat transfer coefficient was average 12% higher than that of the CST. For IGT+SG, average 23% higher than CST was observed.

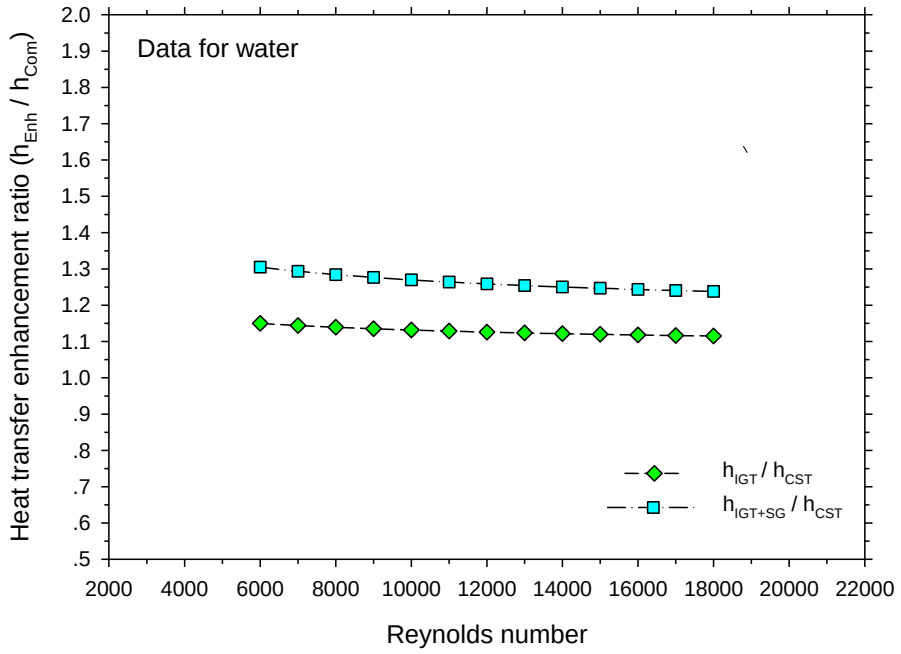

Fig. 5.4 Enhancement ratio versus Reynolds number at various test sections

Variation of the pressure drop across the test section with Reynolds number in CST, IGT and IGT+SG was described in Fig. 5.5. From the results, it was found that the pressure drop increases as Reynolds number increased. Compared with the CST, the pressure drops of for IGT were higher than those of the CST by about 9.93%. It was due to the fact that the grooved surface on the tube wall generate high swirling flow which resulted to produce more flow disturbance. As a sequence, higher pressure drop was obtained. For the case of IGT+SG, although the heat transfer performance of the

IGT+SG was significantly higher than that of the common IGT and CST, however, much more pressure drops were also observed. The pressure drops across the IGT+SG tube were about 2.8 times higher than the common IGT and 2.9 times for CST. It was caused from the fact that six pieces of swirl generator fitted inside the IGT would be strongly interrupt and resist the fluid flow which lead to significantly increase in the pressure drop. Thus, considering the use of the IGT+SG for heat transfer enhancement should be carefully take into account the effect of the pressure drop penalty due to much more pumping power was required.

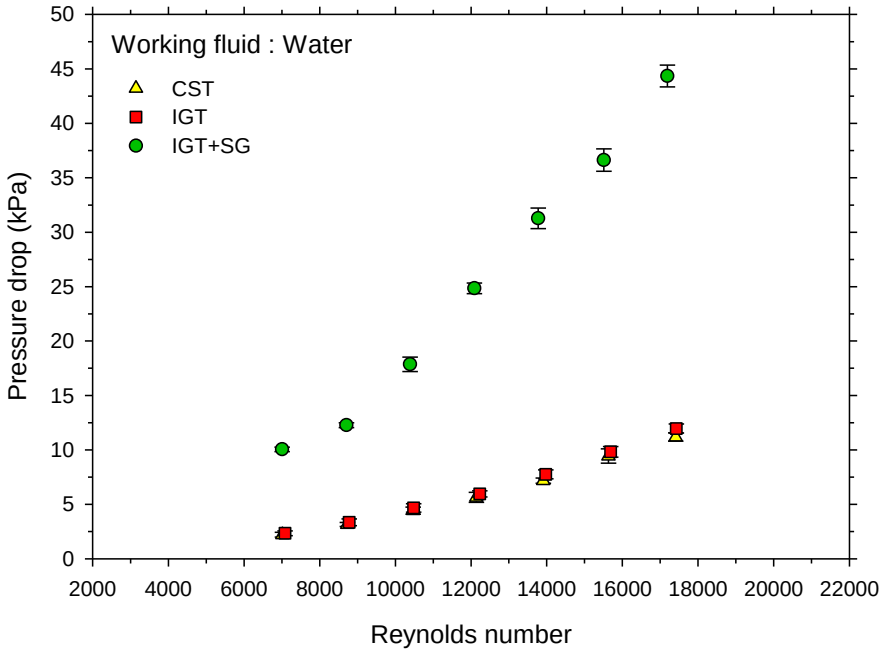

Fig. 5.5 Pressure drop as a function of test section type and Reynolds number

Fig. 5.6 shows the pressure drop ratio as a function of Reynolds number for IGT and IGT+SG. The term of pressure drop ratio means the ratio of the pressure drop between the enhanced tube and the common smooth tube ($\Delta P_{Enh} / \Delta P_{com}$). It clearly seen that the pressure drop ratio of the IGT+SG was significantly larger than that of the IGT approximately 3 times. This resulted in the much more pumping power was needed.

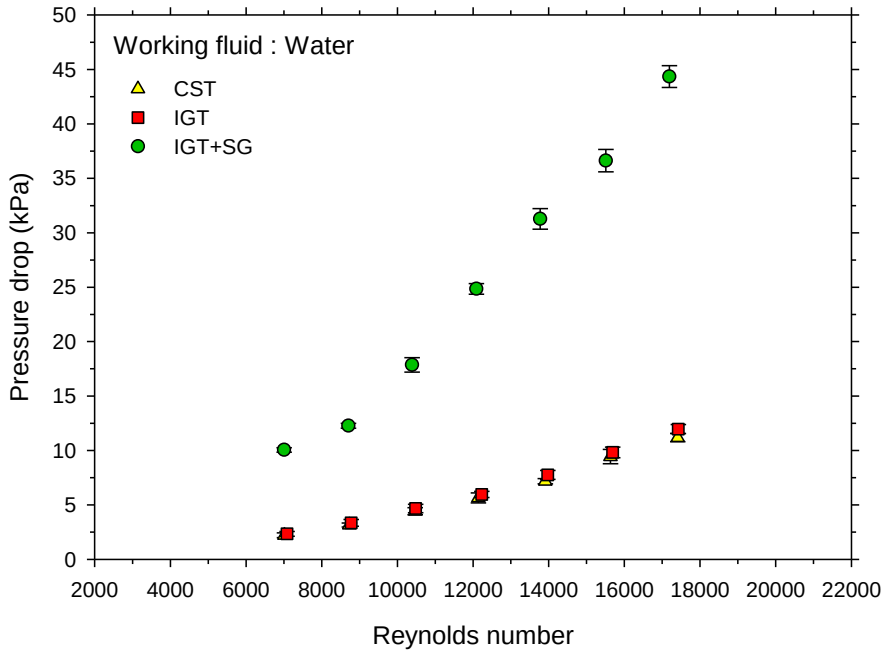

Fig. 5.6 Variation of pressure drop ratio with Reynolds number.

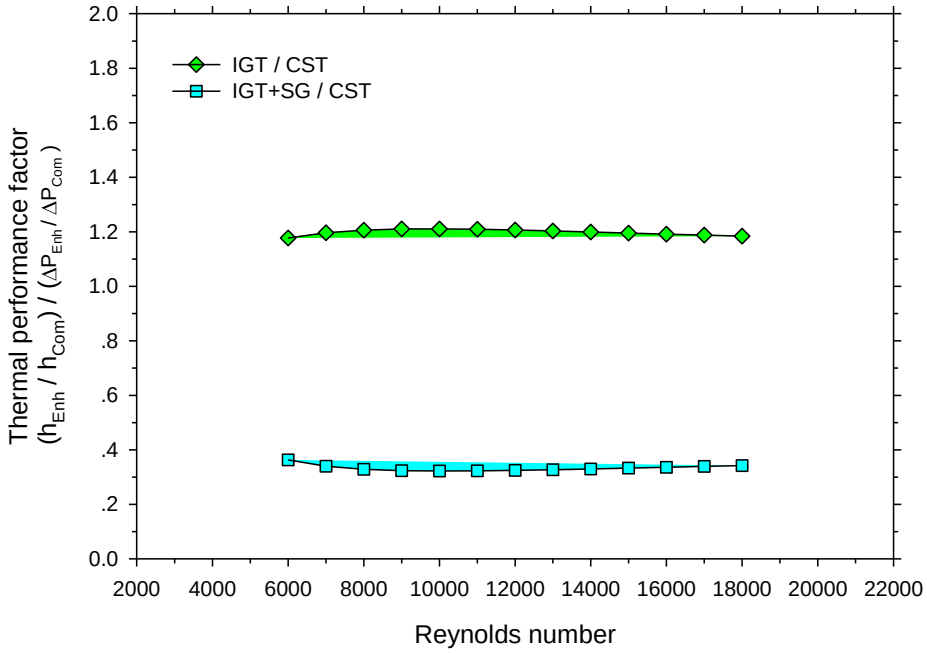

Fig. 5.7 Comparison of the thermal performance factor between common IGT and IGT+SG at various Reynolds number.

To consider the use of some heat transfer enhancement techniques to replace the regular techniques, the term of the thermal performance factor was considered. The term refers

to the ratio of the heat transfer enhancement ratio to the pressure drop ratio. For the present study, the thermal enhancement factors of enhancement techniques such as IGT and IGT+SG were plotted against the Reynolds number as shown in Fig. 5.7. It clearly seen that, for the case of IGT+SG, the thermal performance factor was only around 0.3. This means that the pressure drop ratio was strongly higher than the heat transfer enhancement ratio. It was disadvantaged because the effect of the pressure drop ratio was overcome the enhancement ratio. For the case of IGT, the thermal performance factor was around 1. This behavior indicate that IGT is much more suitable to use for heat transfer enhancement than the IGT+SG. The penalty in the pressure drop can be compensated by increasing of the heat transfer enhancement.

5.3 Effect of particle concentrations of nanofluid on the heat transfer performance and pressure drop of IGT and IGT+SG

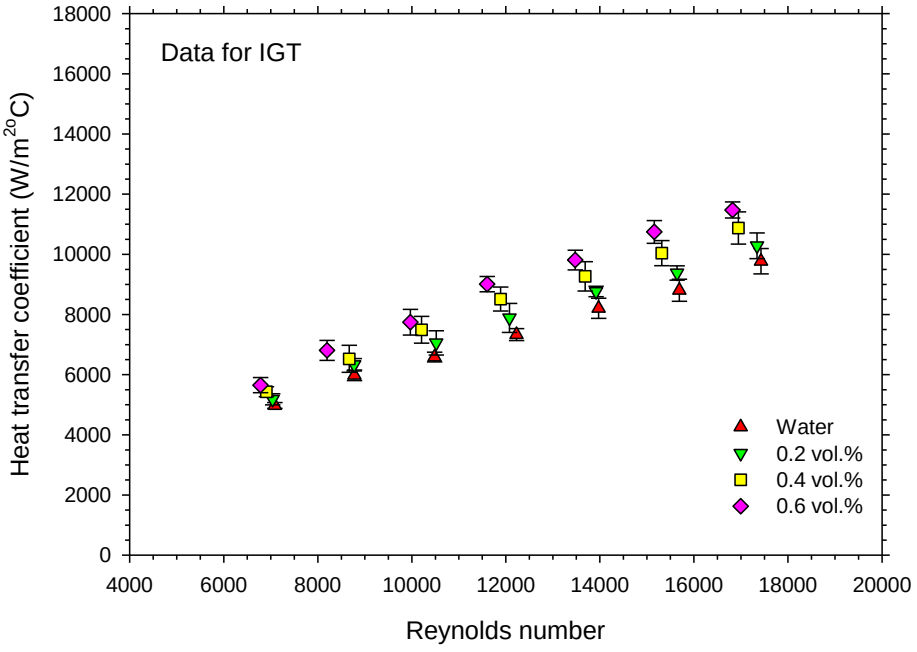

a) data for IGT

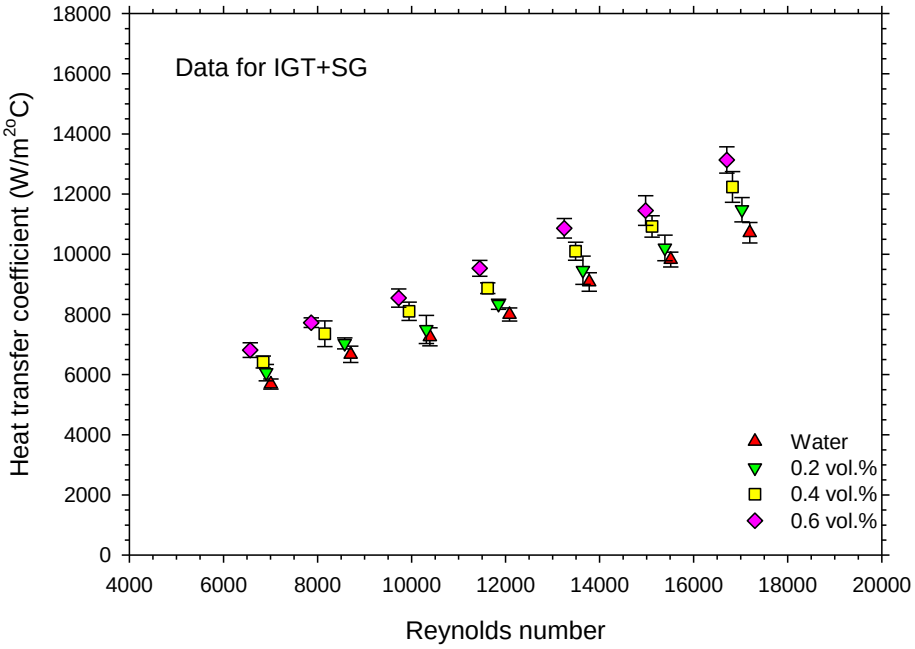

b) data for IGT+SG

Fig. 5.8 Heat transfer coefficient versus Reynolds number as well as particle concentration

As shown in Fig. 5.8(a, b), for both IGT and IGT+SG, the heat transfer performance of the nanofluids are higher than those of the water, and they increase with increasing the Reynolds number as well as the particle volume concentration. The possible reason for this enhancement may be associated with the following: 1) the nanofluid with suspended nanoparticles increases the thermal conductivity of the mixture and 2) a large energy exchange process resulting from the chaotic movement of nanoparticles. Similarly, the enhancement ratio of nanofluids for IGT and IGT+SG are plotted as shown in Fig. 5.9 (a, b). It clearly seen that the enhancement ratio increased with increasing particle concentration. For both IGT and IGT+SG, the enhancement ratio ranged between 5 and 14% for particle loading between 0.2 and 0.6 vol.%. This means

that the nanofluid had higher potential to use as working fluid for heat transfer application compared to conventional base fluid.

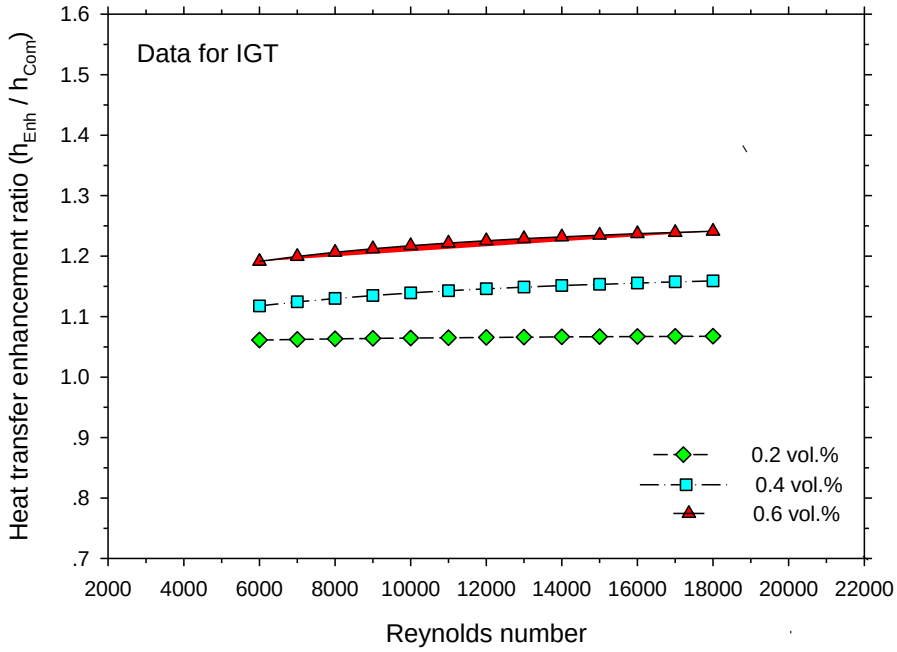

a) data for IGT

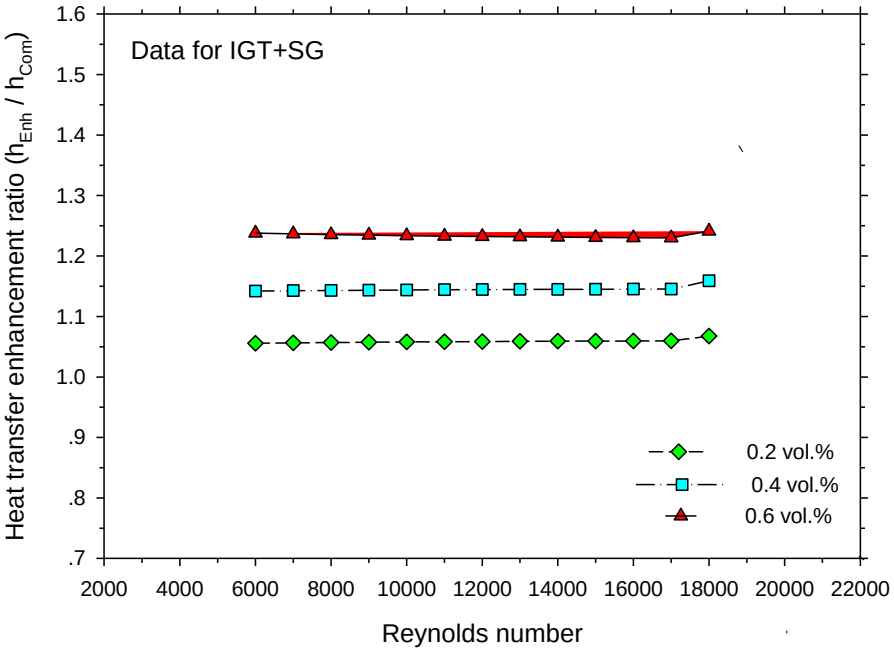

b) data for IGT+SG

Fig. 5.9 Heat transfer enhancement ratio versus Reynolds number as well as particle concentration

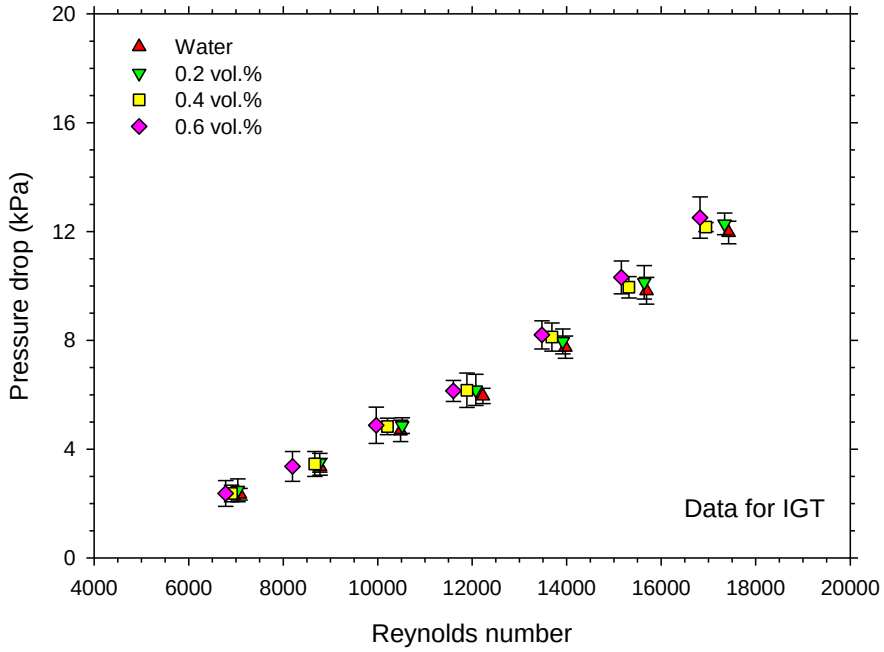

a) data for IGT

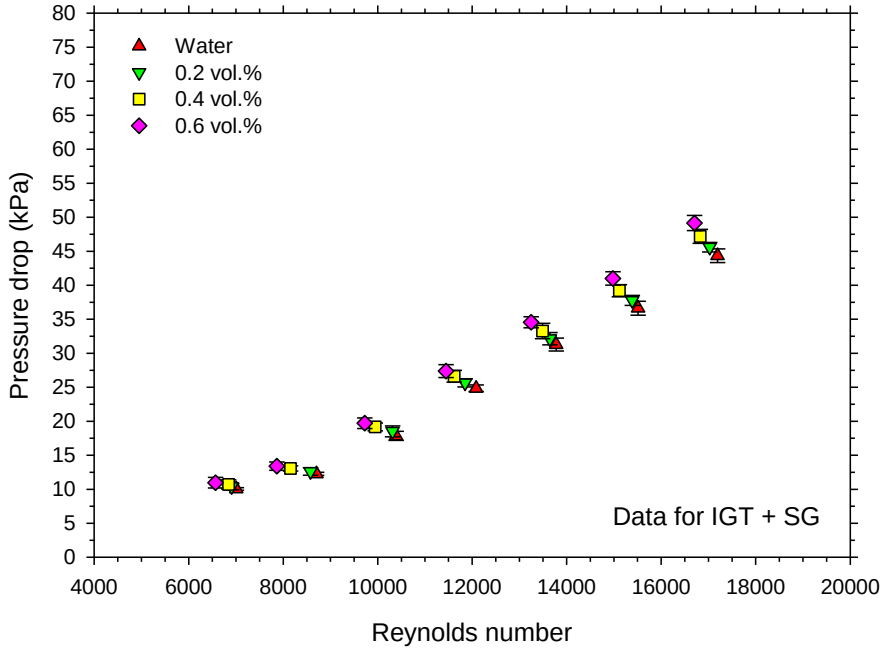

b) data for IGT+SG

Fig. 5.10 Variation of the pressure drop with Reynolds number and particle concentration

As shown in Fig. 5.10, the measured data show that the pressure drop of the nanofluids across the test sections (IGT and IGT+SG) increased with increasing Reynolds number and that there is a small increase with increasing particle concentrations. This means

that using the nanofluids at higher particle volume fraction create a tiny penalty in pressure drop.

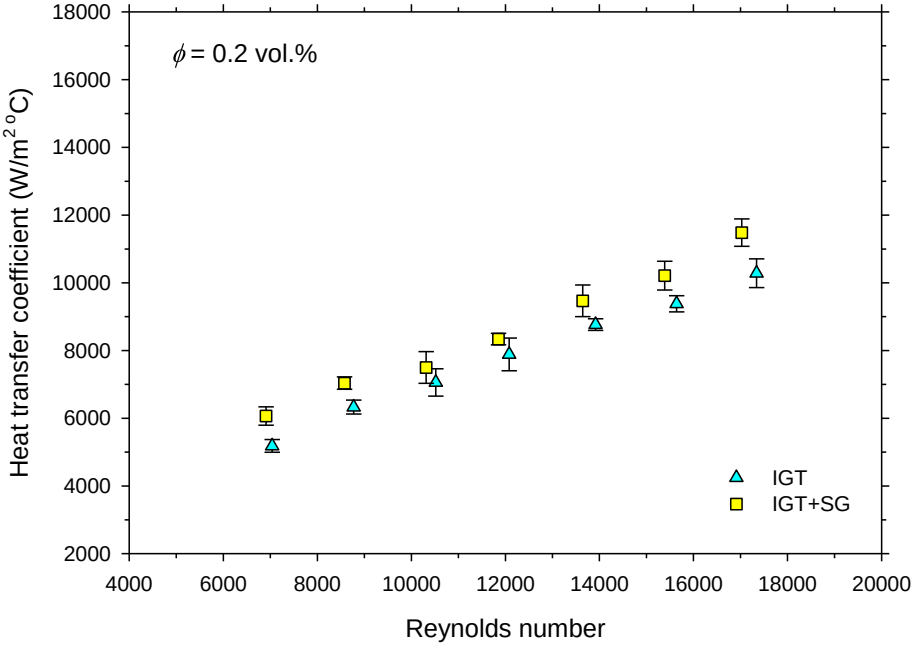

Fig. 5.11 Comparison of the heat transfer coefficient between IGT and IGT+SG at particle concentration of 0.2 vol.%

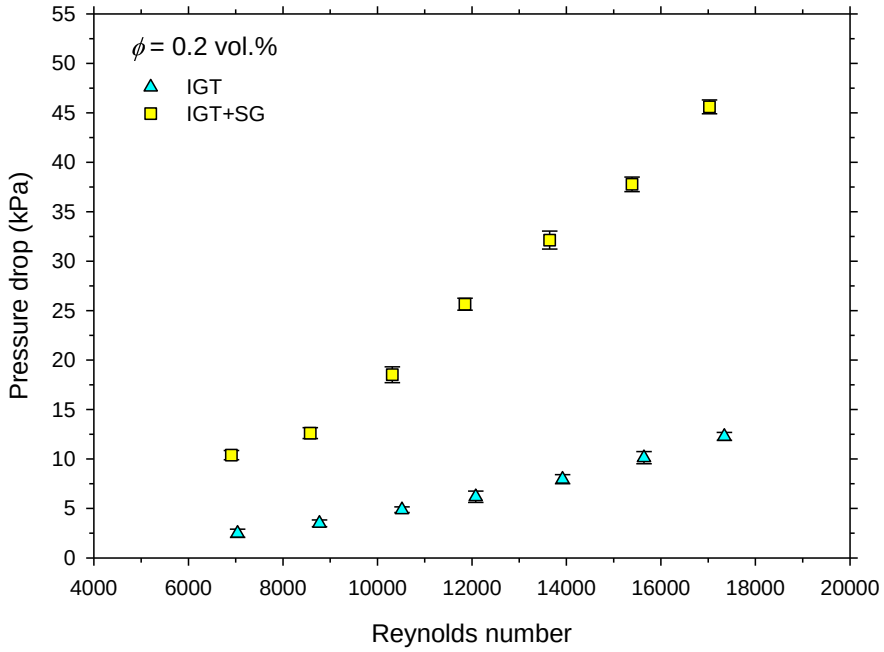

Fig. 5.12 Comparison of the pressure drop between IGT and IGT+SG at particle concentration of 0.2 vol.%

As shown in Fig. 5.11, at particle concentration of 0.2 vol.%, the heat transfer performances of IGT+SG are greater than that those of the IGT average 8%. The results for this enhancement are described in the above-mentioned. However, as shown in Fig. 5.12, for pressure drop, the measured data indicated that the pressure drop across the IGT+SG are greatly higher than the common IGT for several times. This is because the swirl generators fitted inside the grooved tube obstruct and resist the fluid flow which lead to significantly increase in the pressure drop. Moreover, similar tendencies are also observed for the particle concentrations of 0.4 and 0.6 vol.%. Thus, without considering pressure drop, IGT+SG may a suitable case for only heat transfer enhancement due to dramatically pressure drops are created.

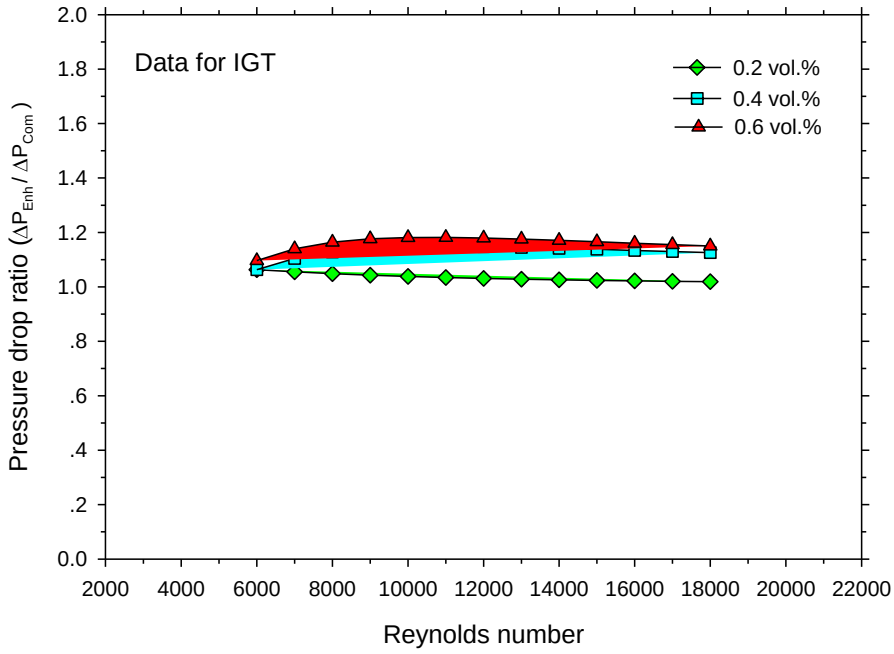

Fig. 5.13 Thermal performance factor versus Reynolds number and particle concentration (data for IGT)

Fig. 5.13 shows the thermal performance factor of IGT as a function of particle concentration. The results indicated that the thermal performance of IGT with particle concentration of 0.2 vol.% was higher than that of the remaining cases. This means that,

for this case, higher heat transfer performance and less penalty in pressure drop were obtained.

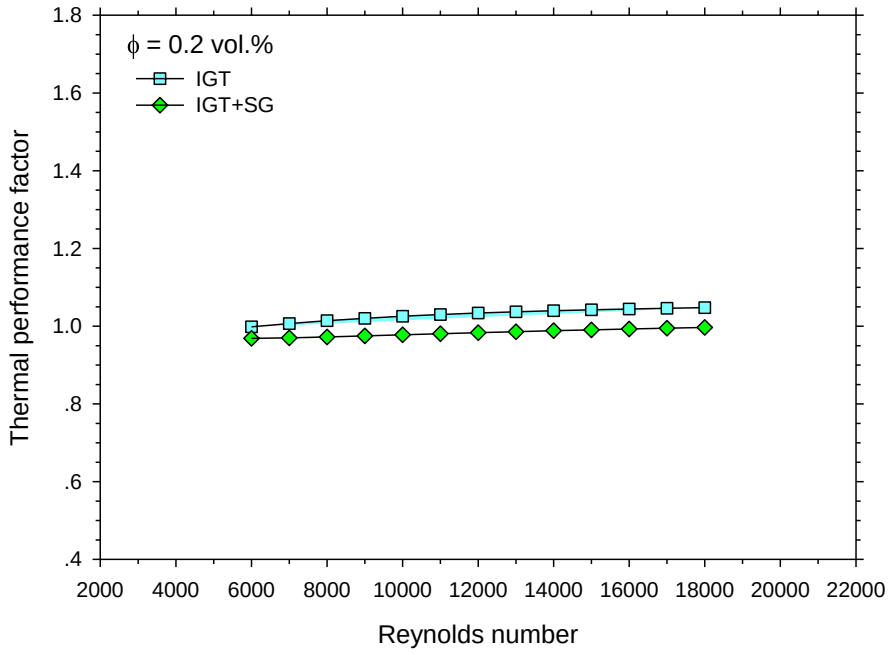

Fig. 5.14 Comparison of the thermal performance factor between IGT and IGT+SG at particle concentration of 0.2 vol.%

Comparison of the thermal performance factor between IGT and IGT+SG at particle fraction of 0.2 vol.%. Although the IGT+SG shows higher heat transfer performance than that of the common IGT, but pressure drop increases dramatically in the same time. Thus, lower thermal performance factors are obtained.

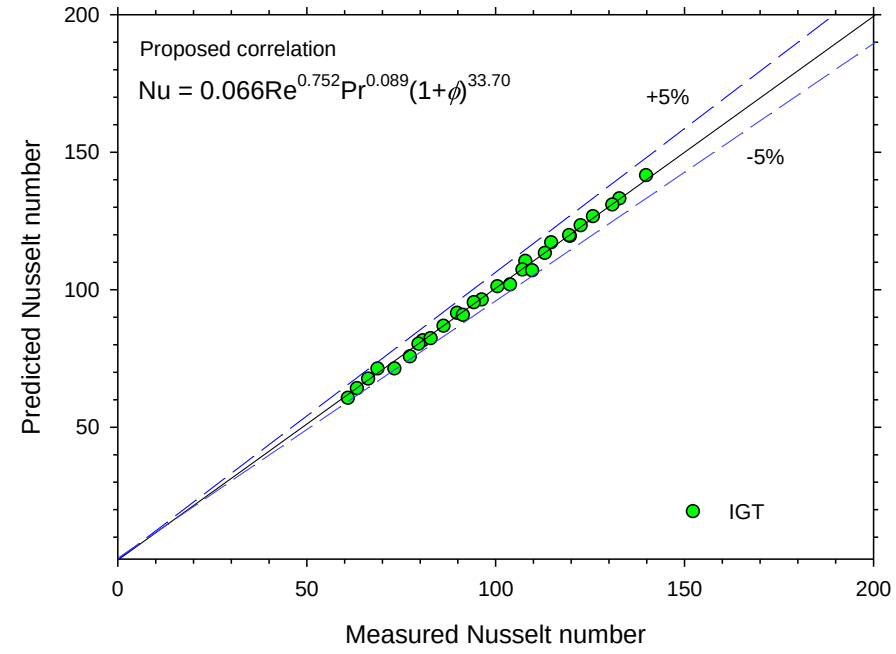

a) IGT

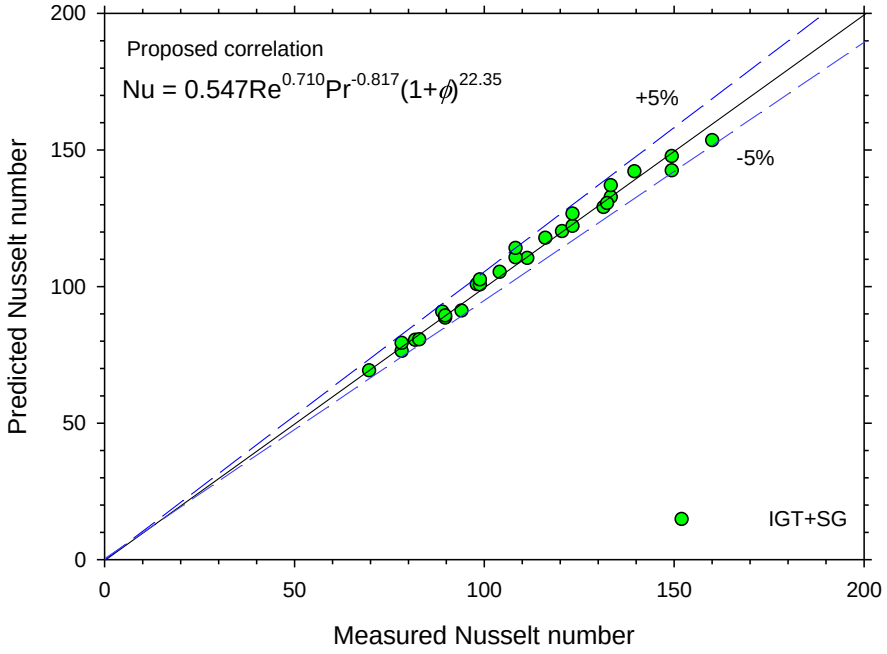

b) IGT+SG

Fig. 5.15 Predicted Nusselt number versus experimental Nusselt number.

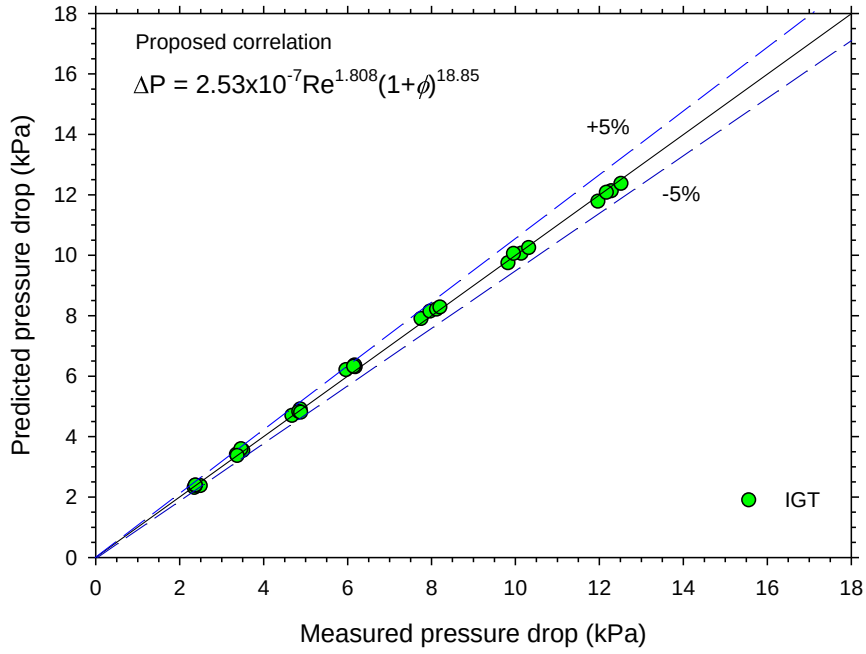

a) IGT

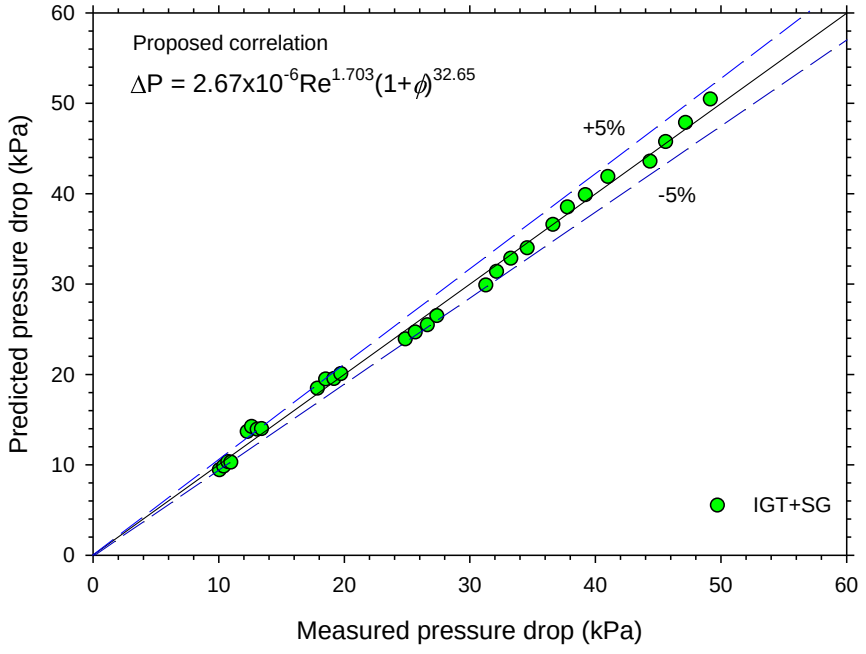

b) IGT+SG

Fig. 5.16 Comparison of the predicted pressure drop and the measured pressure drop.

Finally, the measured data for heat transfer performance are used to establish new heat transfer correlations for predicting the Nusselt number of the nanofluids flowing through common IGT and IGT fitted with freely rotating swirl generators, IGT+SG. The detail of this concern is expressed as follows:

In general, for nanofluids, Nusselt number may be related with the parameters as follows:

$$Nu = f(\mathrm{Re}, \mathrm{Pr}, \phi) \tag{5.3}$$

Considering the above mentioned the equations for predicting the heat transfer performance of nanofluid flowing through IGT and IGT+SG are formed and proposed in the following form:

For IGT:

$$Nu = 0.066\,\mathrm{Re}^{0.752}\,\mathrm{Pr}^{0.089}(1+\phi)^{33.70} \tag{5.4}$$

For IGT+SG:

$$Nu = 0.547\,\mathrm{Re}^{0.710}\,\mathrm{Pr}^{-0.817}(1+\phi)^{22.35} \tag{5.5}$$

The above equations are obtained by curve fitting all the experimental data for the SiO_2-water nanofluids flowing through IGT and IGT+SG. Comparisons of the experimental data with those calculated by the proposed correlations are shown in Fig. 5.15 (a, b). The results show good correspondence between the experimental values and the calculated values by the above equation. It is clearly seen that the majority of the data falls within ± 5% of the proposed equation for both IGT and IGT+SG. The authors would like to introduce that the above equations can be used for predicting the Nusselt number of nanofluids flow in IGT and IGT+SG, particle volume concentration less than 0.6% and Reynolds number range between 6,000 and 18,000.

Similar to the Nusselt number correlation, new correlations which are easy to use for calculating the pressure drop of nanofluids flow through IGT and IGT+SG are proposed in the following form:

For IGT:

$$\Delta P = 2.53x10^{-7}\,\mathrm{Re}^{1.808}(1+\phi)^{18.85} \tag{5.6}$$

For IGT+SG:

$$\Delta P = 2.53x10^{-7}\,\mathrm{Re}^{1.808}(1+\phi)^{18.85} \tag{5.7}$$

As shown in Fig. 5.16 (a, b), the results show that the present correlations gave reasonably good agreement with the experimental data. The majority of the data falls within ± 5% of the proposed equation. The limitations of the above equation are the same as that of the Nusselt number equations.

5.4 Effect of swirl flow on the heat transfer enhancement of microchannel heat sinks

In addition, employing the potential of the swirl flow and nanofluids to enhance the thermal performance can be applied for the case of microchannel heat sinks ($MCHS_s$) in order to remove high heat load. $MCHS_S$ with continuous zigzag flow channel (CZ-HS), and the single cross-cutting zigzag flow channel (CCZ-HS) are used to evaluate the effect of the swirling flow due to cross-cutting of the zigzag flow channel on the thermal performance. The configuration and important dimensions of the CZ-HS and CCZ-HS are depicted in Fig. 5.17 and Table 5.1, respectively. The results are presented as follows:

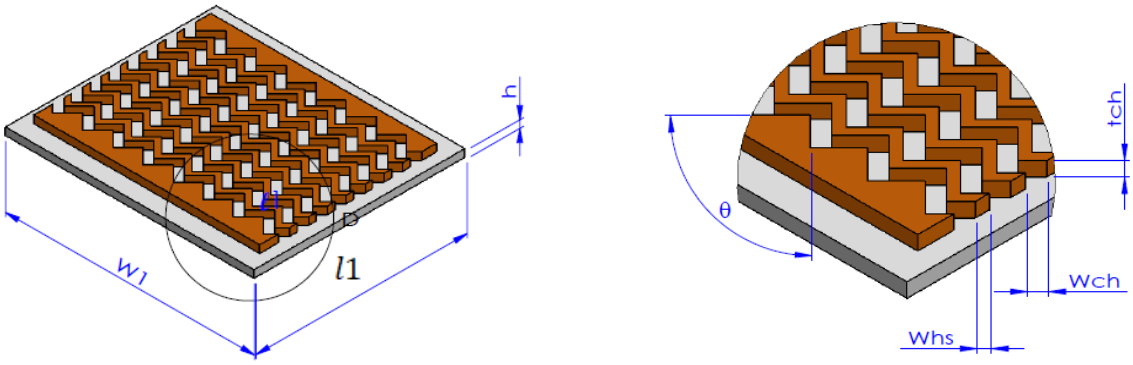

a) CZ-HS

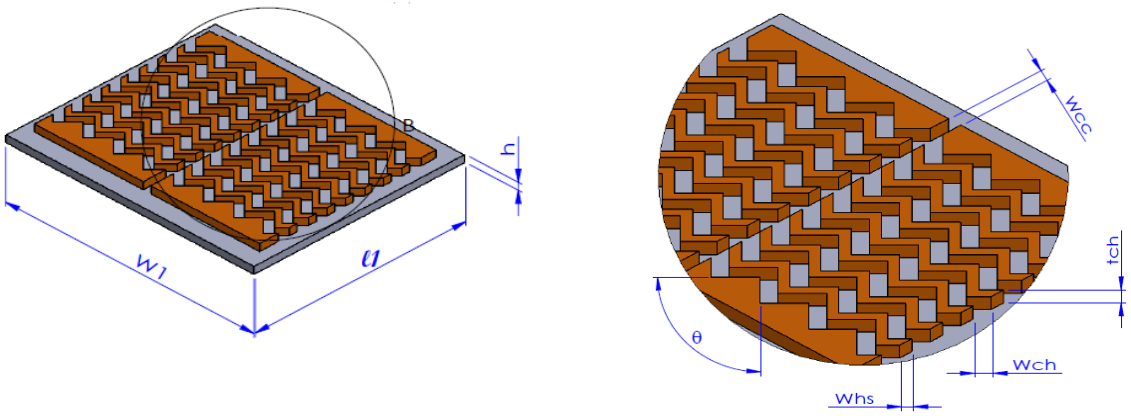

b) CCZ-HS

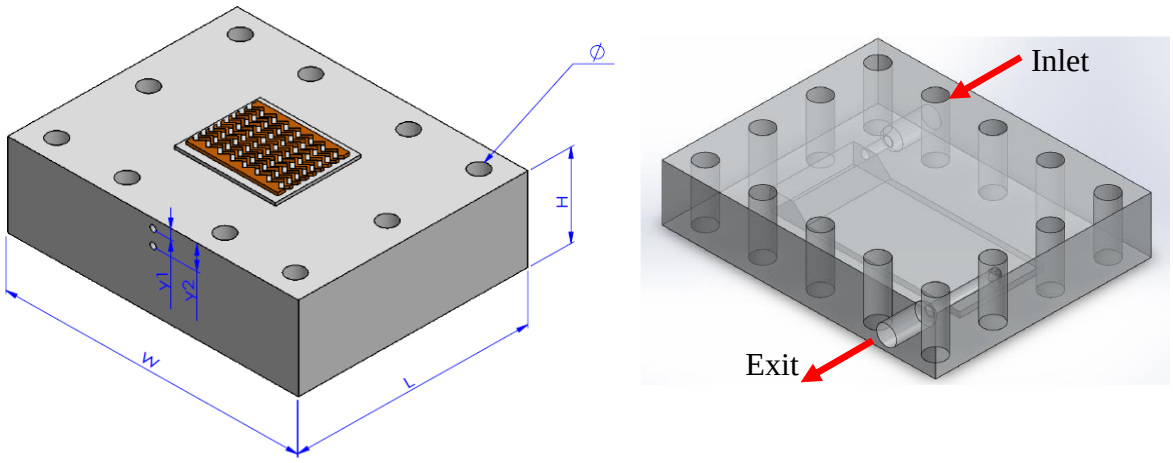

c) Base and cover plate of heat sink

Fig. 5.17 Configuration of the $MCHS_S$ used in the present study.

Table 5.1 Important dimensions of the zigzag flow channel heat sinks used in the present study

Parameter	**CZ-HS**	**CCZ-HS**
W(mm)	95	95
L(mm)	75	75
H(mm)	28	28
W_{ch}(mm)	1	1
t_{ch}(mm)	1	1
W_{hs}(mm)	1	1
W_1(mm)	33	33
l_1(mm)	28	28
h(mm)	1	1
θ (degree)	90^o	90^o
y_1 (mm)	5	5
y_2 (mm)	15	15
w_{cc} (mm)	-	1
$A_{HS}(mm^2)$	1,176	1,238
∅ (mm)	M6x1	M6x1

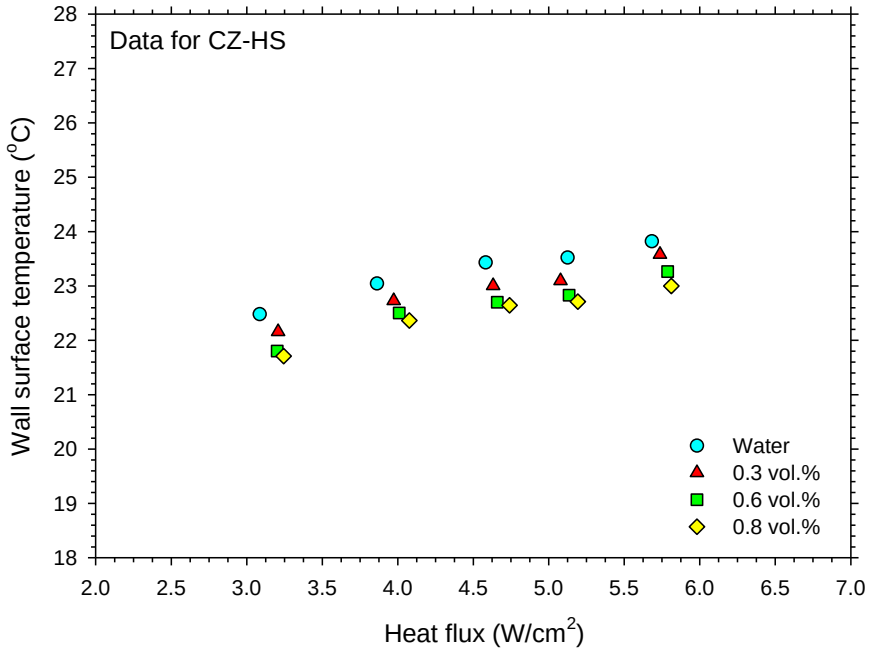

a) data for CZ-HS

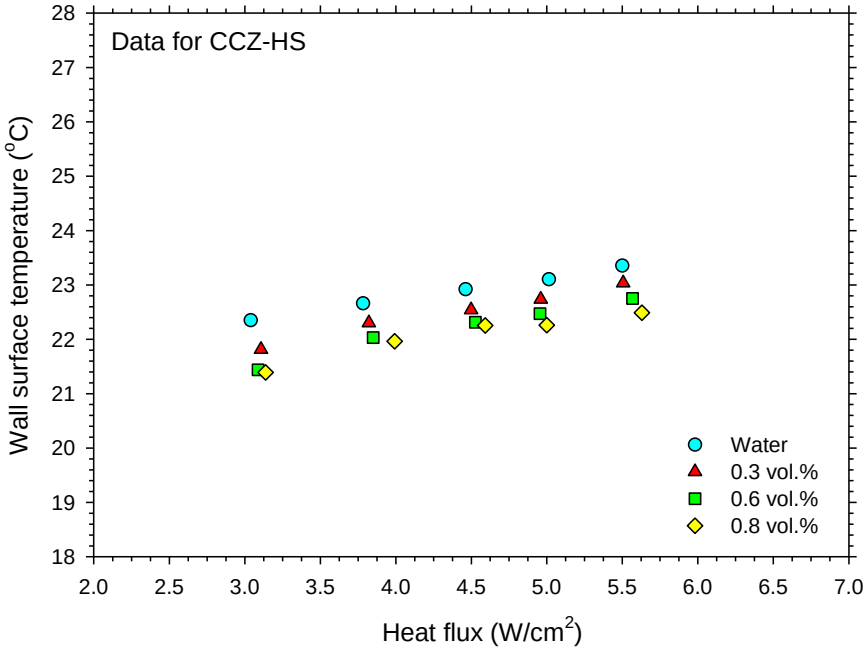

b) data for CCZ-HS

Fig. 5.18 Wall surface temperature versus wall heat flux for various particle concentrations.

Variation of the surface temperature with heat flux as a function of particle concentration is presented in Fig. 5.18. It clearly seen that the surface temperatures of the heat sinks increased with increases in the wall heat flux. Likewise, the surface temperature of MCHS decreases with increasing particle concentration, which means that the nanofluid-cooled heat sink provided better thermal performance than the water-cooled heat sink. This is due to the fact that the nanoparticles suspended in the water enhance the thermal conductivity of the bulk fluid. As a result, a higher heat dissipation rate is obtained, which provides better capability of the system. Moreover, comparing the CZ-HS and CCZ-HS, the experimental data indicate that the surface temperature of CCZ-HS is lower than that of the CZ-HS. This may be due to the effect of the single cross-cutting of the flow channel at the middle plan of CCZ-HS creating a high-intensity disturbance of the fluid flow compared to the CZ-HS, where the fluid flows

continuously through each flow channel. Thus, a lower surface temperature for CCZ-HS is achieved.

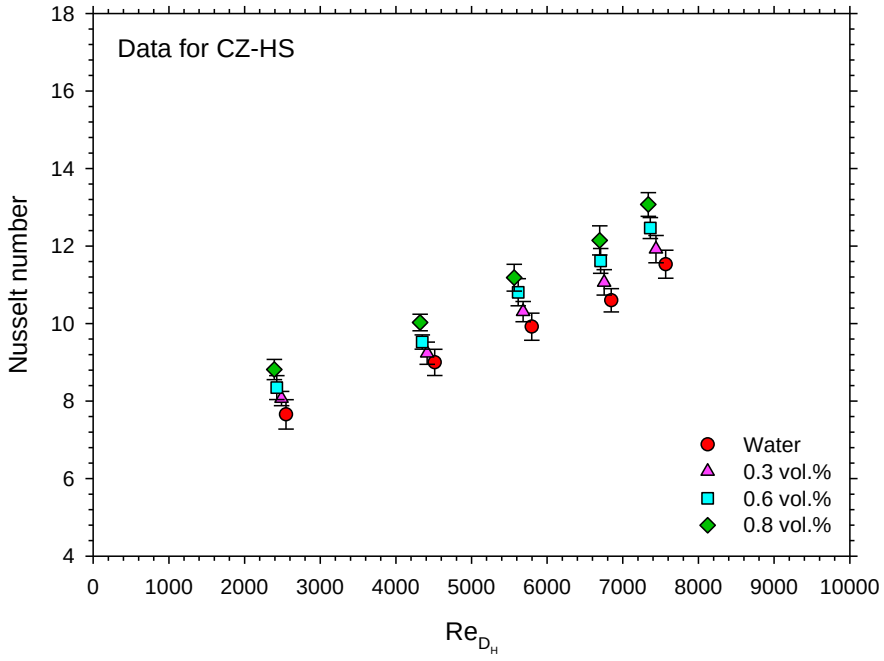

a) data for CZ-HS

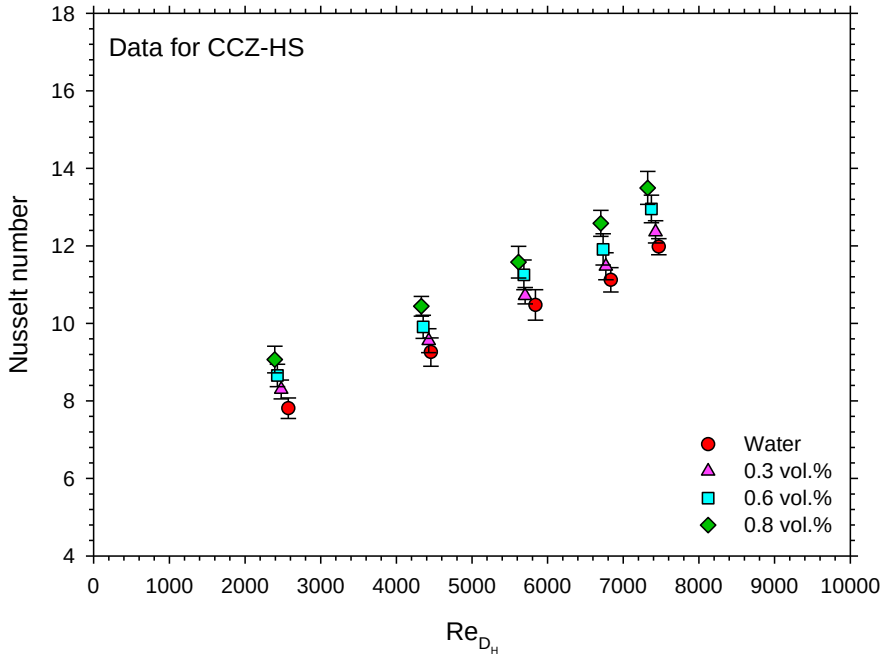

b) data for CCZ-HS

Fig. 5.19 Variation in the Nusselt number and Reynolds number as a function of particle concentrations.

Variations of the measured Nusselt number of CZ-HS and CCZ-HS with the particle concentration and the Reynolds number are shown in Fig. 5.19. The experimental results indicate that the measured Nusselt number increases as the particle concentration and Reynolds number increase. The results also show that the Nusselt number of the nanofluid- cooled heat sink is greater than the case of the water-cooled heat sink by approximately 3–15% with a particle loading ranging between 0.3 and 0.8 vol.%. Furthermore, when comparing CZ-HS and CCZ-HS, it is clear that the thermal performance of CCZ-HS is better than CZ-HS by an average of approximately 2–6%, as shown in Fig. 5.20. this may be due to the fact that for CCZ-HS, single cross-cutting of the flow channel results in dividing the flow area into two regions. When the fluid flows past the first region, direct impingement of the fluid stream to the channel wall of the next region occurs. As a consequence, higher turbulent intensity is attained, resulting in augmentation of the heat-transfer performance.

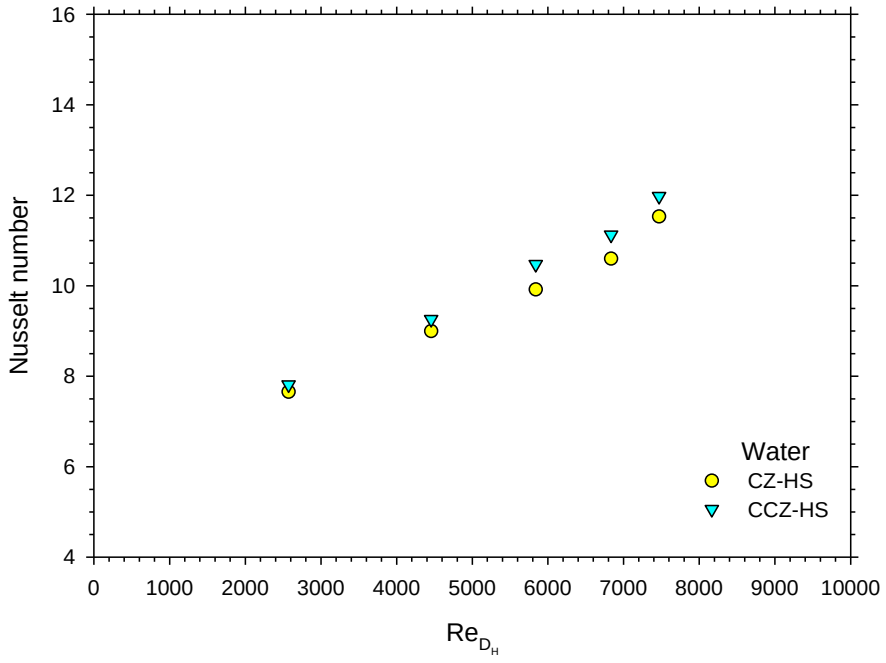

a) data for water

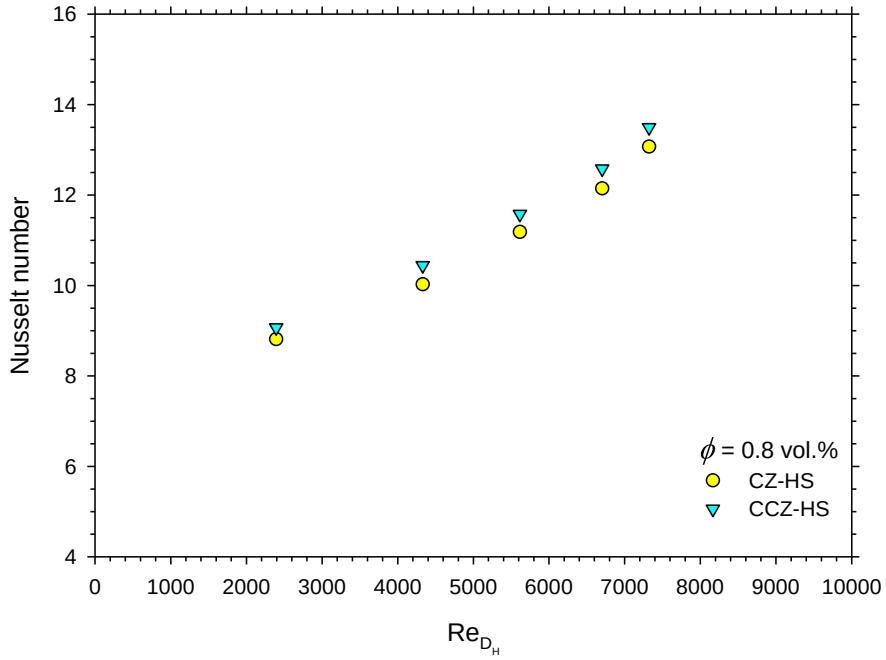

b) data for particle concentration of 0.8 vol.%

Fig. 5.20 Effect of the single cross-cut flow channel on the Nusselt number of the water and nanofluid.

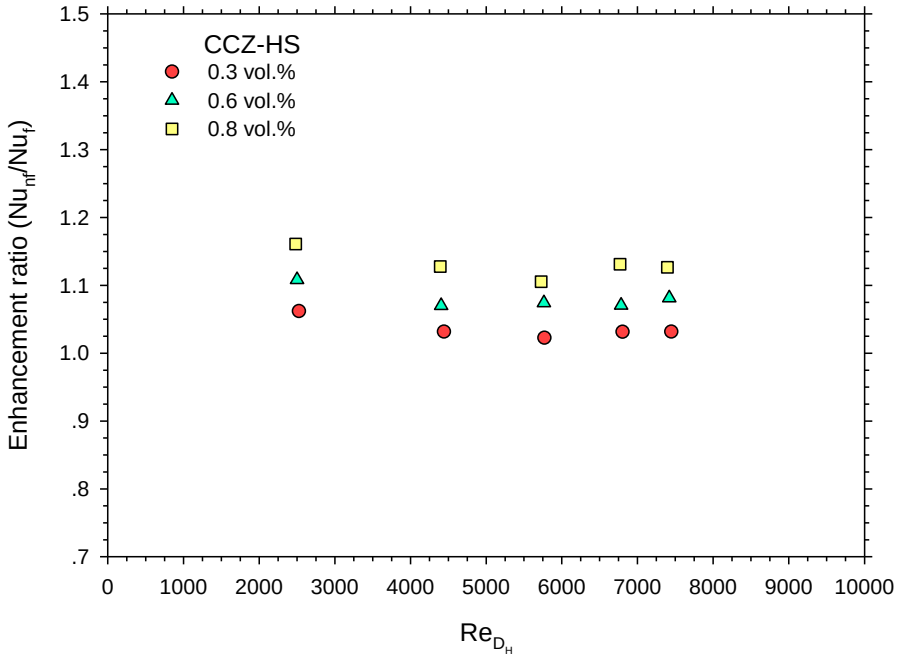

Fig. 5.21 Heat transfer enhancement ratio versus Reynolds number at various particle concentrations.

The enhancement ratio (Nu_{nf}/Nu_w) versus Reynolds number based on hydraulic diameter of the flow channel is illustrated in Fig. 5.21. As described above, the heat sink with the nanofluid-cooled system has a higher thermal performance than the heat sink with the water-cooled system by approximately 3–15% at a particle fraction ranging between 0.3 and 0.8 vol.%. This confirms that the application of nanofluids as a coolant instead of water will enhance the thermal dissipation rate of the system, leading to improvement of the working performance of the heat-transfer equipment.

Figs. 5.22 (a) and (b) show comparison between the experimental data and the calculations, for Nusselt number and pressure drop, respectively. For Nusselt number, the results indicate that the predicted values obtained from the Duangthongsuk and Wongwises equation [49] are much higher than those of the measured data. This is because this equation is established by using the data obtained from the heat sink with pin fin structure which typically gives higher thermal performance than the heat sink with simple flow channel, under the same Reynolds number. Thus, much more heat transfer performance is obtained. However, for the pressure drop, the results show good agreement between the measured values and the calculated values by Duangthongsuk and Wongwises equation. This is because pressure drop across the test section normally depends on the configuration and dimension of the inlet and exit of the test sections, similar to the shape of the flow channel. As a result, an agreement between measured data and the calculated values is observed.

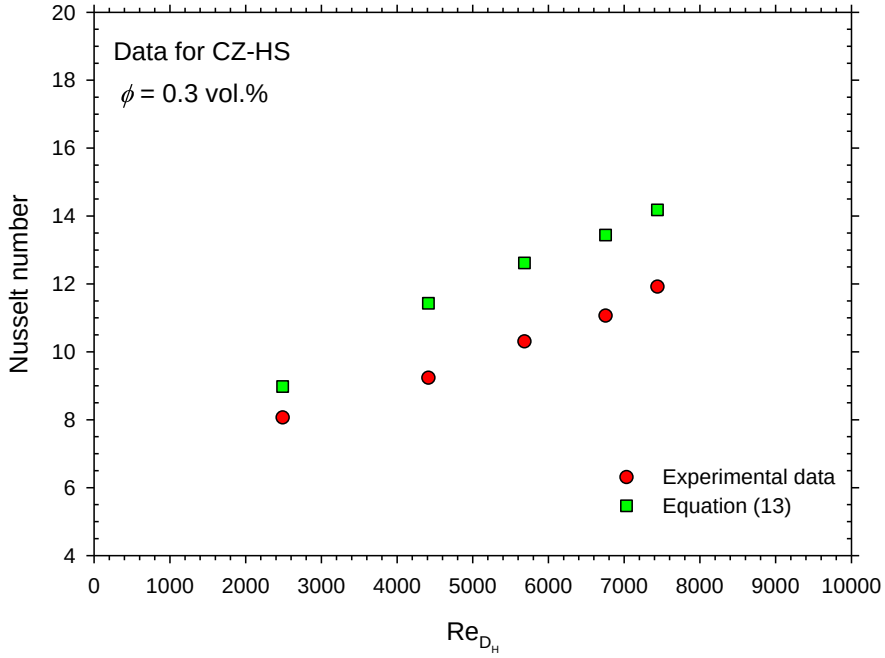

a) Nusselt number

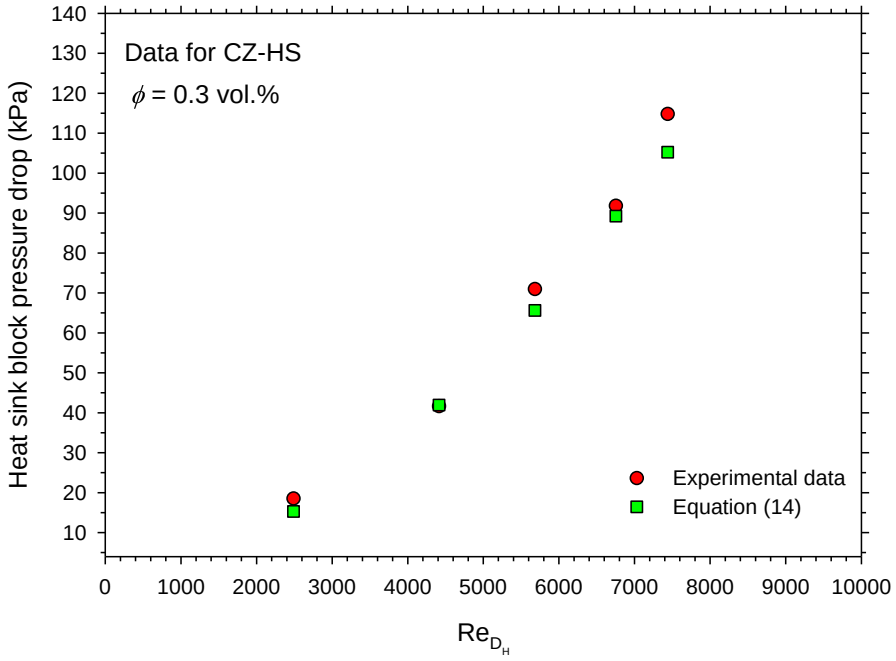

b) Pressure drop

Fig. 5.22 Comparison of the Nusselt number and pressure drop obtained from the experiment and the calulation.

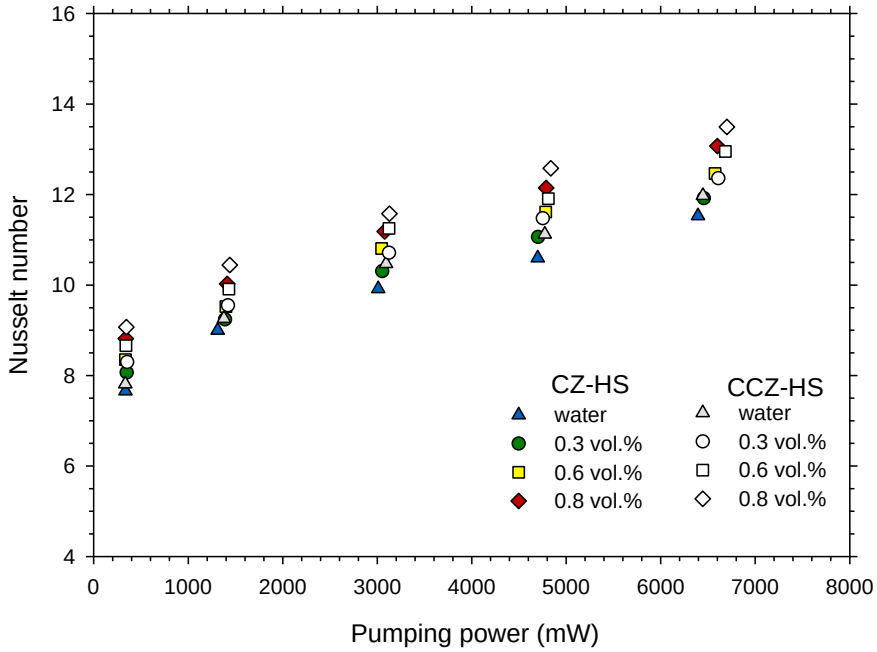

Fig. 5.23 Variation of the Nusselt number and pumping power as a function of particle concentration and heat sink type.

Comparison of the measured Nusselt number for CZ-HS and CCZ-HS as a function of the pumping power at different particle volume fractions is shown in Fig. 5.23. As shown in this figure, at a given pumping power, the Nusselt number of the CCZ-HS is greater than that of the CZ-HS and increases as particle concentration increases. This means that the use of a nanofluid-cooling system provides higher heat-transfer performance than the water-cooling system at a given pumping power. The reasons for the enhancement are described in the above paragraph. Moreover, this observation is consistent with Kim and Kim's [50] study, which indicated that the thermal performance of a heat sink with a cross-cut is significantly greater than a heat sink with multiple cross-cuts. Likely, Chingulpitak and colleges [51] also stated that the cross-cut heat sink gave larger thermal performance than the convectional plate fin heat sink.

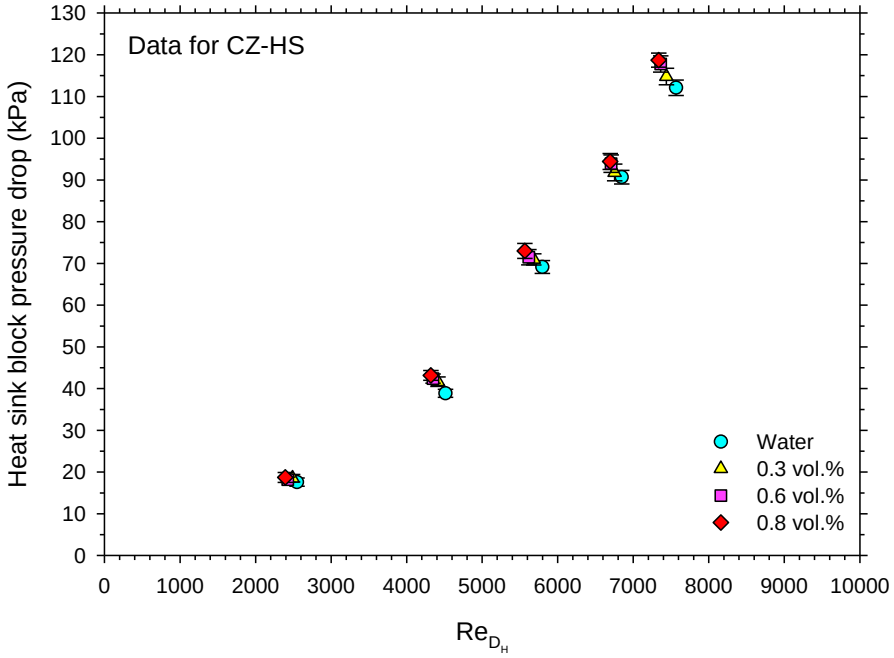

a) data for CZ-HS

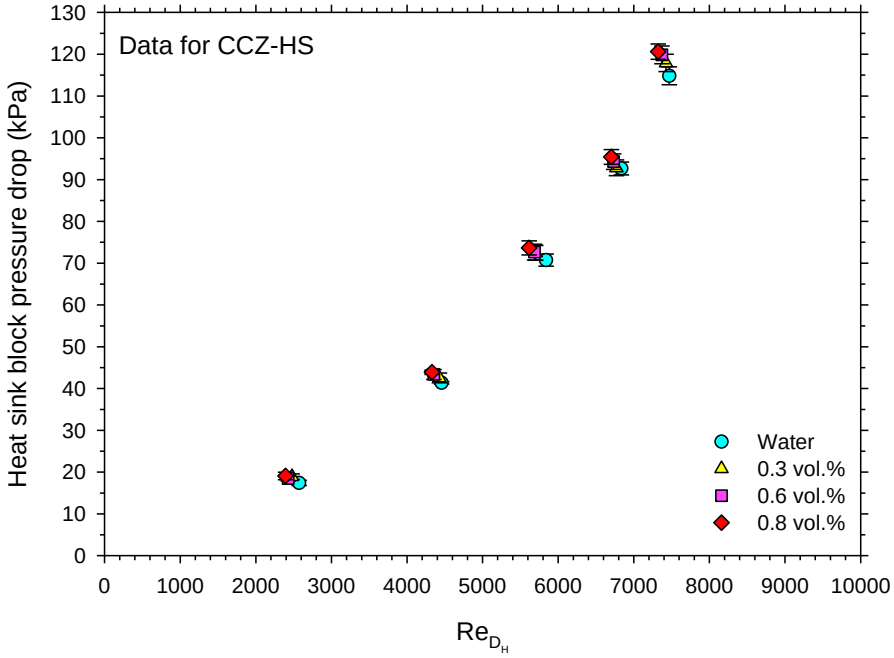

b) data for CCZ-HS

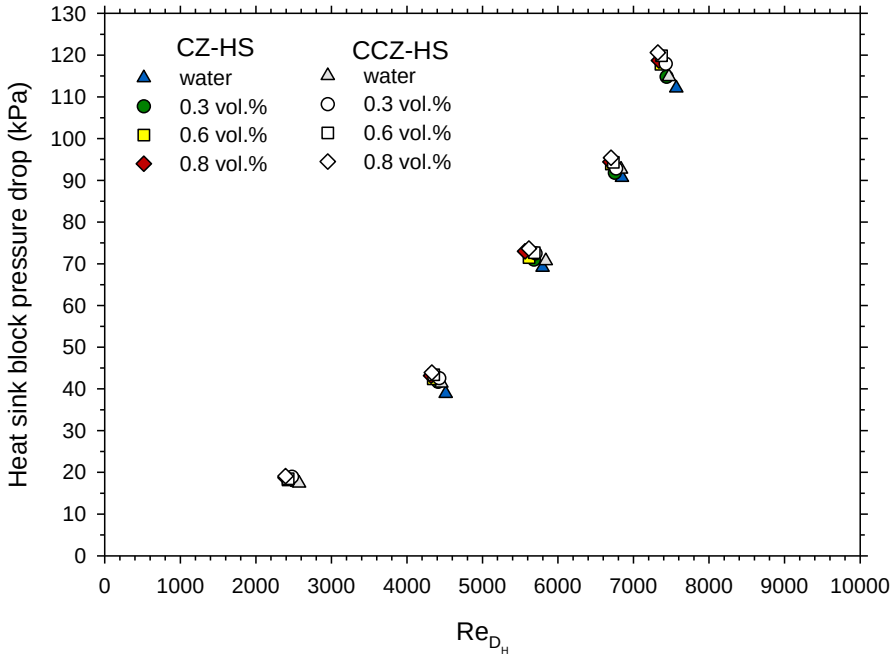

c) effect of single cross-cut flow channel

Fig. 5.24 Heat sink block pressure drop as a function of Reynolds number, particle concentration and heat sink type.

With regard to the pressure drop, Fig. 5.24 shows a comparison of the measured pressure drop across the heat sink for CZ-HS and CCZ-HS as a function of the Reynolds number and particle volume fraction. It is evident that the heat sink block pressure drop increased with increases in the Reynolds number. As the particle concentration increases, a few penalties in the pressure drop are observed. This is an important advantage of the use of nanofluid as a coolant: improving the heat transfer with small or no pressure drop penalties. Moreover, as described in Fig. 5.24c, the pressure drop of CZ-HS is very close to that of CCZ-HS. This means that single cross-cutting of the flow channel leads to enhancement in thermal performance with no extra pressure drop.

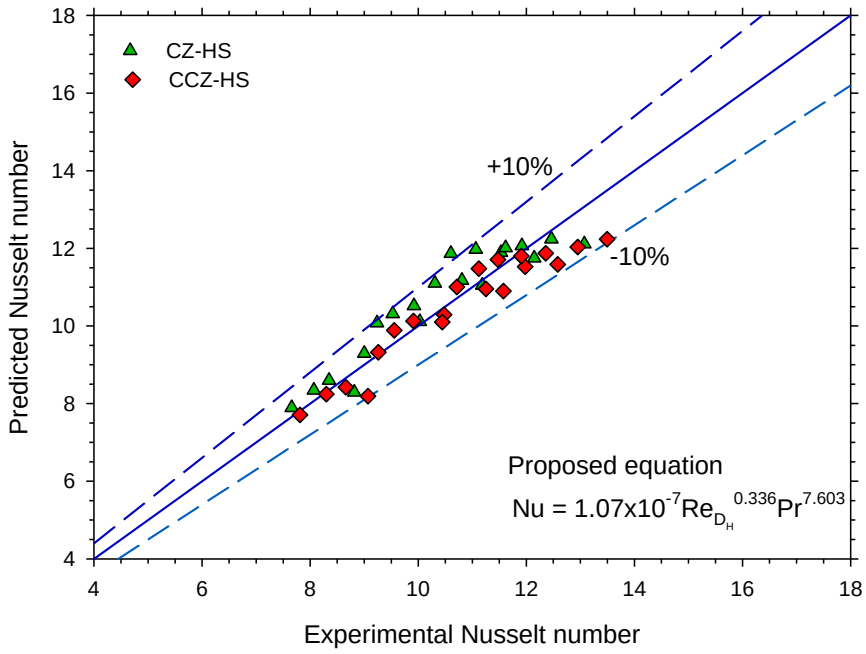

Fig. 5.25 Predicted Nusselt number versus experimental Nusselt number.

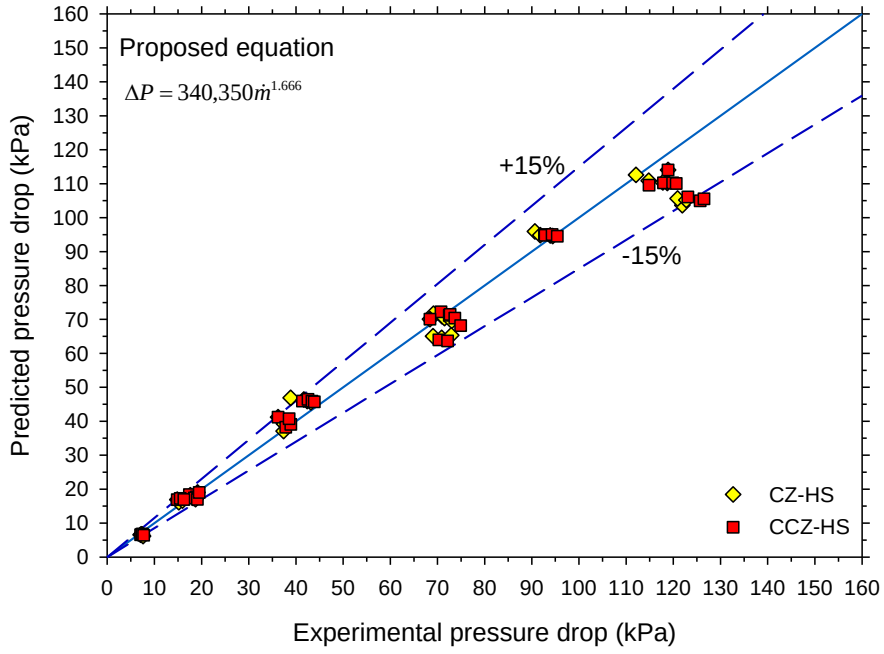

Fig. 5.26 Comparison of the predicted pressure drop and the measured pressure drop.

Finally, the Nusselt number and pressure drop obtained from the experiment are used to form a novel equation to calculate the Nusselt number and pressure drop of nanofluids flowing through MCHS with multiple zigzag flow channel shapes, both with single cross-cutting and continuous flow channels. The established correlations are described as follows:

Generally, the forced convective heat transfer correlation is formed in the following formula:

$$Nu = f\left(\mathrm{Re}_{D_H}, \mathrm{Pr}\right) \tag{5.8}$$

Based on the measured data of the study, the heat-transfer equation to compute the Nusselt number of nanofluid-cooled MCHS with multiple zigzag flow channel structures is presented as follows:

$$Nu = 1.07x10^{-7}\ \mathrm{Re}_{D_H}^{0.336}\ \mathrm{Pr}^{7.603} \tag{5.9}$$

Similarly, a new simple correlation for computing the pressure drop of nanofluids across MCHS with multiple zigzag flow channel shapes is proposed for convenient use as follows:

$$\Delta P = 340{,}350\dot{m}^{1.666}\ \text{(kPa)} \tag{5.10}$$

Thus, the proposed equations are achieved using curve-fitting methodology. The equations are established for all of the measured data for the SiO_2-water nanofluid flow in MCHS with multiple zigzag flow channel structures, both with continuous and single cross-cutting flow channels. The authors would like to recommend that the above equations be used to calculate the Nusselt number and pressure drop of nanofluids flowing through MCHS with multiple zigzag flow channel structures with or without cross-cutting of the flow channel. The scope of equations is described as follows: 1) particle volume concentration less than 0.8 vol.% and 2) Reynolds number based on the hydraulic diameter of each flow channel ranging from 2,500 to 8,000.

As shown in Figs. 5.25 and 5.26, the results indicate that the proposed correlations for Nusselt number and pressure drop gives good results close to the measured data. Most of the data falls within ± 10% for Nusselt number and ± 15% for pressure drop compared with the proposed equations. The results obtained from the proposed correlations show reasonable agreement with the experimental data. These correlations can be used to calculate the Nusselt number and pressure drop of nanofluids flowing in MCHS with multiple zigzag flow channel structures.

CHAPTER 6 CONCLUSION

The objective of this chapter is to present the conclusion of the present study. The important conclusions of this study are expressed as follows:

6.1 Conclusion

The convective heat transfer performance and pressure drop characteristic of a SiO_2–water nanofluid flowing through a common internally grooved tube (IGT) and internally grooved tube fitted with short length tabulator swirl generators (IGT+SG) were experimentally investigated. The following conclusions have been obtained.

- For water, IGT+SG shows highest heat transfer coefficient compared with the IGT and CST around 12% and 24%, respectively. At the same time, highest pressure drops are obtained and greater than those of the IGT and CST average 2.9 and 3.1 times, respectively. Thus, IGT has larger thermal performance factor than the IGT+SG at the same condition.
- The heat transfer coefficient increases with an increasing Reynolds number as well as particle concentration. For case of IGT, the heat transfer coefficients of nanofluid are higher than the common water approximately 6.0 to 22% at particle fraction ranged between 0.2 and 0.6 vol.%.
- The pressure drop of nanofluids increases with increasing Reynolds number and there is a small increase with increasing particle volume concentrations. Similar to the case of common base fluid, IGT gave larger thermal performance factor than that of the IGT+SG for all of the test conditions.

- New heat transfer and pressure drop correlations for predicting the Nusselt number and pressure drop of nanofluids flowing through IGT and IGT+SG are proposed as flows:

  For IGT :

  $$Nu = 0.066\,\mathrm{Re}^{0.752}\,\mathrm{Pr}^{0.089}(1+\phi)^{33.70}$$

  $$\Delta P = 2.53x10^{-7}\,\mathrm{Re}^{1.808}(1+\phi)^{18.85}$$

  For IGT+SG :

  $$Nu = 0.547\,\mathrm{Re}^{0.710}\,\mathrm{Pr}^{-0.817}(1+\phi)^{22.35}$$

  $$\Delta P = 2.53x10^{-7}\,\mathrm{Re}^{1.808}(1+\phi)^{18.85}$$

- The majority of the data falls within ± 5% of the proposed equations. These equations are valid in the range of Reynolds number based on hydraulic diameter between 6,000-18,000 and particle volume concentrations in the range of 0 and 0.6 vol.%.

For two new designs of $MCHS_S$ (CZ-HS and CCZ-HS), the important conclusions are summarized as follows:

- The Nusselt number increases as particle concentration and Reynolds number increase. The heat sink with nanofluid cooling shows a higher Nusselt number than the heat sink cooled by the water by approximately 3–15%.
- The heat sink with multiple zigzag flow channels and CCZ-HS have better thermal performance than the heat sink with continuous multiple zigzag flow channels (CZ-HS) by approximately 2–6%.
- At constant pumping power, the heat transfer performance of CCZ-HS is better than that of CZ-HS.
- As flow rate increases, the pressure drop of the fluid will increase. However, a minor increase in pressure drop is obtained when increasing the particle

concentration. Moreover, a cross-cut of the flow channel has no significant effect on the pressure drop.

- New heat-transfer and pressure-drop equations for predicting the forced convective Nusselt number and pressure drop of nanofluids flow pass the heat sinks with multiple zigzag flow channels are established. The developed correlations are in good agreement with the measured data with an average error of ± 10% for the Nusselt number and 15% for the pressure drop. The correlations are described as follows:

  For the Nusselt number, $Nu = 1.07x10^{-7}\ \mathrm{Re}_{D_H}^{0.336}\ \mathrm{Pr}^{7.603}$

  For the pressure drop, $\Delta P = 340{,}350\dot{m}^{1.666}$

6.2 Recommendations for Future Work

The test apparatus can be improved to study the heat transfer performance and pressure drop of nanofluids flowing through various types of enhanced tube, swirl generator as well as microchannel heat sinks.

REFERENCES

1. Masuda, H., Ebata, A., Teramae, K. and Hishinuma, N., 1993, "Alteration of Thermal Conductivity and Viscosity of Liquid by Dispersing Ultra-Fine Particles (Dispersion of Al_2O_3, SiO_2 and TiO_2 Ultra-Fine Particles)", Netsu Bussei (Japan), Vol.7, No. 4, pp. 227 - 233.

2. Choi, S.U.S., 1995, "Enhancing Thermal Conductivity of Fluids with Nanoparticle", ASME Fluids Engineering Division, Vol. 231, pp. 99 - 105.

3. Duangthongsuk, W. and Wongwises, S., 2009, "Heat Transfer Enhancement and Pressure Drop Characteristics of TiO_2-Water Nanofluid in a Double-Tube Counter Flow Heat Exchanger" International Journal of Heat and Mass Transfer, Vol. 22, pp. 2059 - 2067.

4. Duangthongsuk, W. and Wongwises, S., 2009, "Measurement of Temperature-Dependent Thermal Conductivity and Viscosity of TiO_2-Water Nanofluids", Experimental Thermal and Fluid Sciences, Vol. 33, pp. 706 - 714.

5. Duangthongsuk, W. and Wongwises, S., 2009, "An Experimental Study on the Heat Transfer Performance and Pressure Drop of TiO_2-Water Nanofluids Flowing under a Turbulent Flow Regime", International Journal of Heat and Mass Transfer, Vol. 52, pp. 2059 - 2067.

6. Duangthongsuk, W. and Wongwises, S.,"A Dispersion Model for Predicting the Heat Transfer Performance of TiO_2–Water Nanofluids under a Laminar Flow Regime", International Journal of Heat and Mass Transfer, Vol. 55 (2012), pp. 3138-3146.

7. Goto, M., Inoue, N. and Ishiwatari, N., 2001, "Condensation and Evaporation Heat Transfer of R410A Inside Internally Grooved Horizontal Tubes", International Journal of Refrigeration, Vol. 24 (7), pp. 628-638.

8. Rousseau, P.G., Van Eldik, M. and Greyvenstein, G.P., "Detailed Simulation of Fluted Tube Water Heating Condenser", Eighth International Refrigeration Conference at Purdue University, West Lafayette, IN, USA- July 25-28, 2000

9. www.furukawa.co.jp374

10. Duangthongsuk, W and Wongwises, S., 2013, "An Experimental Investigation into the Heat Transfer and Pressure Drop Characteristics of a Circular Tube Fitted with Rotating Turbine-Type Swirl Generators", Experimental Thermal and Fluid Sciences, Vol. 45, pp. 8-15.

11. Duangthongsuk, W and Wongwises, S., 2013, "Comparison of the Heat Transfer Performance and Friction Characteristics between Fixed (FTSG) and Free Rotation (RTSG) Turbine-Type Swirl Generators Fitted in a Small Circular Tube, Experimental Thermal and Fluid Sciences, Vol. 50, pp. 222-228.

12. Azmi, W.H., Sharma, K.V., Sarma, P.K., Mamat, R., and Anuar, S., 2014, "Comparison of Convective Heat Transfer Coefficient and Friction Factor of TiO2 Nanofluid flow in a Tube with Twisted Tape Inserts", International Journal of Thermal Sciences, Vol.81, pp.84-93.

13. Reddy, M.C.S., and Rao, V.V., 2014, "Experimental Investigation of Heat Transfer Coefficient and Friction Factor of Ethylene Glycol Water Based TiO2 Nanofluid in Double Pipe Heat Exchanger with and Without Helical Coil Inserts", International Communications in Heat and Mass Transfer, Vol.50, pp.68-76.

14. www.techtransfer.anl.gov

15. Wen, D., Ding, Y., 2004, Experimental investigation into convective heat transfer of nanofluids at the entrance region under laminar flow conditions, International Journal of Heat and Mass Transfer, Vol. 47, pp. 5181.

16. Duangthongsuk, W., Wongwises, S., 2010, An experimental study on the heat transfer performance and pressure drop of TiO2-water nanofluids flowing under a turbulent flow regime, International Journal of Heat and Mass Transfer, Vol. 53, pp. 334-344.

17. Das, S. K., Choi, S.U.S., Yu, W. and Pradeep, T., 2008, "Nanofluids: Science and Technology", Wiley

18. Duncan, M.A., and Rouvray, D.H., 1989, Microclusters, Scientific American, pp. 110 – 115.

19. Kimoto, K., Kamilaya, Y., Nonoyama, M. and Uyeda, R., 1963, “An Electron Microscope Study on Fine Metal Particles Prepared by Evaporation in Argon Gas at Low Pressure”, Japan Journal of Applied Physics, Vol. 2, pp. 702 - 713.

20. Granqvist, C.G., and Buhrman, R.A., 1976, “Ultrafine Metal Particles”, Journal of Applied Physics, Vol. 47, No. 5, pp. 2200 – 2219.

21. Suslick, K. S., Fang, M. and Hyeon, T., 1996, “Sonochemical Synthesis of Iron Colloids”, Journal of the American Chemical Society, Vol. 118, No. 47, pp. 11960 - 11961.

22. Chopkar, M, Das, P.K. and Manna, I., 2006, “Synthesis and Characterization of Nanofluid for Advanced Heat Transfer Applications”, Scripta Materialia, Vol. 55, pp. 549 – 552.

23. Akoh, H., Tsukasaki, Y., Yatsuya, S. and Tasaki, A., 1978, “Magnetic Properties of Ferro-Magnetic Ultrafine Particles Prepared by a Vacuum Evaporation on Running Oil Substrate”, Journal of Crystal Growth, Vol. 45, pp. 495 - 500.

24. Wagener, M., Murty, B.S. and Gunther, B., 1997, “Preparation of Metal Nanosuspensions by High-Pressure DC-Sputtering on Running Liquids in

Nanocrystalline and Nanocomposite Materials II", Materials Research Society, Pittsburgh, PA, Vol. 457, pp. 149 - 154.

25. Eastman, J.A., Choi, S.U.S., Li, S., Thompson, L.J. and Lee, S., 1997, "Enhanced Thermal Conductivity through the Development of Nanofluids", Proceeding of the Symposium Nanophase and Nanocomposite Materials II, Materials Research Society, Boston, MA, Vol. 457, pp. 3 - 11.

26. Zhu, H., Lin, Y. and Yin, Y., 2004, "A Novel One-Step Chemical Method for Preparation of Copper Nanofluids", Journal of Colloid and Interface Science, Vol. 277, pp. 100 - 103.

27. Eastman, J.A., Choi, S.U.S., Li, S., Thompson, L.J. and Lee, S., 2001, "Anomalous Thermal Conductivity Enhancement in Nano-tube Suspensions", Applied Physics Letters, Vol. 78, pp. 718 - 720.

28. Choi, S.U.S., Zhang, Z.G., Yu, W., Lockwood, F.E. and Grulke, E.A., 2001, "Anomalous Thermal Conductivity Enhancement in Nano-tube Suspensions", Applied Physics Letters, Vol. 79, pp. 2252 - 2254.

29. Sharma, K.V., Sundar, L.S., and Sarma, P.K., 2009, "Estimation of Heat Transfer Coefficient and Friction Factor in the Transition Flow with Low Volume Concentration of Al_2O_3 Nanofluid flowing in a Circular Tube and with Twisted Tape Insert", International Communications in Heat and Mass Transfer, Vol.36, pp.503-507.

30. Sundar, L.S., and Sharma, K.V., 2010, “Turbulent Heat Transfer and Friction Factor of Al_2O_3 Nanofluid in Circular Tube with Twisted Tape Inserts”, International Journal of Heat and Mass Transfer, Vol.53, pp.1409-1416.

31. Sundar, L.S., and Sharma, K.V., 2010, “Heat Transfer Enhancements of Low Volume Concentration Al_2O_3 Nanofluid and with Longitudinal Strip Inserts in a Circular Tube”, International Journal of Heat and Mass Transfer, Vol.53, pp.4280-4286.

32. Chandrasekar, M., Suresh, S., and Bose, A.C., 2010, “Experimental Studies on Heat Transfer and Friction Factor Characteristics of Al_2O_3/Water Nanofluid in a Circular Pipe Under Laminar Flow with Wire Coil Inserts”, Experimental Thermal and Fluid Science, Vol.34, pp.122-130.

33. Darzi, A.A.R., Farhadi, M., and Sedighi, K., 2014, “Experimental Investigation of Convective Heat Transfer and Friction Factor of Al_2O_3/Water Nanofluid in Helically Corrugated Tube”, Experimental Thermal and Fluid Science, Vol.57, pp.188-199.

34. Wongcharee, K., and Eiamsa-ard, S., 2012, “Heat Transfer Enhancement by Using CuO/Water Nanofluid in Corrugated Tube Equipped with Twisted Tape”, International Communications in Heat and Mass Transfer, Vol.39, pp.251-257.

35. Eiamsa-ard, S., and Wongcharee, K., 2012, “Single-phase Heat Transfer of CuO/Water Nanofluids in Micro-Fin Tube Equipped with Dual Twisted-Tapes”, International Communications in Heat and Mass Transfer, Vol.39, pp.1453-1459.

36. Sekhar, Y.R., Sharma, K.V., Karupparaj, R.T., and Chiranjeevi, C., 2013, "Heat Transfer Enhancement with Al_2O_3 Nanofluids and Twisted Tapes in a Pipe for Solar Thermal Applications", International Conference on Design and Manufacturing, IConDM 2013, Vol.64, pp.1474-1484.

37. Naik, M.T., Fahad, S.S., Sundar, L.S., and Singh. M.K., 2014, "Comparative Study on Thermal Performance of Twisted Tape and Wire Coil Inserts in Turbulent Flow Using CuO/Water Nanofluid", Experimental Thermal and Fluid Science, Vol.57, pp.65-76.

38. Azmi, W.H., Sharma, K.V., Sarma, P.K., Mamat, R., Anuar, S., and Sundar, L.S., 2014, "Numerical Validation of Experimental Heat Transfer Coefficient with SiO_2 Nanofluid Flowing in a Tube with Twisted Tape Inserts", Applied Thermal Engineering, Vol.73, pp.294-304.

39. Darzi, A.A.R., Farhadi, M., Sedighi, K., Shafaghat, R., and Zabihi, K., 2012, "Experimental Investigation of Turbulent Heat Transfer and Flow Characteristics of SiO_2/Water Nanofluid within Helically Corrugated Tubes", International Communications in Heat and Mass Transfer, Vol.39, pp.1425-1434.

40. Maddah, H., Alizadeh, M., Ghasemi, N., and Alwi, S.R.W., 2014, "Experimental Study of Al2O3/Water Nanofluid turbulent Heat Transfer Enhancement in the Horizontal Double Pipes Fitted with Modified Twisted Tapes", International Journal of Heat and Mass Transfer, Vol.78, pp.1042-1054.

41. Eiamsa-ard, S., and Kiatkittipong, K., 2014, “Heat Transfer Enhancement by Multiple Twisted Tape Inserts and TiO2/Water Nanofluid”, Applied Thermal Engineering, Vol.70, pp.896-924.

42. Esmaeilzadeh, E., Almohammadi, H., Nokhosteen, A., Motezaker, A., and Omrani, A.N., 2014, “Study on Heat Transfer and Friction Factor Characteristics of -Al2O3/Water Through Circular Tube with Twisted Tape Inserts with Different Thicknesses”, International Journal of Thermal Sciences, Vol.82, pp.72-83.

43. Azmi, W.H., Sharma, K.V., Sarma, P.K., Mamat, R., Anuar, S., and Sundar, L.S., 2014, “Numerical Validation of Experimental Heat Transfer Coefficient with SiO2 Nanofluid Flowing in a Tube with Twisted Tape Inserts”, Applied Thermal Engineering, Vol.73, pp.294-304.

44. Pak, B. C., Cho, Y. I., 1998, Hydrodynamic and heat transfer study of dispersed fluids with submicron metallic oxide particles, Experimental Heat Transfer, Vol. 11, pp. 151-170.

45. Drew, D.A., Passman, S.L., 1999, Theory of multi component fluids, Springer, Berlin.

46. Hamilton, R.L., Crosser, O.K., 1962, Thermal conductivity of heterogeneous two-component systems, I&EC Fundamental, Vol. 1(3), pp. 187.

47. F. W. Dittus, L. M. K. Boelter, 1930, Heat transfer in automobile radiators of the tubular type. The University of California Publications on Engineering, Vol. 2, pp. 443-461.

48. C.F. Colebrook, 1939, Turbulent flow in pipes, with particular reference to the transition between the smooth and rough pipe laws, Journal of the Institution of Civil Engineers, London, Vol. 11, pp. 133-156.

49. Duangthongsuk, W. and Wongwises, S., 2015, An experimental study on the thermal and hydraulic performances of nanofluids flow in a miniature circular pin fin heat sink, Experimental Thermal and Fluid Sciences, Vol. 33, pp. 706 - 714.

50. Kim, T.Y. and Kim, S.J., 2009, Fluid Flow and Heat Transfer Characteristics of Cross-Cut Heat Sinks, International Journal of Heat and Mass Transfer, Vol. 52, pp. 5358-5370.

51. S. Chingulpitak, N. Chimres, K. Nilpueng, S. Wongwises, 2016, Experimental and numerical investigations of heat transfer and flow characteristics of cross-cut heat sinks, International Journal of Heat and Mass Transfer, Vol. 102, pp. 142–153.

Experimental Thermal and Fluid Science 87 (2017) 30–39

Contents lists available at ScienceDirect

Experimental Thermal and Fluid Science

journal homepage: www.elsevier.com/locate/etfs

An experimental investigation on the heat transfer and pressure drop characteristics of nanofluid flowing in microchannel heat sink with multiple zigzag flow channel structures

Weerapun Duangthongsuk [a,b], Somchai Wongwises [b,*]

[a] Department of Mechanical Engineering, Southeast Asia University, Bangkok, Thailand
[b] Fluid Mechanics, Thermal Engineering and Multiphase Flow Research Lab. (FUTURE), Department of Mechanical Engineering, Faculty of Engineering, King Mongkut's University of Technology Thonburi, Bangmod, Bangkok, Thailand

ARTICLE INFO

Article history:
Received 5 February 2017
Received in revised form 10 April 2017
Accepted 10 April 2017
Available online 20 April 2017

Keywords:
Nusselt number
Pressure drop
Microchannel heat sink
Nanofluid
Cross-cutting

ABSTRACT

This research reports the thermal performance and flow characteristics of nanofluid flows in two different types of microchannel heat sink (MCHS) with multiple zigzag flow channel structures experimentally with regard to the continuous zigzag flow channel (CZ-HS) and the single cross-cutting zigzag flow channel (CCZ-HS). SiO_2 nanoparticles with particle loadings of 0.3, 0.6, and 0.8 vol.% and dispersed in deionized water (DI water) are used as the working medium. Both CZ-HS and CCZ-HS are made from copper material. Their dimensions are approximately 28 × 33 mm. Hydraulic diameter and number of flow channels are equally designed as seven 1-mm flow channels, respectively. The heat transfer area of CZ-HS is approximately 1176 mm^2 and that of CCZ-HS is 1238 mm^2. The effects of single cross-cutting of the flow channel, Reynolds number, and particle concentration on the Nusselt number and pressure drop characteristics are investigated. The experimental data indicate that the nanofluid-cooled heat sink provided larger thermal performance than the heat sink cooled by water of approximately 3–15%. Similarly, the results indicated that the thermal performances of the CCZ-HS are larger than those of the CZ-HS by an average of 2–6%. For the pressure drop, the measured data showed that particle concentration and cross-cutting of the flow channel have a small effect on the pressure-drop data.

1. Introduction

Three decades ago, electronic cooling systems with high heat flux densities were very popular. This trend had gained momentum until now. In the early stages, air cooling systems were widely used. However, the thermal performance of the air-cooled system was quite low due to certain limitations. Later, liquid cooling systems, such as water or other liquids, were used instead of the air-cooling system because the thermal performance of liquids is very high compared to common air and other gases. Currently, microscale and nanoscale heat-transfer devices have become a crucial tool in many common applications, such as integrated circuits (IC), Very-large-scale integration (VLSI) devices, laser-diode arrays, micro heat exchangers, computer chips and biomedical applications. Based on the small size of this equipment, the heat transfer area was limited, and an unprecedentedly high load was also generated. Enhanced cooling capability must be provided to solve the above problem. Improving the thermal performance of the coolants and innovative cooling equipment with special geometric structures is required to eliminate the high heat load generated from the system. In 1981, Tuckerman and Pease [1] first introduced the concept of the microchannel heat sink (MCHS) to increase the heat transfer performance of the cooling system. The hydraulic diameter of MCHS normally ranged between 10 and 1000 mm. They indicated that the thermal performance of the heat sink increased with decreases in the flow-channel diameter. Similarly, in 1993, Masuda and colleges [2] first announced an innovative concept to improve the thermal performance of the coolants using small solid particles dispersed in conventional heat transfer fluid. Later, in 1995, Choi [3] first named the common fluids with a nanoparticle suspension nanofluids, which is still popular at present. A decade ago, many researchers stated that the thermal performance of nanofluids was an order of magnitude higher than common heat transfer fluids and had little or no effect on pressure drop. As a result, using nanofluids as a coolant and flows in MCHS

* Corresponding author.
E-mail address: somchai.won@kmutt.ac.th (S. Wongwises).

http://dx.doi.org/10.1016/j.expthermflusci.2017.04.013
0894-1777/

Nomenclature

A	area, m^2
C_p	specific heat, J/kg °C
d	diameter, m
D_H	hydraulic diameter based on the each flow channel, m
h	heat transfer coefficient, W/m^2 °C and base thickness, mm
H	height, mm
k	thermal conductivity, W/m °C
L	heat sink length, m
$\dot{m}$	mass flow rate, kg/s
n	empirical shape factor
Nu	Nusselt number
ΔP	pressure drop, Pa
q	heat flux, W/cm^2
Q	heat transfer rate, W
$\dot{Q}_v$	volume flow rate, W
Re	Reynolds number
T	temperature, °C
t	channel height, mm
V	mean velocity, m/s
W	heat sink width, mm
W_{pp}	pumping power, W
y	distance from the surface, mm

Greek symbols

ϕ	volume fraction
ψ	sphericity
ρ	density, kg/m^3
μ	viscosity, kg/ms
$\varnothing$	bolt diameter, mm

Subscript

c	cross-sectional
ch	channel
HS	heat sink
in	inlet
out	outlet
p	particles
P	pitch
nf	nanofluid
w	wall, surface and water

with an optimum flow-channel structure called a nanofluid-cooled heat sink is estimated to be a very effective cooling system for removing high-heat densities generated by modern electronic devices. There is a rapidly growing number of studies on this subject. Daungthongsuk and Wongwises [4–7] summarized and explored the published articles with respect to the benefits and use of nanofluid-cooled heat sinks. However, updated studies with respect to the combination of the nanofluid and microchannel heat sink (nanofluid-cooled microchannel heat sink, NCMCHS) are listed in the following text.

Lelea [8] reported the heat-transfer performance of Al_2O_3-water nanofluid flow in a square flow channel MCHS under a laminar flow region numerically. The effects of particle fraction, particle diameter and heating and cooling conditions were evaluated with respect to a constant Reynolds number and heat flux. Nitiapiruk et al. [9] experimentally studied the convective heat transfer coefficient and friction factor of MCHS with multiple rectangular flow channels using TiO2-water nanofluids as coolant. The effects of thermophysical properties of nanofluids on the thermal performance and friction factor were reported. Teja et al. [10] performed a numerical investigation of the heat transfer and flow features of MCHS with rectangular, triangular, pentagonal, and circular flow channels. The CFD technique was used for analysis. In 2015, Malvandi and Ganji [11] investigated the effects of nanoparticle migration and asymmetric heat flux on the heat transfer performance of NCMCHS under uniform magnetic field. Al_2O_3-water nanofluids were used as coolant. Nikkhah et al. [12] presented heat transfer performance of nanofluids in a two-dimensional microchannel, numerically. Functionalized multi-walled carbon nanotube (FMWCNT) nanoparticles dispersed in water with particle fraction of 0.12 and 0.25 vol.% were conducted. Microchannel walls were surrounded under a periodic wall heat flux. Effect of the slip boundary conditions were taken into account. Karimipour [13] numerically investigated on the forced convective heat transfer of nanofluids flow in a microchannel using the lattice Boltzmann method. Various types of nanoparticles such as Ag, Cu and Al_2O_3 were dispersed in water. Effects of particle volume fraction and slip coefficient on the thermal performance were presented. Likewise, Karimipour et al. [14] used the lattice Boltzmann method to describe the heat transfer performance of water–Cu nanofluids flowing through a microchannel under laminar flow regime. In 2016, Azizi et al. [15] experimentally examined the thermal and hydraulic performances of NCMCHS. Cu nanoparticles dispersed in water with different particle weight fractions were used as coolant, and flow was studied in a cylindrical MCHS under a laminar flow regime. Wu et al. [16] presented the effectiveness of Al_2O_3-water nanofluid flow in MCHS to provide criteria about the optimum amount of nanofluids when used with MCHS.

In the abovementioned studies, many researchers stated that the thermal performance of NCMCHS was significantly greater than MCHS cooled by water and that little penalty in pumping power was obtained. However, most studied the thermal performance and pressure drop of NCMCHS using a numerical approach. Moreover, only single or multiple straight flow channels were examined. Thus, the target of the present work is to evaluate the heat transfer performance of nanofluid flow in a new type of microchannel heat sink. $MCHS_s$ with two different multiple zigzag flow channel structures is constructed and used as test sections. The first is the continuous zigzag flow channel (CZ-HS), and the second is the single cross-cutting zigzag flow channel (CCZ-HS). These are new type of flow channel structures that have never been seen in the published literature. They are made from copper material with dimensions of 28 × 33 mm, a hydraulic diameter of 1 mm, and 7 flow channels, equally. The heat transfer area of CZ-HS and CCZ-HS are approximately 1176 mm^2 and 1238 mm^2, respectively. Particle concentrations of 0.3, 0.6, and 0.8 vol.% are tested. Effect of the single cross-cutting flow channel, Reynolds number, and particle concentrations on the thermal and flow characteristics are investigated.

2. Experimental set-up

In this study, an experimental apparatus is designed to evaluate the Nusselt number and pressure drop of a nanofluid-cooled heat sink and then compared to the data for a water-cooled heat sink. The working medium flows through microchannel heat sinks with multiple CZ-HS and CCZ-HS structures. The experimental system is

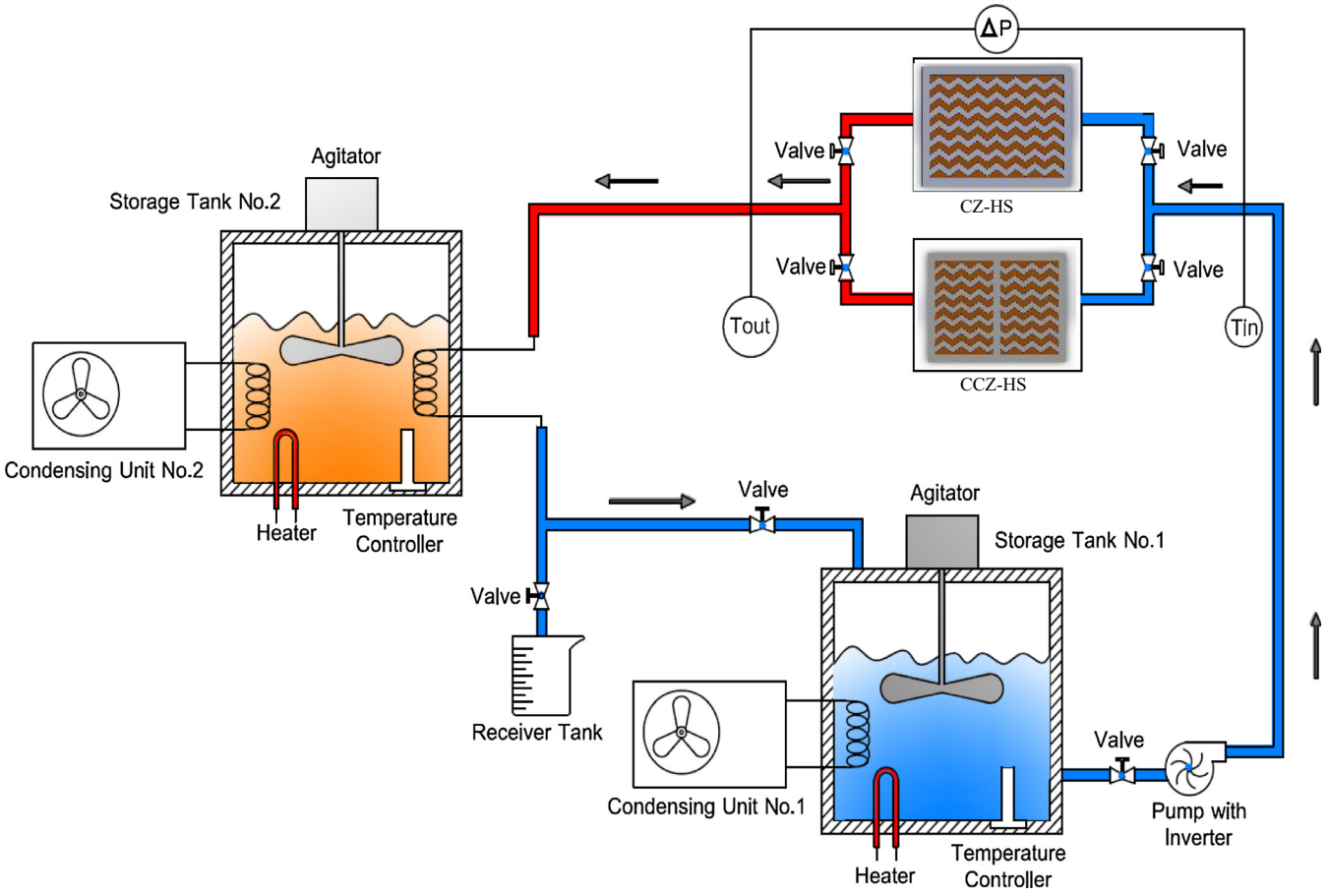

Fig. 1. Schematic diagram of the experimental system used in the present work.

schematic, as described in Fig. 1. It mainly consists of the two test sections (CZ-HS and CCZ-HS), two storage tanks, a receiver tank, and a pump with an inverter. Fig. 2 and Table 1 illustrate the configurations and importance dimensions of the $MCHS_S$ used in the present study, respectively. Both CZ-HS and CCZ-HS are made of copper material. The transparency material is used to make the cover plate of the MCHS and placed at the upper side of the test section to completely seal the flow channels, as depicted in Fig. 2C. An electric heater with a capacity of 100 W is attached at the lower side of the test section to simulate the heat load, which can be varied using a variac with a 10-A capacity. Stainless steel material is used to construct the two storage tanks with a volume of 15 L. For tank 1, a 2-kW electric heater and 3.5-kW cooling capacity coil are equipped inside the tank to adjust the temperature of the working fluid to the required value using a thermostat. Similarly, a 3.5-kW cooling coil is placed in tank 2 and used to decrease the temperature of the working fluid that exits from the test section to the temperature of tank 1. A thermostat is also used to control the fluid temperature inside tank 2. This tank is required to reach steady-state condition. The receiver tank is used to measure the fluid flow rate by means of measuring the mass of discharged fluid per unit time. The fluid flow rate can be varied by using an inverter to control the frequency of the pump. The bulk fluid temperatures are measured using T-type thermocouples and located at the inlet and exit on the test section. To estimate the surface temperature, two T-type thermocouples are positioned at 5 mm and 15 mm from the upper side surface of the heat sink to measure the temperature gradient. Later, the surface temperature of the heat sink is calculated. To measure the heat sink block pressure drop, two digital pressure gages are placed at the inlet and exit of the test section. To certify the precision and reliability of the experimental data, all instruments are calibrated as shown in Table 2. During the test run, the following parameters are measured, such as the bulk fluid temperatures of the working fluid, temperature of the test section, fluid flow rates, and pressure at the both ends of the test section. All data are recorded after steady-state condition has been achieved.

3. Sample preparation

To provide the nanofluids, the 2-step method is used. SiO_2 nanoparticles with an average diameter of 15 nm are used and dispersed in the DI water at particle volume fractions of 0.3, 0.6, and 0.8 vol.%. First, SiO_2 nanoparticles are dispersed and stirred in the DI water at the required particle concentration under stirring action. Secondly, a 500-W ultrasonic vibrator sonicates the nanofluid continuously for 2 h to eliminate the agglomeration of ultrafine nanoparticles. The thermophysical properties of SiO_2 nanoparticle are expressed in Table 3.

4. Calculation methodology

For this work, the Nusselt number and pressure drop of SiO_2-water nanofluids flow in MCHS with two different zigzag flow channels (CZ-HS and CCZ-HS) are presented. The data for water and nanofluids are compared. The following relevant equations are considered to compute the thermal performance and pressure drop of the working fluid. The correlations are described as follows:

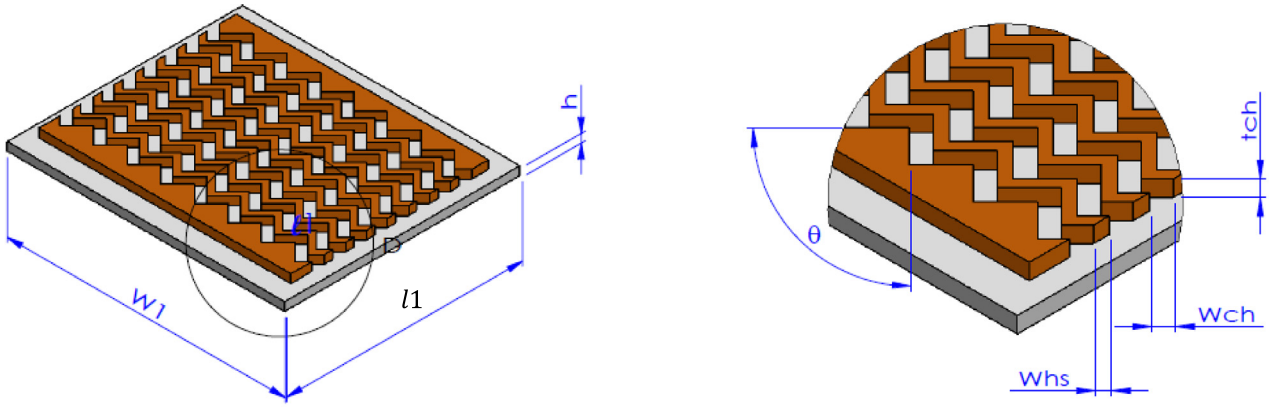

a) CZ-HS

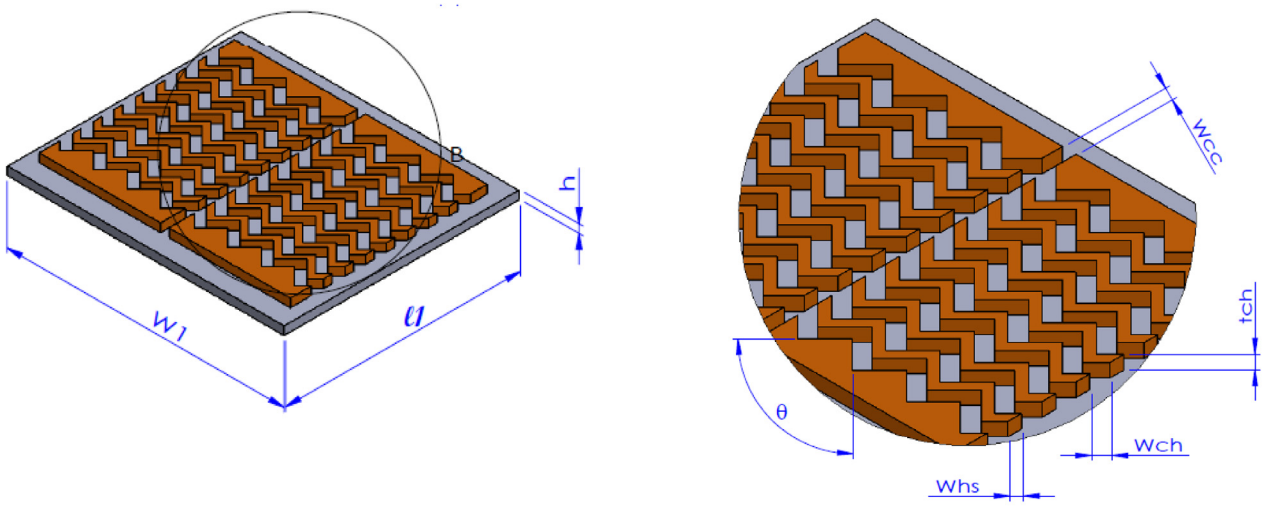

b) CCZ-HS

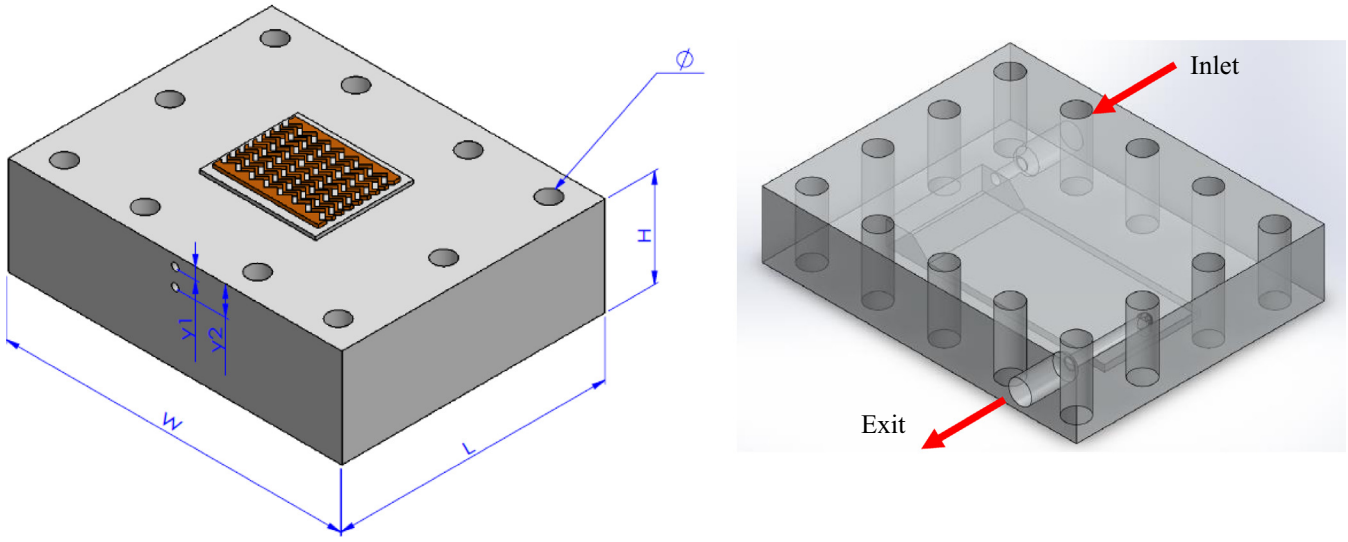

c) Base and cover plate of heat sink

Fig. 2. Configuration of the $MCHS_S$ used in the present study.

Table 1
Important dimensions of the zigzag flow channel heat sinks used in the present study.

Parameter	CZ-HS	CCZ-HS
W (mm)	95	95
L (mm)	75	75
H (mm)	28	28
W_{ch} (mm)	1	1
t_{ch} (mm)	1	1
W_{hs} (mm)	1	1
W_1 (mm)	33	33
l_1 (mm)	28	28
h (mm)	1	1
θ (degree)	90°	90°
y_1 (mm)	5	5
y_2 (mm)	15	15
w_{cc} (mm)	–	1
A_{HS} (mm^2)	1176	1238
∅ (mm)	M6x1	M6x1

Table 2
Experimental system uncertainties.

Parameter	Uncertainty (%)
Pressure measurement (kPa)	±0.05
Temperature (°C)	±0.1
Electronic balance (g)	±0.6
Heat transfer coefficient (W/m^2 °C)	±8

Table 3
Thermophysical properties of SiO_2 nanoparticle.

Properties	SiO_2 nanoparticle
Mean diameter, d_p	15 nm
Thermal conductivity, k	1.37 W/m °C
Specific heat, Cp	0.742 kJ/kg °C
Density, ρ	2648 kg/m^3

The Nusselt number of the nanofluids can be calculated using the following equations:

$$h_{nf} = \frac{Q_{nf}}{A_{HS}(T_w - T_{nf})} \tag{1}$$

$$Nu_{nf} = \frac{h_{nf} D_H}{k_{nf}} \tag{2}$$

The heat transfer rate of the nanofluids presented in Eq. (1) can be computed from

$$Q_{nf} = \dot{m}_{nf} Cp_{nf} (T_{out} - T_{in})_{nf} \tag{3}$$

in which A_{HS} is the heat transfer area, D_H is the hydraulic diameter based on each flow channel, h_{nf} is the heat transfer coefficient of the nanofluid, k_{nf} is the thermal conductivity of the nanofluid, Nu_{nf} is the Nusselt number of the nanofluid, Q_{nf} is the heat transfer rate, T_w is the surface temperature of the test section, and T_{nf} is the bulk temperature of the nanofluid.

As shown in Eq. (1), the surface temperature (T_w) of the test section is necessary to calculate the heat transfer coefficient. Thus, a T-type thermocouple is inserted at the two different points of the test section (5 mm (T_1) and 10 mm (T_2) from the top surface) to measure the temperature gradient. Then, the surface temperature of the test section is computed using Eq. (4) as follows:

$$T_w = T_1 - \frac{y_1}{y_2}(T_2 - T_1) \tag{4}$$

in which T_1 and T_2 are the temperature 5 mm and 10 mm from the top surface, respectively, y_1 is the distance between T_W and T_1, and y_2 is the distance between T_1 and T_2.

The Reynolds number based on hydraulic diameter of the flow channel is calculated from

$$Re_{D_H} = \frac{\rho_{nf} V_c D_H}{\mu_{nf}} \tag{5}$$

The hydraulic diameter of the each flow channel is calculated as follows:

$$D_H = \frac{4A_c}{p_c} \tag{6}$$

where ρ_{nf} is the density of the nanofluid, V_c is the mean fluid velocity of the each flow channel, μ_{nf} is the viscosity of the nanofluid, A_c is the cross-sectional area of the each flow channel, and p_c is the perimeter of each flow channel.

From the above equations, it evident that the thermophysical properties of the nanofluid are important. The following correlations are used to calculate the thermal conductivity, viscosity, density, and specific heat. The bulk temperature is considered to compute the thermophysical properties. The relevant equations are expressed as follows:

For thermal conductivity, the Hamilton and Crosser model [17] is used as shown in Eq. (7).

$$k_{nf} = \left[\frac{k_p + (n-1)k_w - (n-1)\phi(k_w - k_p)}{k_p + (n-1)k_w + \phi(k_w - k_p)}\right] k_w \tag{7}$$

$$n = 3/\psi \tag{8}$$

The Einstein model [18] is used for computing the viscosity of the nanofluid, as expressed in Eq. (9):

$$\mu_{nf} = (1 + 2.5\phi)\mu_w \tag{9}$$

where ϕ is the volume fraction of nanoparticle, k is the thermal conductivity, ψ is the sphericity (1 for the spherical shape and 0.5 for the cylindrical shape), n is the empirical shape factor, and μ is the viscosity.

To calculate the specific heat and density of the nanofluids, Pak and Cho's [19] correlations are used and are expressed as follows:

$$Cp_{nf} = \phi Cp_p + (1 - \phi) Cp_w \tag{10}$$

$$\rho_{nf} = \phi \rho_p + (1 - \phi)\rho_w \tag{11}$$

in which Cp is the specific heat, ρ is the density, and the subscripts nf, p, and w presented in the above equations are the nanofluid, nanoparticles, and water, respectively.

Lastly, the pressure drop across the test section is measured and then used to calculate the pumping power as follows:

$$W_{pp} = \dot{Q}_V \Delta P \tag{12}$$

where W_{pp} is the pumping power, ΔP is the measured pressure drop across the test section, and $\dot{Q}_V$ is the measured volume flow rate of the working medium.

Finally, the measured Nusselt number and pressure drop are compared with those obtained from the heat transfer and pressure drop correlations proposed by Duangthongsuk and Wongwises [5]. The correlations are shown below:

For Nusselt number;

$$Nu = 1463 Re_{D_H}^{0.418}\ Pr^{-4.09} \tag{13}$$

For pressure drop;

$$\Delta P = 16,542 \dot{m}^{1.760} \tag{14}$$

5. Results and discussion

Variation of the surface temperature with heat flux as a function of particle concentration is presented in Fig. 3. It clearly seen that the surface temperatures of the heat sinks increased with increases

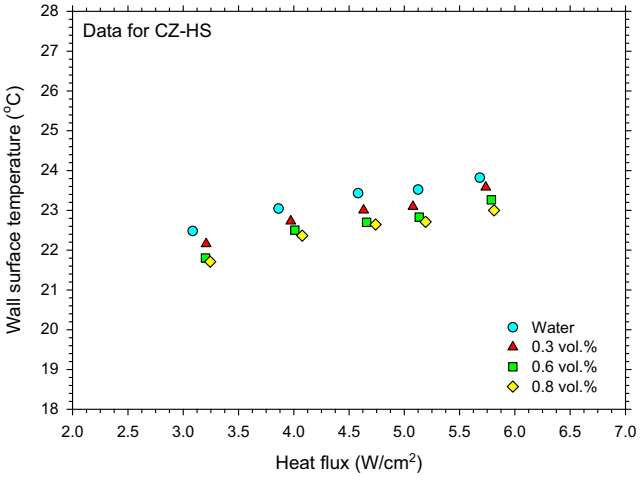

a) data for CZ-HS

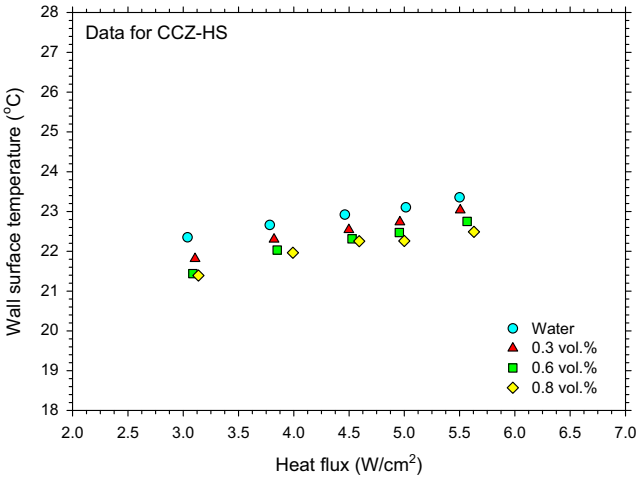

b) data for CCZ-HS

Fig. 3. Wall surface temperature versus wall heat flux for various particle concentrations.

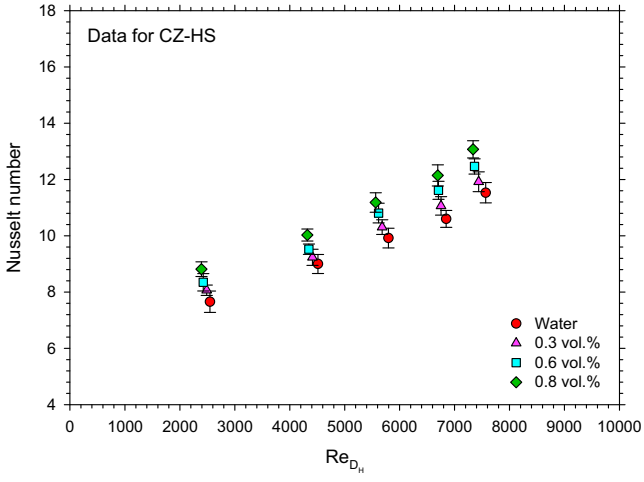

a) data for CZ-HS

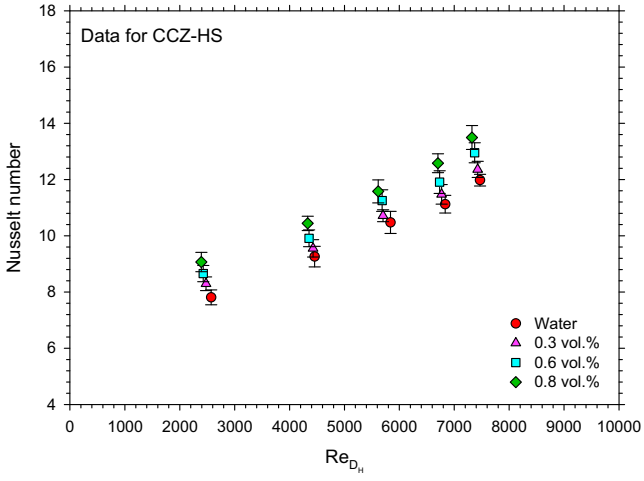

b) data for CCZ-HS

Fig. 4. Variation in the Nusselt number and Reynolds number as a function of particle concentrations.

in the wall heat flux. Likewise, the surface temperature of MCHS decreases with increasing particle concentration, which means that the nanofluid-cooled heat sink provided better thermal performance than the water-cooled heat sink. This is due to the fact that the nanoparticles suspended in the water enhance the thermal conductivity of the bulk fluid [20]. As a result, a higher heat dissipation rate is obtained, which provides better capability of the system. Moreover, comparing the CZ-HS and CCZ-HS, the experimental data indicate that the surface temperature of CCZ-HS is lower than that of the CZ-HS. This may be due to the effect of the single cross-cutting of the flow channel at the middle plan of CCZ-HS creating a high-intensity disturbance of the fluid flow compared to the CZ-HS, where the fluid flows continuously through each flow channel. Thus, a lower surface temperature for CCZ-HS is achieved.

Variations of the measured Nusselt number of CZ-HS and CCZ-HS with the particle concentration and the Reynolds number are shown in Fig. 4. The experimental results indicate that the measured Nusselt number increases as the particle concentration and Reynolds number increase. The results also show that the Nusselt number of the nanofluid- cooled heat sink is greater than the case of the water-cooled heat sink by approximately 3–15% with a particle loading ranging between 0.3 and 0.8 vol.%. Furthermore, when comparing CZ-HS and CCZ-HS, it is clear that the thermal performance of CCZ-HS is better than CZ-HS by an average of approximately 2–6%, as shown in Fig. 5. This may be due to the fact that for CCZ-HS, single cross-cutting of the flow channel results in dividing the flow area into two regions. When the fluid flows past the first region, direct impingement of the fluid stream to the channel wall of the next region occurs. As a consequence, higher turbulent intensity is attained, resulting in augmentation of the heat-transfer performance.

The enhancement ratio (Nu_{nf}/Nu_w) versus Reynolds number based on hydraulic diameter of the flow channel is illustrated in Fig. 6. As described above, the heat sink with the nanofluid-cooled system has a higher thermal performance than the heat sink with the water-cooled system by approximately 3–15% at a particle fraction ranging between 0.3 and 0.8 vol.%. This confirms that the application of nanofluids as a coolant instead of water will enhance the thermal dissipation rate of the system, leading to improvement of the working performance of the heat-transfer equipment.

Fig. 7(a) and (b) shows comparison between the experimental data and the calculations, for Nusselt number and pressure drop, respectively. For Nusselt number, the results indicate that the predicted values obtained from the Eq. (13) are much higher than

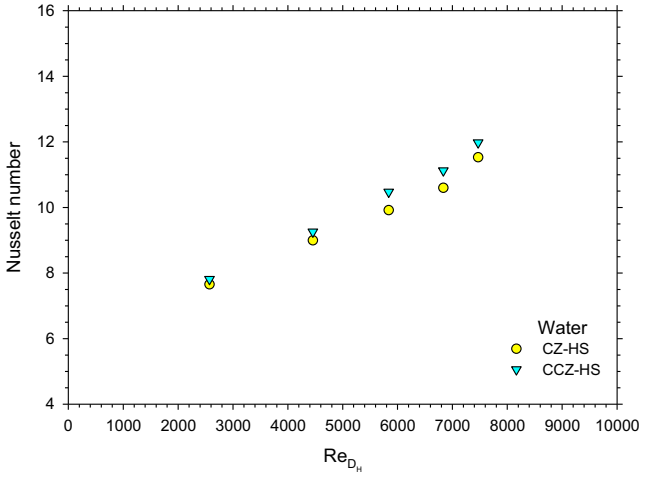

a) data for water

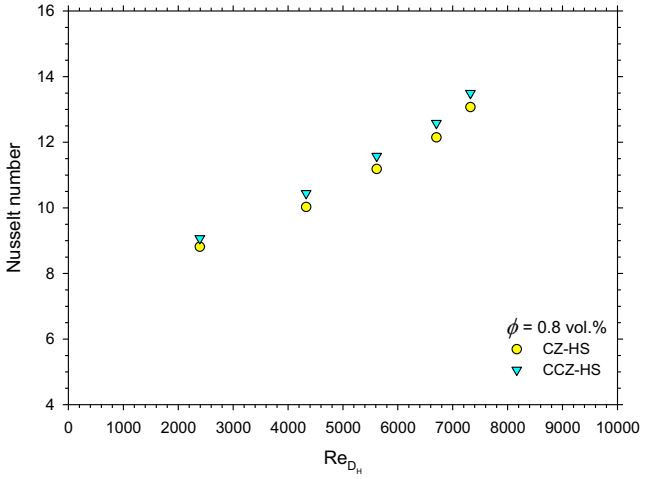

b) data for particle concentration of 0.8 vol.%

Fig. 5. Effect of the single cross-cut flow channel on the Nusselt number of the water and nanofluid.

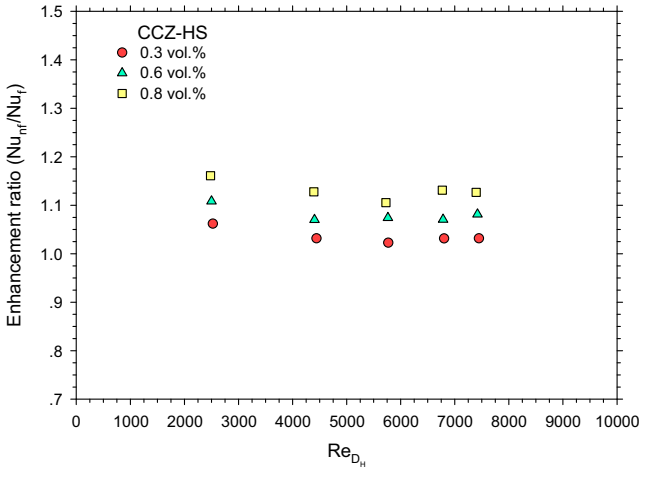

Fig. 6. Heat transfer enhancement ratio versus Reynolds number at various particle concentrations.

those of the measured data. This is because Eq. (13) is established by using the data obtained from the heat sink with pin fin structure

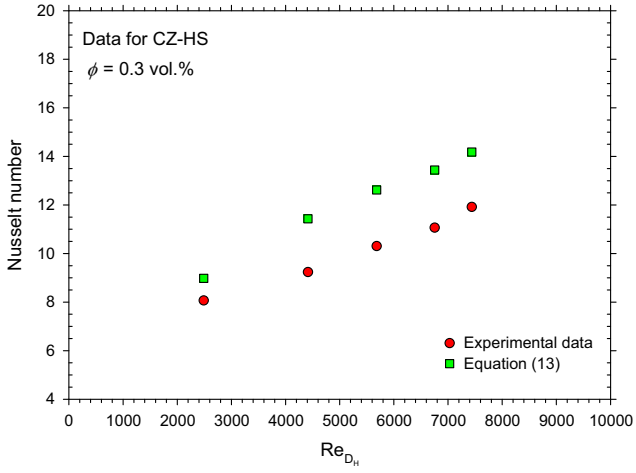

a) Nusselt number

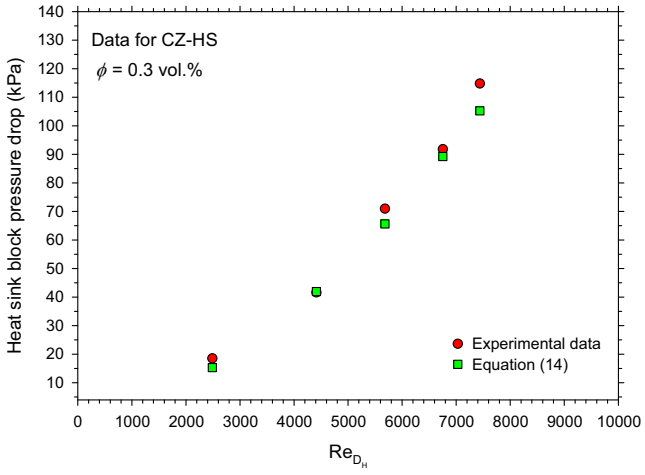

b) Pressure drop

Fig. 7. Comparison of the Nusselt number and pressure drop obtained from the experiment and the calculation.

which typically gives higher thermal performance than the heat sink with simple flow channel [21], under the same Reynolds number. Thus, much more heat transfer performance is obtained. However, for the pressure drop, the results show good agreement between the measured values and the calculated values by Eq. (14). This is because pressure drop across the test section normally depends on the configuration and dimension of the inlet and exit of the test sections, similar to the shape of the flow channel. As a result, an agreement between measured data and the calculated values is observed.

Comparison of the measured Nusselt number for CZ-HS and CCZ-HS as a function of the pumping power at different particle volume fractions is shown in Fig. 8. As shown in this figure, at a given pumping power, the Nusselt number of the CCZ-HS is greater than that of the CZ-HS and increases as particle concentration increases. This means that the use of a nanofluid-cooling system provides higher heat-transfer performance than the water-cooling system at a given pumping power. The reasons for the enhancement are described in the above paragraph. Moreover, this observation is consistent with Kim and Kim's [22] study, which indicated that the thermal performance of a heat sink with a cross-cut is significantly greater than a heat sink with multiple cross-cuts. Likely, Chingulpitak and colleges [23] also stated that

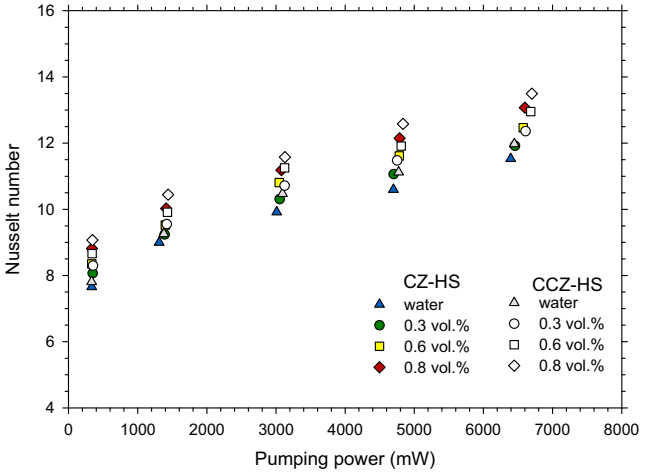

Fig. 8. Variation of the Nusselt number and pumping power as a function of particle concentration and heat sink type.

the cross-cut heat sink gave larger thermal performance than the convectional plate fin heat sink.

With regard to the pressure drop, Fig. 9 shows a comparison of the measured pressure drop across the heat sink for CZ-HS and CCZ-HS as a function of the Reynolds number and particle volume fraction. It is evident that the heat sink block pressure drop increased with increases in the Reynolds number. As the particle concentration increases, a few penalties in the pressure drop are observed. This is an important advantage of the use of nanofluid as a coolant: improving the heat transfer with small or no pressure drop penalties. Moreover, as described in Fig. 9c, the pressure drop of CZ-HS is very close to that of CCZ-HS. This means that single cross-cutting of the flow channel leads to enhancement in thermal performance with no extra pressure drop.

Finally, the Nusselt number and pressure drop obtained from the experiment are used to form a novel equation to calculate the Nusselt number and pressure drop of nanofluids flowing through MCHS with multiple zigzag flow channel shapes, both with single cross-cutting and continuous flow channels. The established correlations are described as follows:

Generally, the forced convective heat transfer correlation is formed in the following formula:

$$Nu = f(Re_{D_H}, Pr) \tag{15}$$

Based on the measured data of the study, the heat-transfer equation to compute the Nusselt number of nanofluid-cooled MCHS with multiple zigzag flow channel structures is presented as follows:

$$Nu = 1.07 \times 10^{-7} Re_{D_H}^{0.336}\ Pr^{7.603} \tag{16}$$

Similarly, a new simple correlation for computing the pressure drop of nanofluids across MCHS with multiple zigzag flow channel shapes is proposed for convenient use as follows:

$$\Delta P = 340,350\dot{m}^{1.666} \quad \text{(kPa)} \tag{17}$$

Thus, the proposed equations are achieved using curve-fitting methodology. The equations are established for all of the measured data for the SiO_2-water nanofluid flow in MCHS with multiple zigzag flow channel structures, both with continuous and single cross-cutting flow channels. The authors would like to recommend that the above equations be used to calculate the Nusselt number and pressure drop of nanofluids flowing through MCHS with multiple zigzag flow channel structures with or without cross-cutting of the flow channel. The scope of equations is described as follows:

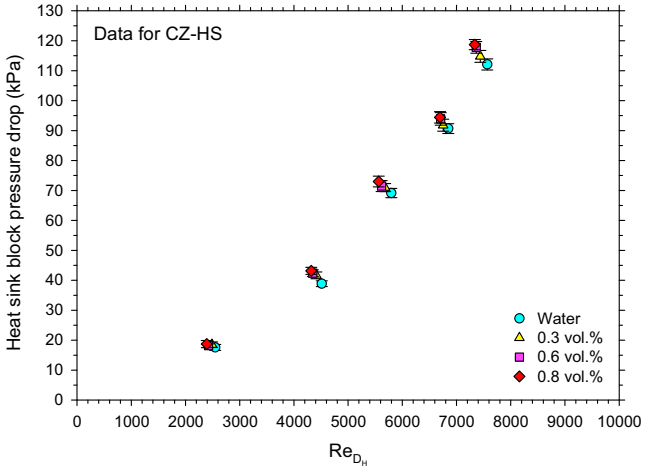

a) data for CZ-HS

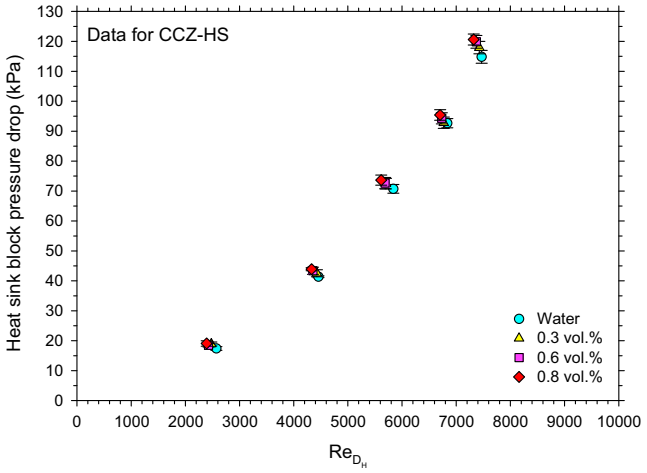

b) data for CCZ-HS

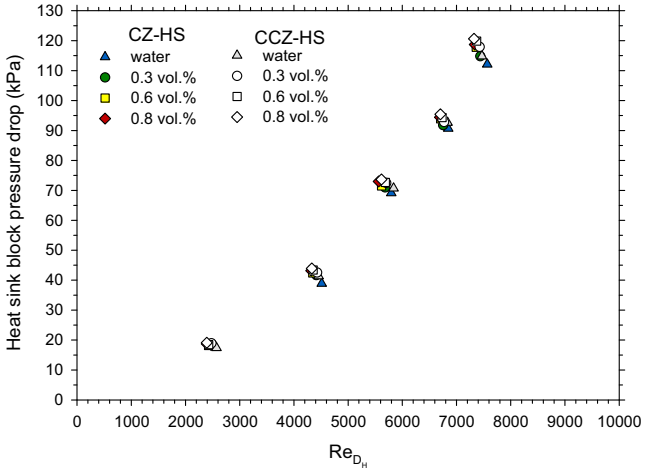

c) effect of single cross-cut flow channel

Fig. 9. Heat sink block pressure drop as a function of Reynolds number, particle concentration and heat sink type.

(1) particle volume concentration less than 0.8 vol.% and (2) Reynolds number based on the hydraulic diameter of each flow channel ranging from 2500 to 8000.

As shown in Figs. 10 and 11, the results indicate that the proposed correlations for Nusselt number and pressure drop gives

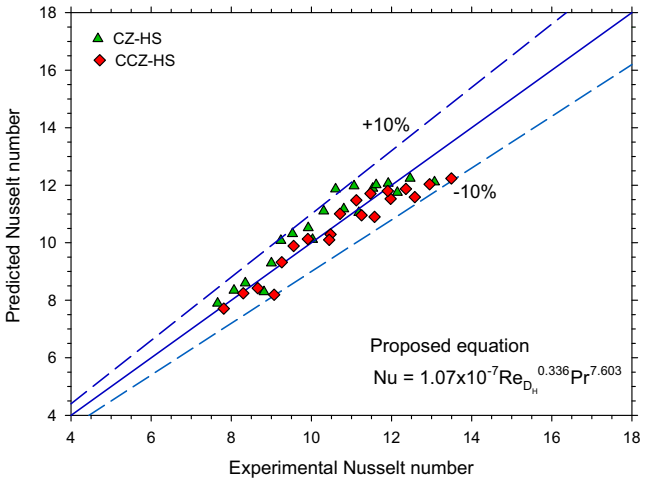

Fig. 10. Predicted Nusselt number versus experimental Nusselt number.

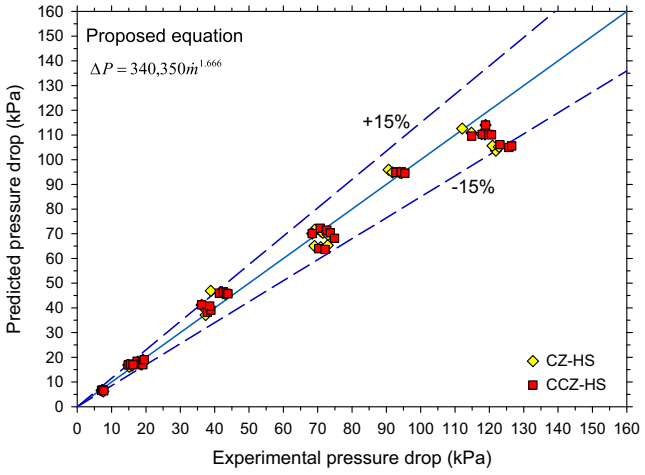

Fig. 11. Comparison of the predicted pressure drop and the measured pressure drop.

good results close to the measured data. Most of the data falls within ±10% for Nusselt number and ±15% for pressure drop compared with the proposed equations. The results obtained from the proposed correlations show reasonable agreement with the experimental data. These correlations can be used to calculate the Nusselt number and pressure drop of nanofluids flowing in MCHS with multiple zigzag flow channel structures.

6. Conclusions

In this work, the convective heat transfer and pressure drop of a novel type of microchannel heat sink are experimentally studied. Two new designs of $MCHS_S$ with a multiple zigzag flow channel are tested. The first one is the continuous zigzag flow channel (CZ-HS), and another is the zigzag flow channel with a single cross-cutting at the middle position (CCZ-HS). SiO_2-water nanofluids with particle loading of 0.3, 0.6, and 0.8 vol.% are examined. The effects of particle concentration, Reynolds number, and single cross-cutting of the flow channel on the thermal performance and pressure drop are presented. The resultant findings of the present study are described as follows:

- The Nusselt number increases as particle concentration and Reynolds number increase. The heat sink with nanofluid cooling shows a higher Nusselt number than the heat sink cooled by the water by approximately 3–15%.
- The heat sink with multiple zigzag flow channels and CCZ-HS have better thermal performance than the heat sink with continuous multiple zigzag flow channels (CZ-HS) by approximately 2–6%.
- At constant pumping power, the heat transfer performance of CCZ-HS is better than that of CZ-HS.
- As flow rate increases, the pressure drop of the fluid will increase. However, a minor increase in pressure drop is obtained when increasing the particle concentration. Moreover, a cross-cut of the flow channel has no significant effect on the pressure drop.
- New heat-transfer and pressure-drop equations for predicting the forced convective Nusselt number and pressure drop of nanofluids flow pass the heat sinks with multiple zigzag flow channels are established. The developed correlations are in good agreement with the measured data with an average error of ±10% for the Nusselt number and 15% for the pressure drop. The correlations are described as follows:

  For the Nusselt number, $Nu = 1.07 \times 10^{-7} Re_{D_H}^{0.336}\ Pr^{7.603}$

  For the pressure drop, $\Delta P = 340,350\dot{m}^{1.666}$

Acknowledgement

The authors acknowledge the financial support provided by the "Research Chair Grant" National Science and Technology Development Agency (NSTDA), the Thailand Research Fund (TRF) and the Office of the Higher Education Commission (Grant No. TRG5880269), the National Research University Project (NRU) and King Mongkut's University of Technology Thonburi through the "KMUTT 55th Anniversary Commemorative Fund".

References

[1] D.B. Tuckerman, R.F.W. Pease, High performance heat sinking for VLSI, IEEE Electron Device Lett. 2 (5) (1981) 126–129.
[2] H. Masuda, A. Ebata, K. Teramae, N. Hishinuma, Alteration of thermal conductivity and viscosity of liquid by dispersing ultra-fine particles (Dispersion of Al_2O_3, SiO_2 and TiO_2 Ultra-Fine Particles), Netsu Bussei 7 (4) (1993) 227–233.
[3] S.U.S. Choi, Enhancing thermal conductivity of fluids with nanoparticle, ASME Fluids Eng. Div. 231 (1995) 99–105.
[4] W. Duangthongsuk, A.S. Dalkilic, S. Wongwises, Convective heat transfer of Al_2O_3-water nanofluids in a microchannel heat sink, Curr. Nanosci. 8 (3) (2012) 317–322.
[5] W. Duangthongsuk, S. Wongwises, An experimental study on the thermal and hydraulic performances of nanofluids flow in a miniature circular pin fin heat sink, Exp. Therm. Fluid Sci. 66 (2015) 28–35.
[6] W. Duangthongsuk, S. Wongwises, Heat transfer and pressure drop in a pin fin heat sink using nanofluids as coolant, Adv. Mater. Res. 1105 (2015) 253–258.
[7] W. Duangthongsuk, S. Wongwises, A comparison of the heat transfer performance and pressure drop of nanofluid-cooled heat sinks with different miniature pin fin configurations, Exp. Therm. Fluid Sci. 68 (2015) 111–118.
[8] D. Lelea, The performance evaluation of Al_2O_3/water nanofluid flow and heat transfer in microchannel heat sink, Int. J. Heat Mass Transf. 54 (2011) 3891–3899.
[9] P. Nitiapiruk, O. Mahian, A.S. Dalkilic, S. Wongwises, Performance characteristics of a microchannel heat sink using TiO_2/water nanofluid and different thermophysical models, Int. Commun. Heat Mass Transfer 47 (2013) 98–104.
[10] V.S. Teja, A. Ramakrishna, R. Rao, Numerical study of different cross-sectional stacked microchannel heat sink, Int. J. Eng. Res. Technol. 3 (8) (2014) 54–59.
[11] A. Malvandi, D.D. Ganji, Effects of nanoparticle migration and asymmetric heating on magnetohydrodynamic forced convection of alumina/water nanofluid in microchannels, Eur. J. Mech. B/Fluids 52 (2015) 169–184.
[12] Z. Nikkhah, A. Karimipour, M. Reza Safaei, P. Forghani-Tehrani, M. Goodarzi, M. Dahari, S. Wongwises, Forced convective heat transfer of water/functionalized multi-walled carbon nanotube nanofluids in a microchannel with oscillating heat flux and slip boundary condition, Int. Commun. Heat Mass Transfer 68 (2015) 69–77.

[13] A. Karimipour, New correlation for Nusselt number of nanofluid with Ag/Al_2O_3/Cu nanoparticles in a microchannel considering slip velocity and temperature jump by using lattice Boltzmann method, Int. J. Therm. Sci. 91 (2015) 146–156.
[14] A. Karimipour, A. Hossein Nezhadb, A. D'Orazio, M. Hemmat Esfe, M. Reza Safaei, E. Shirani, Simulation of copper-water nanofluid in a microchannel in slip flow regime using the lattice Boltzmann method, Eur. J. Mech. B/Fluids 49 (2015) 89–99.
[15] Z. Azizi, A. Alamdari, M.R. Malayeri, Thermal performance and friction factor of a cylindrical microchannel heat sink cooled by Cu-water nanofluid, Appl. Therm. Eng. 99 (2016) 970–978.
[16] J. Wu, J. Zhao, J. Lei, B. Liu, Effectiveness of nanofluid on improving the performance of microchannel heat sink, Appl. Therm. Eng. 101 (2016) 402–412.
[17] R.L. Hamilton, O.K. Crosser, Thermal conductivity of heterogeneous two-component systems, Ind. Eng. Chem. Fundam. 1 (3) (1962) 187–191.
[18] D.A. Drew, S.L. Passman, Theory of Multi Component Fluids, Springer, Berlin, 1999.
[19] B.C. Pak, Y.I. Cho, Hydrodynamic and heat transfer study of dispersed fluids with submicron metallic oxide particles, Exp. Heat Transf. 11 (1998) 151–170.
[20] M. Hemmat Esfe, H. Rostamian, M. Afrand, A. Karimipour, M. Hassani, Modeling and estimation of thermal conductivity of MgO–Water/EG (60:40) by artificial neural network and correlation, Int. Commun. Heat Mass Transfer 68 (2015) 98–103.
[21] H. Shafeie, O. Abouali, K. Jafarpur, G. Ahmadi, Numerical study of heat transfer performance of single-phase heat sinks with micro pin-fin structures, Appl. Therm. Eng. 58 (2013) 68–76.
[22] T.Y. Kim, S.J. Kim, Fluid flow and heat transfer characteristics of cross-cut heat sinks, Int. J. Heat Mass Transf. 52 (2009) 5358–5370.
[23] S. Chingulpitak, N. Chimres, K. Nilpueng, S. Wongwises, Experimental and numerical investigations of heat transfer and flow characteristics of cross-cut heat sinks, Int. J. Heat Mass Transf. 102 (2016) 142–153.